

UCLA

UCLA Electronic Theses and Dissertations

Title

Kinetic Competition Growth Mechanism and Phase Manipulation of Silicide Nanowires in Solid State Reaction

Permalink

<https://escholarship.org/uc/item/4jf35993>

Author

Chen, Yu

Publication Date

2014

Peer reviewed|Thesis/dissertation

UNIVERSITY OF CALIFORNIA

Los Angeles

Kinetic Competition Growth Mechanism and Phase Manipulation
of Silicide Nanowires in Solid State Reaction

A dissertation submitted in partial satisfaction of the
requirements for the degree Doctor of Philosophy
in Materials Science and Engineering

by

Yu Chen

2014

© Copyright by

Yu Chen

2014

ABSTRACT OF THE DISSERTATION

Kinetic Competition Growth Mechanism and Phase Manipulation
of Silicide Nanowires in Solid State Reaction

by

Yu Chen

Doctor of Philosophy in Materials Science and Engineering

University of California, Los Angeles, 2014

Professor Yu Huang, Chair

The first phase selection and the phase formation sequence between metal and silicon (Si) couples are indispensably significant to microelectronics. With increasing scaling of device dimension to nano regime, established thermodynamic models in bulk and thin film fail to apply in one dimensional (1-D) nanostructures. Herein, we use a kinetic competition model to explain the phase formation sequence of 1-D nickel (Ni) silicides: multiple Ni silicides coexist at the initial stage and then the fastest one wins out as the first phase in a following growth competition. With kinetic parameters extracted from in-situ transmission electron microscope (TEM) observations, we quantitatively explain the unique size

dependant first phase formation and the phase formation sequence changes in 1-D structures. We can further control the first phase by selectively enhancing or suppressing the growth rate of silicides through template structure modifications. Growth rate diffusion limited phases can be greatly enhanced in a porous Si nanowire (NW) template due to short diffusion paths. On the other hand, a thick aluminum oxide (Al_2O_3) shell around the NW is applied to impede the growth of large volume diffusion limited phases including $\text{Ni}_{31}\text{Si}_{12}$, $\delta\text{-Ni}_2\text{Si}$ and $\theta\text{-Ni}_2\text{Si}$. Moreover, a thin platinum (Pt) interlayer between Si and Ni is used to suppress the nucleation of NiSi_2 . Together, with the thick shell and Pt interlayer, we can suppress all competing silicides and render slow growing NiSi to form as the first phase. The resistivity of Pt doped NiSi (denoted as Ni(Pt)Si) NW are found compatible to pure NiSi from a two terminal and four terminal measurement. Controlled formation of $\text{Ni}_{31}\text{Si}_{12}$, $\delta\text{-Ni}_2\text{Si}$, $\theta\text{-Ni}_2\text{Si}$, NiSi or NiSi_2 as the first phase has also been achieved. To examine the kinetic competition model, 1-D cobalt (Co) and palladium (Pd) silicide formations are also studied and analyzed kinetically. A thick shell is found effective to suppress the Pd silicide NW broken at the interface.

The dissertation of Yu Chen is approved.

King-Ning Tu

Xiangfeng Duan

Yu Huang, Committee Chair

University of California, Los Angeles

2014

Table of Contents

Chapter 1 Introduction	1
Chapter 2 Si NW template synthesis and sample preparation	8
2.1 Growth of Si NW with diameter control.....	8
2.2 Fabrication of porous Si NW.....	8
2.3 Preparation of TEM membranes.....	10
2.4 Preparation of metal/Si NW diffusion couples.....	11
Chapter 3 Kinetic competition model and size dependant phase formation sequence of Ni silicide	13
3.1 Si NW size dependant first phase formation of Ni silicides.....	13
3.2 Failure of interfacial strain energy model in explaining silicide phase formation sequence in 1-D structures.....	16
3.3 Failure of effective formation heat model in explaining silicide phase formation sequence in 1-D structures.....	19
3.4 Kinetic competition model and multiple phases coexistence in the initial stage.....	21
3.5 Contact area between Ni and Si NW does not limit the Ni supply.....	23
3.6 Growth rate of Ni silicides and kinetic parameters extracted from in-situ TEM.....	26
3.7 Thermal stability of Ni silicides.....	34

Chapter 4 Phase manipulation through template modulations.....	37
4.1 Importance of Ni silicide phase manipulation.....	37
4.2 Ni silicides formation in porous Si NWs.....	38
4.3 Ni silicides formation in solid Si NWs with compressive shells.....	42
4.4 Ni silicides formation in solid Si NWs with Pt interlayers.....	46
4.5 Ni silicides formation in solid Si NWs with compressive shell and Pt interlayers.....	46
4.6 Pt distribution in Ni(Pt)Si crystal structure.....	48
4.7 Demonstration of Ni silicides phase control in Si NW templates.....	53
Chapter 5 Influence of the additional Pt atoms on NiSi formation and its electrical propertie.....	57
5.1 Electrical properties of Ni(Pt)Si NWs from two terminal measurements.....	57
5.2 Fabrication of long Ni(Pt)Si NWs.....	58
5.3 Electrical properties of Ni(Pt)Si NWs from four terminal measurements.....	59
5.4 Wider processing windows of Ni(Pt)Si than pure NiSi.....	63
Chapter 6 Phase formation in other silicide systems.....	65
6.1 Phase formation of Co silicide.....	65
6.2 Phase formation in Pd silicide.....	69
Chapter 7 Summary.....	73
References.....	76

Acknowledgments

I would never have been able to finish my dissertation without the guidance of my committee members and selfless supports from my family, friends and my wife. I would like to express my deepest appreciation to them.

First of all, I appreciate Prof. Yu Huang, my Ph.D. research advisor, offered me financial supports and the opportunity to join Functional Nanostructures Lab to work with smart and diligent people. Her guidance and creativity has always led me to accomplish challenging tasks. During these years, I have never been short of encouragement, trust, and inspiration from her which I thank the most.

I would also like to thank my committee members, Prof. Xiangfeng Duan, Prof. King-Ning Tu, Prof. Mark S. Goorsky and Prof. Bruce S. Dunn for their mentorships and valuable suggestions. I am also lucky having very close cooperation with Prof. Duan and his students. From those team works, I am exposed to many new fields and learn a lot from people with diverse backgrounds. Prof. Tu, as one of the greatest experts on nanomaterials, silicide systems and kinetic studies, gave me many important suggestions which became part of the major points in my study.

I thank my great research partners: Dr. Yung Chen Lin, Dr. Chun-Wei Huang, Ms. Ya Hsuan Chuang and Mr. Hung Chieh Cheng for their selfless helps. I would never forget the happiness and frustration we shared to have solid data to support our studies. I thank Dr.

Yung Chen Lin, Dr. Xiaojing Huang, Dr. Lixin Liu, Dr. Woojong Yu, Mr. Tze-Bin Song, Dr. Lingyan Ruan, Dr. Hailong Zhou, Dr. Gong Liu, Dr. Rui Cheng, Mr. Udayabagya Halim, Mr. Yongjia Li, Mr. Chain Lee, Mr. Jonathan Shaw, Mr. Boris Voloskiy and Mr. Zhaoyang Lin for inviting me to join their projects and sharing their wisdoms. Those works open a wide window to me to understand the interesting nanoscale world.

I also appreciate the technical supports and important discussions from Prof. Lih J. Chen, Prof. Wen-Wei Wu, Dr. Sergey Prikhodko, Dr. Noah Bodzin, Dr. Stephan Kraemer, Dr. Tom Mates and Dr. Yunbin Guan. It is not easy to have long term distant cooperation with people outside the department, campus or even in other countries. I appreciate their warm and professional helps.

In addition, I want to show my appreciation to my family and close friends in Chinese for their supports.

謝謝我的父母，陳進通先生、周淑媛女士對我的鼓勵和支持，沒有他們的對我的悉心栽培和心靈輔導，我不可能成為家族裡第一個大學畢業生，並且成功出國獲得博士學位，我感激他們無盡的付出。謝謝我的弟弟陳睿在我異鄉求學期間，一肩扛起侍奉父母的重責大任，讓我能夠專心致力於研究，順利畢業。謝謝葉佳喜媽咪，斯蘋，芋茹的體諒，在我成家之後，暫時免除我對家裡的責任，讓我能夠沒有後顧之憂的讀書。

我也很感謝我的朋友們，在我讀書期間豐富了我的生命歷程。謝謝巫嘉

恩和張睿思淨化了我的靈魂，謝謝陳天白無微不至的貼心，無形的為我化解了一次又一次的難關，謝謝許宛晴願意真誠地與我分享她的生命經驗以及課業知識，謝謝李宜秋協助我解決生活上大小事，讓我在洛杉磯能安穩的生活下來，謝謝楊士德雪中送炭的羊肉爐，謝謝張馨云助我走過最初的適應期，謝謝張維軒、葉雅婷讓我看到幸福和諧的婚姻生活，以及在逆境求生的意志，謝謝張立德、王超逸溫暖了我的胃，溫暖了我的心，灌醉了斯穰的肝，謝謝莊亞璇、鄭弘杰在承受巨大壓力的同時，燃燒自己的小宇宙，提供我最真誠的協助，謝謝何旻璟讓我的而立之路不孤單，謝謝王秋燕在研究上和生活中的無私分享，謝謝陳嘉伶、陳欣蘋不吝讓我借鏡她們自身的寶貴經驗，謝謝劉小葳爽朗豪邁的笑聲，驅走我們生活中的陰霾，謝謝劉楫平、劉佩宜用開朗樂觀的態度，提醒我能保持正面積極，謝謝巫俊志、江怡慧從不間斷的關懷，謝謝蔡宇淳、魏志君分享的各種生活知識與美食，謝謝王伯原的體諒和偶爾的溫馨接送情，謝謝李家恩教我在美國生活必備的談判入門。

最後，也是最重要的，謝謝斯穰，一路上風雨相伴，無怨無悔，體貼入微，關心倍至，放棄高薪繁華的空姐生活，回歸質樸本色。願以此論文，獻給你們。

VITA

EDUCATION

- 2005-2007 MS, National Tsing Hua University (Hsinchu, Taiwan)
Materials Science and Engineering, supervised by Prof. Lih J. Chen
- 2001-2005 BS, National Tsing Hua University (Hsinchu, Taiwan)
Materials Science and Engineering

EXPERIENCE

- 2009-2014 Research assistant in Functional Nanostructures Lab (UCLA)
- 2006-2007 Teaching assistant in transmission electron microscopy (Graduate class, NTHU)
- 2005-2007 Research assistant in Nano Structures and Dynamics Lab (NTHU)

AWARDS/SCHOLARSHIPS

- 2014 Harry M. Showman Prize
- 2014 Chinese-American Engineers and Scientists Association of Southern California
Scholarship
- 2014 First Prize Winner of Science as Art Competition in 2014 Materials Research Society
Meeting (Spring)
- 2013 Best Presentation Award in Southern California Society for Microscopy &
Microanalysis
- 2013 Young Scientist Award, Asia-Pacific Conference on Semiconducting Silicides

PUBLICATIONS

- **Kinetic manipulation of silicide phase formation in Si nanowire templates.** Chen, Y., Lin, Y.-C., Zhong, X., Cheng, H.-C., Duan, X., & Huang, Y. (2013). *Nano Lett.*, 13(8), 3703-3708.
- **Kinetic competition model and size-dependent phase selection in 1-D nanostructures.** Chen, Y., Lin, Y.-C., Huang, C.-W., Wang, C.-W., Chen, L.-J., Wu, W.-W., & Huang, Y. (2012). *Nano Lett.*, 12(6), 3115-3120.
- **Crystallinity control of ferromagnetic contacts in stressed nanowire templates and the magnetic domain anisotropy.** Lin, Y.-C., Chen, Y., Chen, R., Ghosh, K., Xiong, Q., & Huang, Y. (2012). *Nano Lett.*, 12(8), 4341-4348.
- **The growth and applications of silicides for nanoscale devices.** Lin, Y.-C., Chen, Y., & Huang, Y. (2012). *Nanoscale*, 4(5), 1412-1421.
- **Detection of spin polarized carrier in silicon nanowire with single crystal MnSi as magnetic contacts.** Lin, Y.-C., Chen, Y., Shailos, A., & Huang, Y. (2010). *Nano Lett.*, 10(6), 2281-2287.
- **Growth of nickel silicides in Si and Si/SiO_x core/shell nanowires.** Lin, Y.-C., Chen, Y., Xu, D., & Huang, Y. (2010). *Nano Lett.*, 10(11), 4721-4726.
- **Domain wall motion in synthetic Co₂Si nanowires.** Liu, G., Lin, Y.-C., Liao, L., Liu, L., Chen, Y., Liu, Y., Weiss, N. O., et al. (2012). *Nano Lett.*, 12(4), 1972-6.
- **High Density Catalytic Hot Spots in Ultrafine Wavy Nanowires.** Huang, X., Zhao, Z., Chen, Y., Chiu, C.-Y., Ruan, L., Liu, Y., Li, M., Duan, X., & Huang, Y. (2014). *Nano Lett.*, DOI: 10.1021/nl501137a.

- **A versatile strategy to the selective synthesis of Cu nanocrystals and the in situ conversion to CuRu nanotubes.** Huang, X., Chen, Y., Chiu, C.-Y., Zhang, H., Xu, Y., Duan, X., & Huang, Y. (2013). *Nanoscale*, 5(14), 6284–90.
- **Monodisperse Cu@PtCu nanocrystals and their conversion to hollow-PtCu nanostructures for methanol oxidation.** Huang, X., Chen, Y., Zhu, EB, Xu, YX., Duan, XF & Huang, Y. " (2013). *J. Mater. Chem., A1* (46), 14449-14454
- **Palladium-based nanostructures with highly porous features and perpendicular pore channels as enhanced organic catalysts.** Huang, X., Li, Y., Chen, Y., Zhou, E., Xu, Y., Zhou, H., Duan, X., et al. (2013). *Angew. Chem. Int. Ed. (English)*, 52(9), 2520–4.
- **Plasmonic and catalytic AuPd nanowheels for the efficient conversion of light into chemical energy.** Huang, X., Li, Y., Chen, Y., Zhou, H., Duan, X., & Huang, Y. (2013). *Angew. Chem. Int. Ed. (English)*, 52(23), 6063–7.
- **A facile strategy to Pt₃Ni nanocrystals with highly porous features as an enhanced oxygen reduction reaction catalyst.** Huang, X., Zhu, E., Chen, Y., Li, Y., Chiu, C.-Y., Xu, Y., Lin, Z., et al. (2013). *Adv. Mater.*, 25(21), 2974–2979.
- **A rational design of carbon-supported dispersive Pt-based octahedra as efficient oxygen reduction reaction catalysts.** Huang, X., Zhao, Z., Chen, Y., Zhu, E., Li, M., Duan, X. & Huang, Y. *Energy Environ. Sci.* 7 (9), 2957-2962.
- **Nanoscale joule heating and electromigration enhanced ripening of silver nanowire contacts.** Song, T., Chen, Y., Chung, C., Yang, Y., Bob, B., Duan, H., Li, G., Tu, K. N., Huang, Y. & Yang, Y. (2014). *ACS Nano*, 8 (3), 2804–2811.
- **Chemical vapor deposition growth of monolayer MoSe₂ nanosheets.** Shaw, J., Zhou, H., Chen, Y., Weiss, N., Liu, Y., Huang, Y. & Duan, X. (2014) *Nano Res.* 7(4) 1-7.
- **Biomimetic synthesis of an ultrathin platinum nanowire network with a high twin density for enhanced electrocatalytic activity and durability.** Ruan, L., Zhu, E., Chen, Y., Lin, Z., Huang, X., Duan, X. & Huang, Y. (2013). *Angew. Chem. Int. Ed. (English)*, 52(48), 12557-81.
- **Gold clusters alloyed to nanoporous palladium surfaces as highly active bimetallic oxidation catalysts.** Li, Y., Zhu, E., Chen, Y., Chiu, C., Yu, H., Huang, X., Hicks, R. & Huang, Y. (2013). *ChemSusChem* 6 (10), 1868-1872
- **Vertically stacked multi-heterostructures of layered materials for logic transistors and complementary inverters.** Yu, W. J., Li, Z., Zhou, H., Chen, Y., Wang, Y., Huang, Y., & Duan, X. (2013). *Nat. Mater.*, 12(3), 246–52.
- **A rational design of cosolvent exfoliation of layered materials by directly probing liquid–solid interaction,** Halim, U., Zheng, C. R., Chen, Y., Lin, Z., Jiang, S., Cheng, R., Huang, Y. & Duan, X. (2013) *Nat. Commun.*, 4, 2213.
- **Chemical vapour deposition growth of large single crystals of monolayer and bilayer graphene.** Zhou, H., Yu W. J., Liu, L., Cheng, R., Chen, Y., Huang, X., Liu, Y., Wang, Y., Huang, Y. & Duan, X. (2013) *Nat. Commun.*, 4, 2096.
- **High-frequency self-aligned graphene transistors with transferred gate stacks.** Cheng, R., Bai, J., Liao, L., Zhou, H., Chen, Y., Liu, L., Lin, Y.-C., et al. (2012). *Proc. Natl. Acad. Sci. U.S.A.*, 109(29), 11588–92.
- **High-yield chemical vapor deposition growth of high-quality large-area AB-stacked bilayer graphene.** Liu, L., Zhou, H., Cheng, R., Yu, W. J., Liu, Y., Chen, Y., Shaw, J., et al. (2012). *ACS Nano*, 6(9), 8241–9.
- **A systematic study of atmospheric pressure chemical vapor deposition growth of large-area monolayer graphene.** Liu, L., Zhou, H., Cheng, R., Chen, Y., Lin, Y.-C., Qu, Y., Bai, J., et al. (2012). *J. Mater. Chem.*, 22(4), 1498.
- **Au(Si)-filled β-Ga₂O₃ nanotubes as wide range high temperature nanothermometers.** Gong, N. W., Lu, M. Y., Wang, C. Y., Chen, Y., & Chen, L. J. (2008). *Appl. Phys. Lett.*, 92(7), 073101.(Cover)

Chapter 1 Introduction

Size does matter. In low dimensional nanostructures, unique material properties and superior functions are available due to size and geometry effect. For example, low temperature superplasticity has been reported in nanocrystalline nickel, aluminum alloy and nickel aluminide due to their suppressed grain boundary sliding and thus less deformation within nanograined structures.¹ Thermal conductivity of Si NW has also been found much lower than that in bulk Si while its Seebeck coefficient and resistivity remain similar² which makes Si NW a good thermal electric material due to size and geometry effect. While many unique properties of nanostructured materials have been discovered and interrogated extensively in the past few decades,³⁻⁵ fundamental material processes at this scale leave much to be desired for. For instance, nanoscale Si electronics have attracted much attention, wherein the contact engineering is of paramount importance leading to reliable and high device performance at this scale.⁶⁻⁸ The thermodynamics and kinetics properties of metallic silicide phases have been extensively studied in two-dimensional (2-D, thin film) and three-dimensional (3-D, bulk) structures for its significance in microelectronic applications.⁹⁻¹¹ NiSi, the most conductive silicide, have served as nanocontacts in integrated circuits due to its low resistivity, high current densities, clean interface with Si, shallow trench and compatibility to self alignment silicide process (salicide).¹² However, during the annealing to fabricate NiSi contacts, other high resistive Ni silicides including Ni₃Si, Ni₃₁Si₁₂,

θ -Ni₂Si, δ -Ni₂Si, Ni₃Si₂ and NiSi₂ could also form in the solid state reaction and degrade the performance.¹² Therefore, to manufacture repeatable, high quality and high yields of NiSi nanocontacts, it is very important to understand the fundamental phase transformation mechanism and to control the NiSi formation.

In thin-film and bulk structures, the binary element silicide phase formation sequences and the first formed silicide phases are predicted by several models. In 1976, Walser and Bené proposed a thermodynamic model to predict the first phases of silicide systems.¹³ They supposed the first phase is the one with largest free energy drop in the phase transformation. In their words, “The first compound nucleated in planar binary reaction couples is the most stable congruently melting compound adjacent to the lowest-temperature eutectic on the bulk equilibrium phase diagram.” This model successfully explains the first phase formation in 67 binary silicide systems (of which are 84 in total.) However, it does not consider the real atomic concentration of metal and Si at the growth interface which is not always equal to the final composition ratio in silicides. Therefore, there is an extra diffusion process required for the limited element to diffuse to the interface which may suppress the thermodynamic favorable phase to nucleate. Pretorius et al. thus introduced the concept of effective heat of formation model to modify Walser and Bené’s model.¹⁴⁻¹⁷ In Pretorius’s model, formation heat (enthalpy, ΔH^0) was used as estimation to the free energy (ΔG) which is reasonable in

solid state reaction due to little entropy changes. The definition of the effective heat is as follow:

$$\Delta H_{\text{eff}} = \Delta H^0 \times \frac{\text{effective concentration of limiting element}}{\text{composition concentration of limiting element}}$$

Here, effective concentration of limiting element is its actual atomic concentration at the growth interface. Pretorius used the concentration at the minimum liquidus in phase diagram to approach the real concentration at the metal/Si interface. And, to further consider the difficulty of phases with high nucleation barrier to appear, the non-congruent phases are ruled out from the first phase candidate list. Pretorius's model successfully predicted more of the first phase formation in silicide systems than Walser and Bené's model. However, as it comes to Ni-Si system, the predicted first phase NiSi (-39.4 kJ/mole) is conflict with the experimentally observed first phase: δ -Ni₂Si (-37.6 kJ/mole). Although the small difference in effective formation heat between these two phases could fall in the estimation error range, the effective heat of formation model still does not consider the kinetic obstacles and cannot explain the disappearance of thermodynamic favorable phases. A kinetic model is thus required to explain the phase formation.

Gosele et al. and d'Heurle et al. explained the first formed phase from the kinetics theories.^{18,19} The kinetic model assumes all phases could simultaneously grow at the initial stage as individual domains next to each other. The first formed phase is the one with the fastest growth rate (i.e. fastest supply of diffusive atoms, Ni in Ni-Si case) which will

consume the slower growth phases. For Ni-Si system, δ -Ni₂Si forms as the first phase due to its lower kinetic barrier and higher diffusivity for Ni to diffuse in δ -Ni₂Si which provides faster Ni supply to δ -Ni₂Si growth fronts. After δ -Ni₂Si grows out, the appearance of the second phase will have to wait until δ -Ni₂Si reaches a critical thickness about 2 μ m, above which the second phase could form and grows with δ -Ni₂Si simultaneously. The kinetic model successfully predicts the first phases in many 2-D silicide systems including Ni-Si and explains the following phase transformation.

In thin film structure, the reported experiment results exhibit a famous formation sequence of Ni silicide: δ -Ni₂Si normally forms as the first phase at 200-350 °C and then reacts with underneath Si to form NiSi at 350-750 °C. Above 750-1000 °C, NiSi will transfer into a high temperature phase NiSi₂ which is very stable and will not reversely transfer to NiSi and Si even when it is cooled again.^{20,21} However, the Ni silicide phase formation sequence and the first formed phase are found altered in 1-D nanostructures. θ -Ni₂Si, NiSi and NiSi₂ (instead of δ -Ni₂Si) have been reported to form as the first phase in 1-D structures from many groups.²²⁻²⁵ Of most of these studies, NiSi₂, known as a nucleation controlled phase in 2-D structures and usually appears at above 750 °C, takes over the conventional first phase δ -Ni₂Si and becomes the dominating first phase at 300-800 °C. Lu et al., found NiSi forms as the first phase in a point contact structure.²⁶ Dellas et al. reported the NW orientation dependant first phase formation at 350-700 °C with θ -Ni₂Si, NiSi and NiSi₂ observed as the

first phases under different conditions.²⁷ The phase formation sequence alternation may be attributed to the unique kinetics behaviours in 1-D structures.

Very interestingly, the nucleation and diffusion mechanisms in 1-D structures have been found to deviate from that of bulk and of thin film system.^{28,29} Chou et al. found Ni and Co silicides nucleate from a homogeneous site in a NW instead of a heterogeneous site which means the nucleation activation barrier changes a lot in 1-D structures.²⁸ Holmberg et al. reported the diffusion path of Au in Ge NW has also changed and causes a 5 order slower diffusion process than that in bulk Ge.²⁹ Since the first phase selection and the following formation sequence is determined from a kinetic competition, different nucleation barrier height and diffusion mechanism in 1-D structures could lead to the altered phase transformation results. For now, there is no consistent explanation to quantitatively understand why the phase formation sequence and the first phase changes in 1-D structures. Therefore, systematic investigation and understanding of are prescribed to achieve predictable and reliable contacts for high performance nanodevices.

In this study, the phase transformation sequence of Ni-Si binary system in a Si NW template is extensively and systematically interrogated over a wide range of temperatures. Unique size dependant first phase selection is found for the first time. The coexistence of multiple phases at initial stages is clearly captured to confirm that the non-first phases are not limited by nucleation. Taking the benefits of NW's geometry, we do not need to damage or

change the structure of NW to monitor this initial stage which allows us to observe the real kinetic behaviors with an in-situ TEM. From our results, selection of first phases is governed by a kinetic growth competition regarding the interfacial reaction rate (including nucleation) and Ni diffusion rate in silicides. With kinetic parameters extracted from in-situ TEM observations, the competition model is applied to predict the first phase and yields a reasonable critical Si NW diameter. Beyond this critical diameter, the first phase can be switched from diffusion rate limited phase (θ -Ni₂Si) to interfacial limited phase (NiSi₂) at 800 °C.

With the understanding of the kinetic competition, we further apply Si NW template modulations to selectively enhance or hinder the growth rates of targeted Ni silicides in a Si NW, and demonstrate that Ni₃₁Si₁₂, δ -Ni₂Si, θ -Ni₂Si, NiSi and NiSi₂ can emerge as the first contacting phase at the silicide/Si interface through these modulations.³⁰ Firstly, the growth rates of silicides are selectively tuned through template structure modifications. It is demonstrated that the growth rate of diffusion limited phases can be enhanced in a porous Si NW due to a short diffusion path, which suppresses the formation of interface limited NiSi₂. In addition, we show that a confining thick shell can be applied around the Si NW to hinder the growth of the silicides with large volume expansion during silicidation, including Ni₃₁Si₁₂, δ -Ni₂Si and θ -Ni₂Si. Secondly, a platinum (Pt) interlayer between the Ni source and the Si NW is shown to effectively suppress the formation of the phases with low Pt solubility,

including the dominating NiSi_2 . Together, with the combined applications of thick shells and Pt interlayer, the lowest resistive NiSi phase can form as the first phase in a solid NW with a Pt interlayer to suppress NiSi_2 and a thick shell to hinder $\text{Ni}_{31}\text{Si}_{12}$, $\delta\text{-Ni}_2\text{Si}$ and $\theta\text{-Ni}_2\text{Si}$ simultaneously. The resistivity of Ni(Pt)Si NW has been measured from two and four terminal structures and is found compatible to pure NiSi. In addition, formations of Co and Pd silicides from Si NW have also been studied to examine the competition model. With a thick shell to confine the volume expansion, NW breaking at $\text{Pd}_2\text{Si}/\text{Si}$ interface due to Poisson's effect is suppressed.

Chapter 2 Si NW template synthesis and sample preparation

2.1 Growth of Si NW with diameter control

Si NWs are grown through vapor-liquid-solid method with Au nanocatalysts.³¹ 1-10 nm sputtered Au film is deposited and then annealed at 550 °C to form Au nanoparticles. Size of the Au nanoparticles which is important to control the diameter of Si NWs can be tuned through initial Au film thickness and annealing time. For small NWs, commercial mono-dispersed Au colloid particles (British Biocell International Ltd) are used as the catalysts. SiH₄ is decomposed to serve as the Si source and carried by forming gas (5 % H₂ and 95 % N₂) at 450-550 °C for 10-40 mins to grow Si NW. After the growth, sample is cooled down in the furnace. The total pressure is 30 torr with the silane partial pressure of about 2 torr. As shown in Fig. 1, Si NWs are typically single crystal with diameter of 7-230 nm and length of 15-20 μm with [111] orientation. The scanning electron microscope (SEM) image in Fig. 1a shows the diameter and length of Si NWs are uniform.

2.2 Fabrication of porous Si NW

Porous Si [111] NWs are prepared with a wet-etching process from Si <111> wafers.³² The Si wafers are first cleaned with water, acetone, and isopropanol for 5 mins each in a sonicator. Photoresist AZ5214 is used to protect the back side (unpolished side) of Si wafer in the etching. Then the whole wafer is immersed into buffered oxide etchant (BOE, commercial

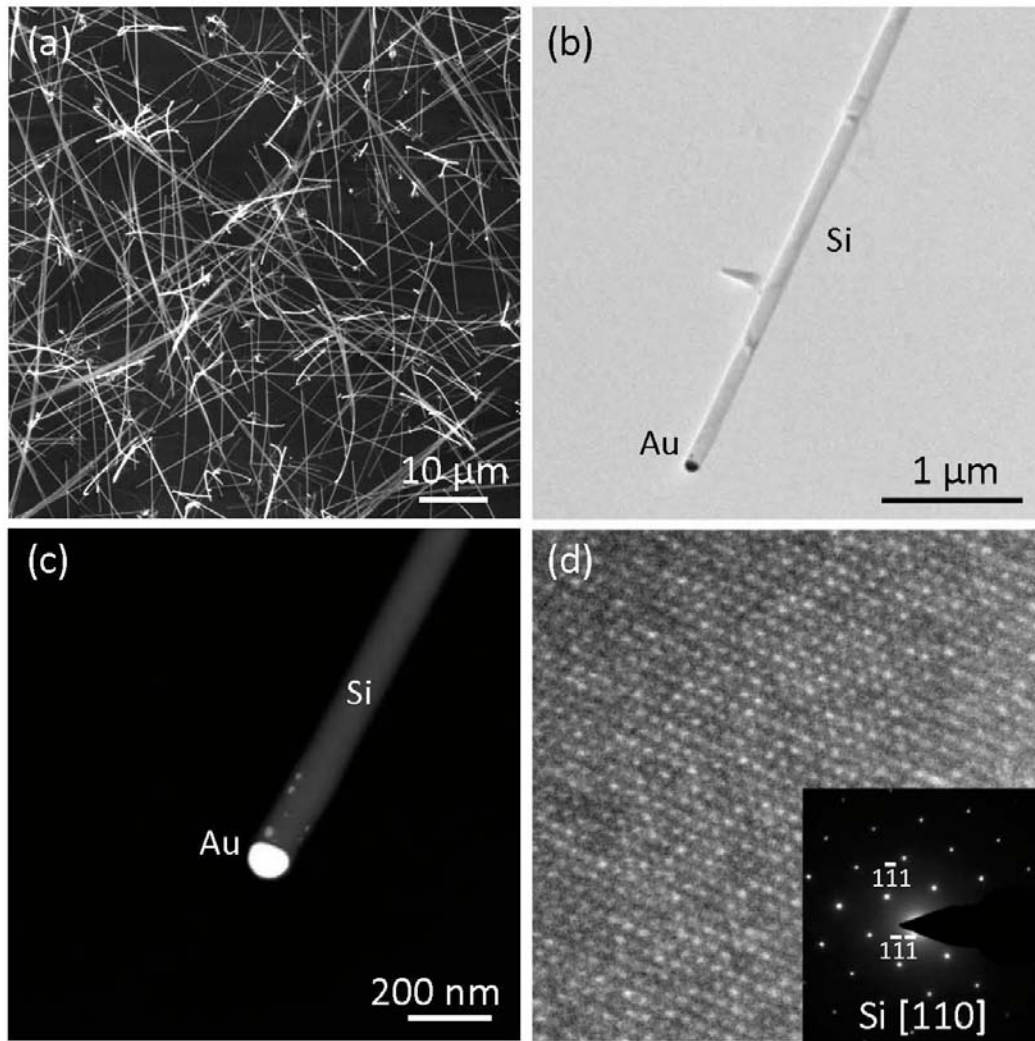


Fig. 1 Characterization of Si NW. (a) SEM image of Si NWs. (b) TEM image of a Si NW with an Au catalyst on the tip. (c-d) high angle annular dark field (HAADF) and high resolution images of Si NW in (b). Inset in (d) the selective area electron diffraction (SAED) pattern of the Si NW

HF buffered solution) for 10 mins to remove the surface oxide and result in hydrogen (H) terminated surface. A very thin silver (Ag) film is deposited onto the H-terminated surface by electroless deposition. After a short annealing, Ag film transforms into nanoparticles which serve as catalysts in the following etching. With the catalysts, Si wafers is put into an etching solution of 4.8 M HF and 0.1-0.6 M H₂O₂ for 60 mins. The local area with Ag nanoparticles

will be etched to form an array of Si NW. Some small Ag particles will be left on the side wall of Si NWs during the etching and further etch the NW in radial direction to form a porous structure. After the etching, porous Si NWs are soaked into concentrated nitric acid longer than 1 hour to remove Ag particles. The wafer with porous Si NW is then washed by water and dried by nitrogen flow for couple times.

2.3 Preparation of TEM membranes

To observe the growth of silicide NW in a TEM, we need to fabricate the Si nitride TEM membrane. As shown in Fig. 2, a 40 nm thick low stressed Si nitride is deposited on both side of $\langle 100 \rangle$ Si wafers in a low pressure chemical vapor deposition (LPCVD) chamber at 550-650 °C for 10 mins. NH_3 and SiCl_2H_2 are used as precursors to form Si nitride. After the nitride deposition, back side of the Si wafers is then patterned through photolithography. $100 \times 100 \mu\text{m}$, $300 \times 300 \mu\text{m}$ or $500 \times 500 \mu\text{m}$ window areas are exposed (without photoresist covered) and etched by reactive ion etcher (RIE). The remaining Si nitride at the back side then serves as a hard mask when the wafer is etched by 35 % KOH solution at 80 °C for hours. Due to the anisotropy etching of Si facets in KOH, the slow etched {111} facets will remain and form a wedge structure at the sides of the windows.³³ The whole structure is then washed by water. With a 40 nm thick low stress Si nitride film suspended on top of the window, the membrane can serve as the mechanical supporting substrate for our TEM observations.

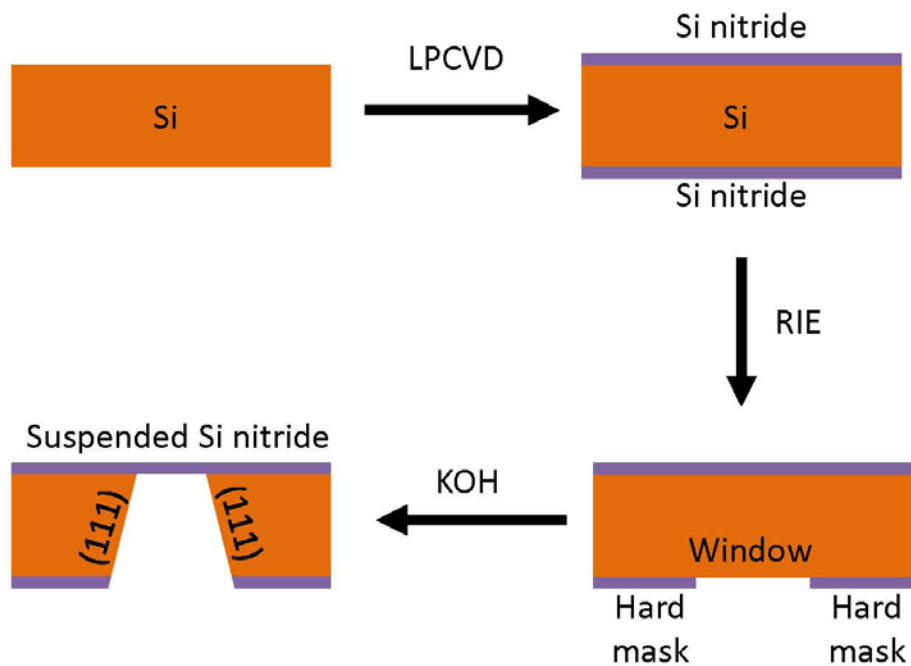


Fig. 2 Process flow of Si nitride TEM membrane fabrication.

2.4 Preparation of metal/Si NW diffusion couples

Free standing Si NWs are sonicated into ethanol solution and dispersed on top of Si nitride membranes or substrates. The whole sample is then baked for 15 mins at 170 °C on a hot plate to get rid of the water molecule. Two layered photoresist are spin coated on top of the samples which allows the metal film to be easily lifted-off later. MMA (MicroChem Corp. 8.5 MMA EL9) is first coated at 4000 rpm for 1 min and then baked for 2 min at 170 °C. After that, PMMA (MicroChem Corp. 495 PMMA A4) is coated at 5000 rpm for 1 min and also baked for another 2 min. E-beam lithography is used to expose the designed area to allow NWs been partially covered by metal pads as shown in Fig. 3. After sample been developed in a mixed isopropanol solution (methyl isobutyl ketone: isopropanol = 3:1), 70

nm thick, 400 nm to 2 μm width metal pads are deposited by an e-beam evaporator in a vacuum order of 10^{-8} Torr. To provide good contacts between metal and Si, BOE is used to remove native oxides before the depositions of metal films. Samples are loaded into deposition chamber right after the BOE treatment and then annealed at 300-800 $^{\circ}\text{C}$ for different durations in in-situ TEM. (JEOL CX100 TEM and JEOL JEM-2000V equipped with Gatan heating holder). High resolution image and characterizations of silicides NW are performed with FEI Titan at 300 KV. Cross section TEM sample are prepared within FEI Nova 600 focus ion beam (FIB) and SEM images are taken in FEI Nova 230 (field emission). The electrical properties are measured in a Lakeshore TTP4 probe station.

Chapter 3 Kinetic competition model and size dependant phase formation sequence of

Ni silicide

3.1 Si NW size dependant first phase formation of Ni silicides

During the annealing process, Ni diffuses into Si NW and forms Ni silicides (Fig. 3a). Multiple silicide phases are identified growing from underneath of Ni pads into the Si NW template. Cubic NiSi₂ (space group 225, Fm $\bar{3}$ m, a=5.416 Å), orthogonal NiSi (space group 62, Pnma, a=5.180 Å, b=3.340 Å and c=5.620 Å), hexagonal θ -Ni₂Si (space group 194, P6₃/mmc a=3.805 Å and c=4.890 Å), orthogonal δ -Ni₂Si (space group 62, Pnma, a=4.990 Å, b=3.720 Å and c=7.030 Å) and hexagonal Ni₃₁Si₁₂ (space group 150, P321, a=6.671 Å and c=12.288 Å) are confirmed from high resolution images and fast Fourier transform (FFT)/SAED patterns at two or more different zone axis (Fig. 4). The atomic structures of NiSi₂, δ -Ni₂Si and Ni₃₁Si₁₂ are close to previously reported silicides NWs grown with chemical vapor deposition.³⁴⁻³⁶ According to phase diagram, hexagonal θ -Ni₂Si which is thermodynamically stable only above 816 °C with composition range from Ni:Si=1.564 to 1.941 is different from orthogonal δ -Ni₂Si (line product, stable down to room temperature.)³⁷ Since the growth time of silicides in Si NW template is short and no higher temperature post-annealing is applied, metastable θ -Ni₂Si can remain as the first phase which was consistent with the observation in [112] Si NW template.²⁷

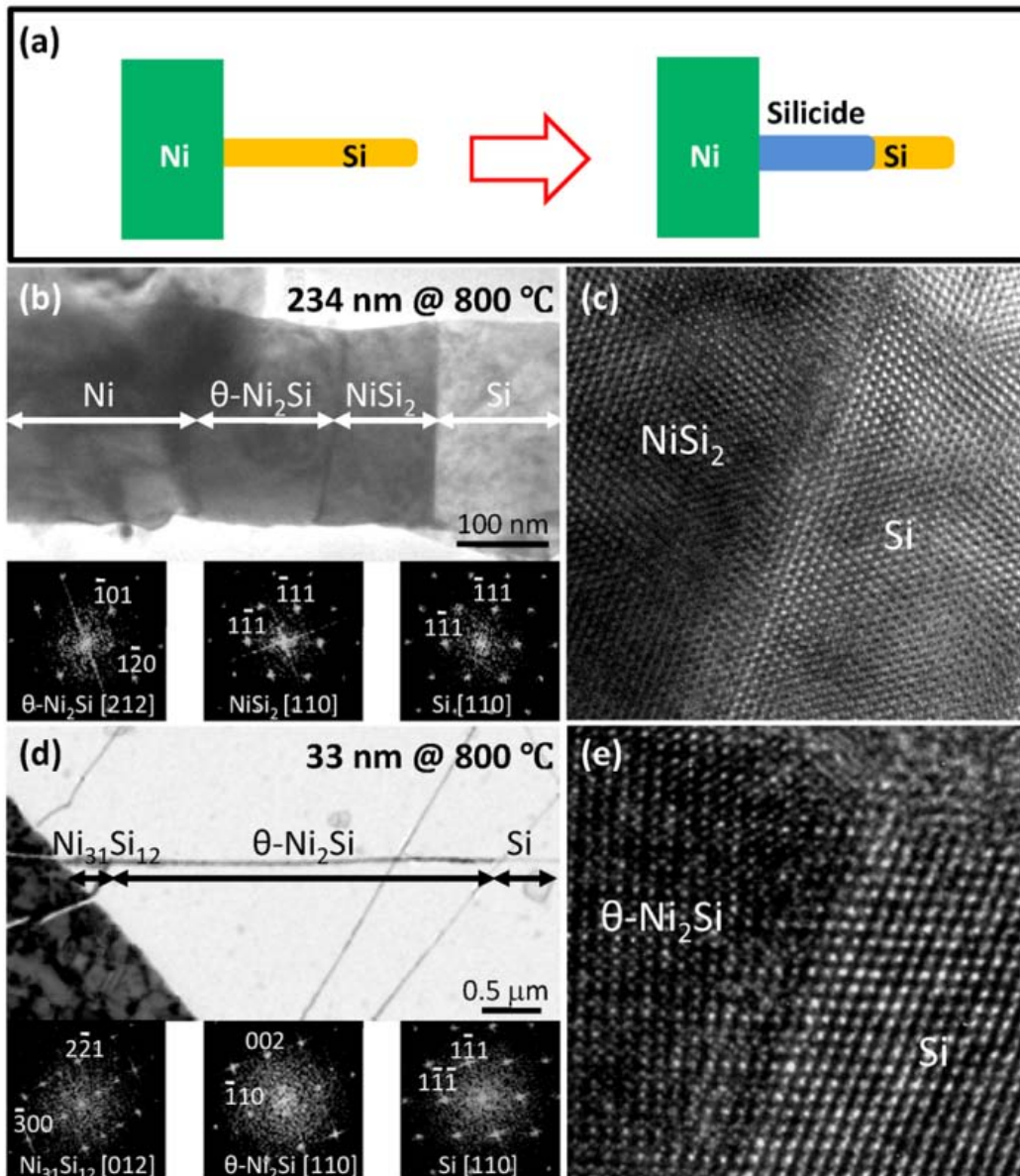


Fig. 3 Size dependant first phase selection at 800 °C. (a) Schematics of typical diffusion structure. (b-c) Silicides formed in a 234 nm Si NW grown at 800 °C for 30 secs. (b) Image and FFT patterns of θ -Ni₂Si, NiSi₂ and Si. (c) Epitaxial interface between NiSi₂ and Si. (d-e) Silicides formed in a 33 nm Si NW grown at 800 °C for 30 secs. (d) Image and FFT patterns of Ni₃₁Si₁₂, θ -Ni₂Si and Si. (e) Epitaxial interface between θ -Ni₂Si and Si.

Through identification of silicide phases with TEM, at 800 °C, a significant size dependant first phase selection is observed, i.e.: while NiSi₂ remains as the first phase in a Si NW larger than 150 nm (Fig. 3b-c), θ -Ni₂Si takes over NiSi₂ and becomes the first phase in a Si NW

with diameter smaller than 70 nm (Fig. 3d-e). However, it is observed that at lower temperatures, 300-650 °C, NiSi₂ emerges as the first phase in all examined Si NW templates with diameter of 27-213 nm (Fig. 5 and Fig. 6). Epitaxial relations NiSi₂[110]//Si[110], NiSi₂($\bar{1}11$)//Si($\bar{1}11$) are found between NiSi₂ and Si (Fig. 5b,d,f,h and Fig. 6b,d). With systematic studies, we rule out Si/silicide interfacial strained energies (at epitaxial interfaces) and effective heat of formation difference among phases as key contributors (see chap. 3.2-3.3), but confirm that the kinetic growth competition determines the first phase formation in Si NW templates.

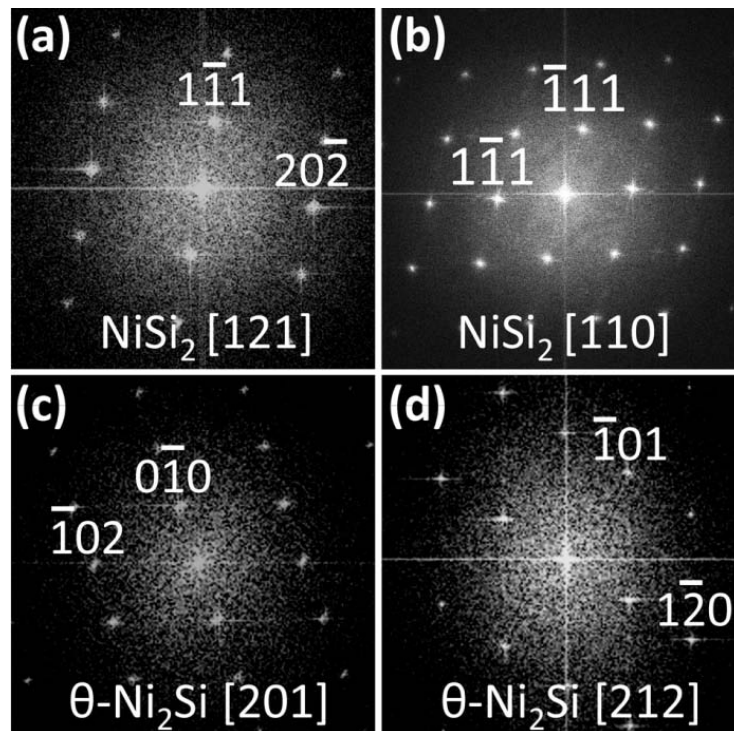


Fig. 4 FFT patterns of NiSi₂ and θ -Ni₂Si. (a-b) FFT of NiSi₂ corresponding to zone axis [121] and [110] at the same spot. NiSi₂ is the only Ni silicide phase which fits both patterns. (c-d) FFT of θ -Ni₂Si corresponding to zone axis [201] and [212] at the same spot. θ -Ni₂Si is the only Ni silicide phase which fits both patterns.

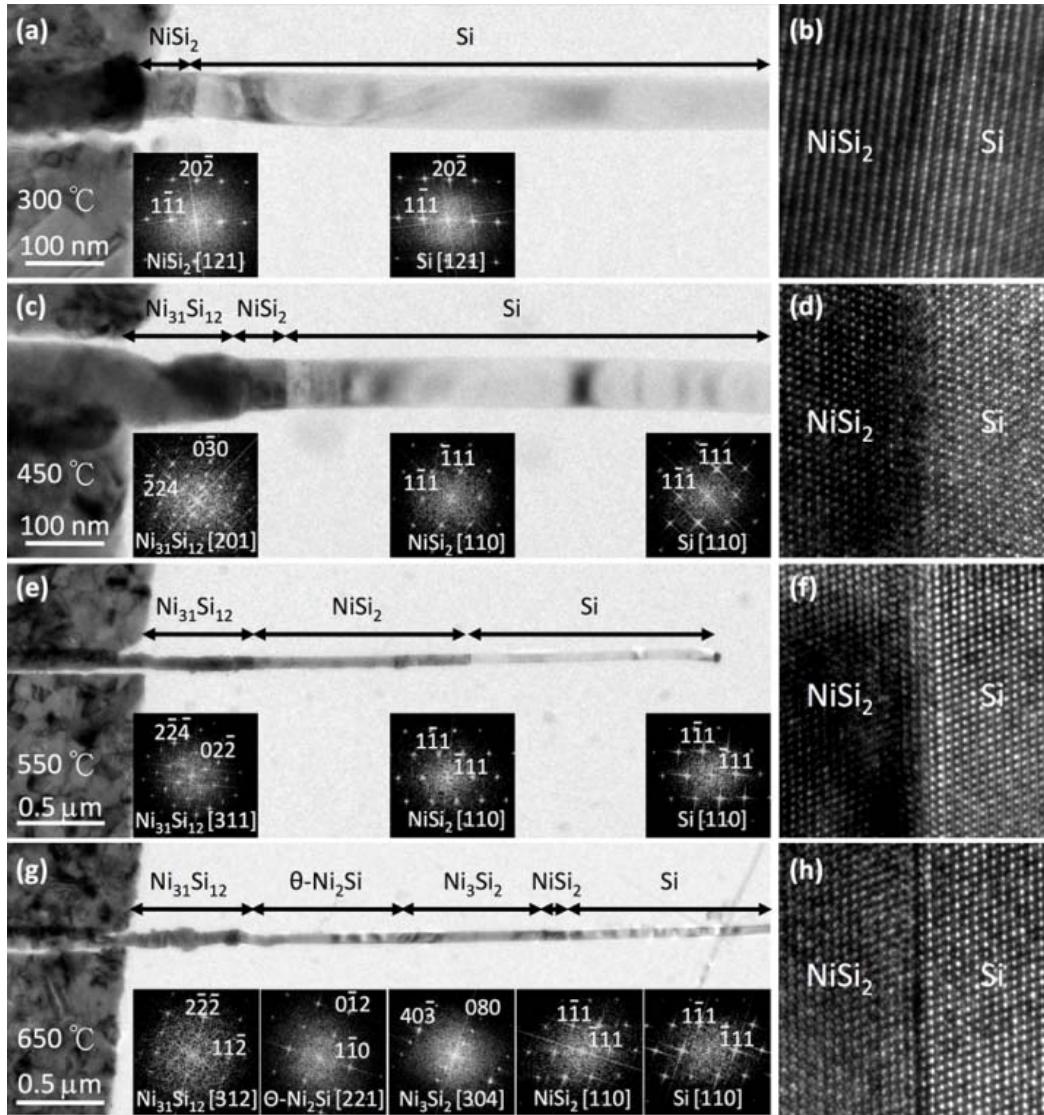


Fig. 5 TEM images of silicides formation sequence and silicide/Si interface in ~ 50 nm Si NW templates annealed at various temperature. NiSi_2 emerges as the first phase in all cases from 300 to 650 °C. (a-b) 300 °C for 30 mins, (c-d) 450 °C for 30 s, (e-f) 550 °C for 30 s and (g-h) 650 °C for 30s. There is no silicide grow out from Ni pad below 300 °C within one hour. All NiSi_2 /Si interface keeps epitaxial relation of NiSi_2 [110]//Si[110], $\text{NiSi}_2(\bar{1}11)$ //Si($\bar{1}11$).

3.2 Failure of interfacial strain energy model in explaining silicide phase formation

sequence in 1-D structures

Previous studies had suggested that the interfacial strained energy between silicide/Si may play an important role in first phase formation in 1-D structures.²⁷ However, in our study, two

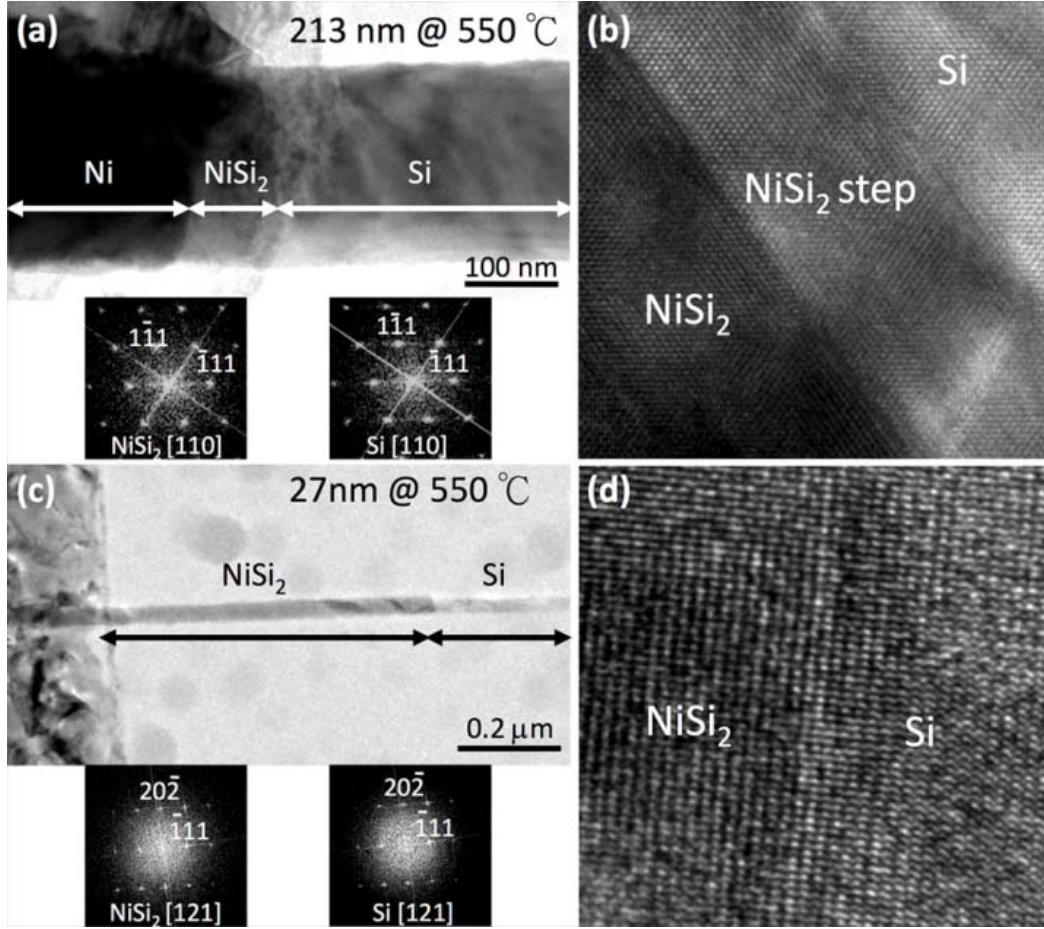


Fig. 6 TEM images of first phase observation at 550 °C in 27 to 213 nm Si NW template. NiSi₂ emerges as the first phase in both cases. (a-b) Silicides formed in 213 nm Si NW grown at 550 °C for 4 mins. (a) Image and FFT patterns of NiSi₂ and Si. (b) Epitaxial interface between NiSi₂ and Si. (c-d) Ni silicides formed in 27 nm Si NW grown at 550 °C for 30 secs. (c) Image and FFT patterns of NiSi₂ and Si. (d) Epitaxial interface between NiSi₂ and Si. Both NiSi₂/Si interface keeps epitaxial relation of NiSi₂ [110]//Si[110], NiSi₂($\bar{1}\bar{1}\bar{1}$)//Si($\bar{1}\bar{1}\bar{1}$).

epitaxial relations between θ -Ni₂Si and Si were simultaneously observed and identified as

below:

$$\theta\text{-Ni}_2\text{Si}[110]//\text{Si}[110], \theta\text{-Ni}_2\text{Si}(002)//\text{Si}(1\bar{1}\bar{1}) \quad [1]$$

with misfit of $f = \frac{d_{\theta\text{-Ni}_2\text{Si}(\bar{1}\bar{2}0)} - d_{\text{Si}(2\bar{2}0)}}{d_{\text{Si}(2\bar{2}0)}} = \frac{1.902 - 1.920}{1.920} = -0.94\%$

and $\theta\text{-Ni}_2\text{Si}[110]//\text{Si}[110]$, $\theta\text{-Ni}_2\text{Si}(2\bar{2}\bar{1})//\text{Si}(1\bar{1}1)$ [2]

$$f = \frac{d_{\theta\text{-Ni}_2\text{Si}(0\bar{1}2)} - d_{\text{Si}(2\bar{2}0)}}{d_{\text{Si}(2\bar{2}0)}} = \frac{1.964 - 1.920}{1.920} = 2.29\%$$

$$f = \frac{d_{\theta\text{-Ni}_2\text{Si}(110)} - d_{\text{Si}(2\bar{0}2)}}{d_{\text{Si}(2\bar{0}2)}} = \frac{1.902 - 1.920}{1.920} = -0.94\%$$

Here, f is mismatch between atomic spacing d_x of Si and silicides ($f = \frac{d_{\text{silicide}} - d_{\text{Si}}}{d_{\text{Si}}}$).

Relation [1] is consistent with observations in previous reports while [2] was never found in thin film or bulk system.³⁸ Misfits between $\theta\text{-Ni}_2\text{Si}$ and Si are -0.94% and -0.94% to Si along two hexagonal directions in relation [1] and 2.29% and -0.94% in [2]. If interfacial strained energy dominated the first phase selection, it should always adopt the smallest mismatch in epitaxial relation: in our case relation [1].

In addition, among all silicides, NiSi_2 with CaF_2 structure has the smallest lattice mismatch (-0.21%) to Si in epitaxial relation [3]:

$\text{NiSi}_2[110]//\text{Si}[110]$, $\text{NiSi}_2(\bar{1}11)//\text{Si}(\bar{1}11)$ [3]

$$f = \frac{d_{\text{NiSi}_2\{220\}} - d_{\text{Si}\{220\}}}{d_{\text{Si}\{220\}}} = \frac{1.916 - 1.920}{1.920} = -0.21\%$$

However NiSi_2 is not always the most competitive phase in the Si NWs we studied. These observations infer that the interfacial strained energy between silicides and silicon is not a key contributor to the first phase formation of silicides in Si NW. In addition, Dellas et al. have found $\theta\text{-Ni}_2\text{Si}$ with 5 and 0.1% mismatch formed as first phase in [112] Si NW from 350-700 °C,²⁷ which is larger than that of the NiSi_2/Si (0.21-0.52%)^{39,40} under the same

conditions, the non-dominant role of interfacial strained energy in 1-D silicides growth competition is again confirmed.

$$f = \frac{d_{NiSi_2\{220\}} - d_{Si\{220\}}}{d_{Si\{220\}}} = \frac{1.9160 - 1.9200}{1.9200} = -0.21\%$$

$$f = \frac{d_{NiSi_2\{111\}} - d_{Si\{111\}}}{d_{Si\{111\}}} = \frac{3.1190 - 3.1354}{3.1354} = -0.52\%$$

3.3 Failure of effective formation heat model in explaining silicide phase formation sequence in 1-D structures

Effective heat of formation model is used to predict the first phase selection from thermodynamics in thin film and bulk system. However, our observations of NiSi₂ predominance at 300-650 °C (Fig. 5 and Fig. 6), the size dependant first phase transition (Fig. 3) and the coexistence of multiple phases at initial stage (Fig. 7 and Fig. 8) challenge the application of effective heat of formation model to 1-D nanostructures. (1) According to the model, “the congruent phase with the highest negative effective heat of formation at the concentration of the lowest eutectic temperature in phase diagram is the first phase to form”.¹⁵ In Ni-Si couple, the lowest eutectic point on phase diagram is at composition of Ni_{0.535}Si_{0.465} which gives value of effective heat of formation of δ-Ni₂Si (-37.64 kJ/mol), NiSi (-39.43 kJ/mol) and NiSi₂ (-20.44 kJ/mol). It shows δ-Ni₂Si and NiSi have larger driving force (formation energy drop) than NiSi₂, especially, NiSi₂ as a non-congruent phase is not even in the candidate pool due to difficulty of nucleation and the required composition

fluctuation in transformation. The consistent appearance of NiSi_2 hence cannot be explained by the effective heat of formation.

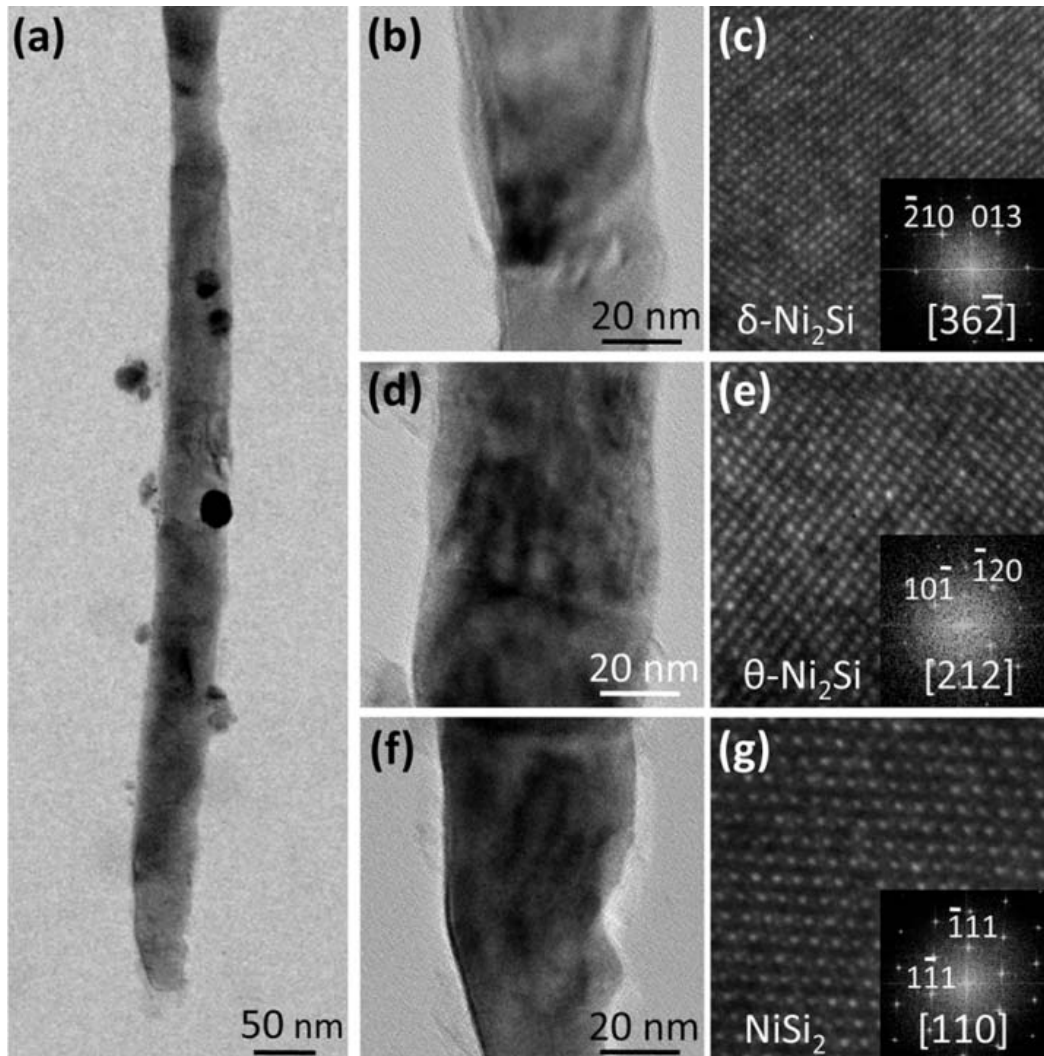


Fig. 7 Coexistence of silicides at initial growth stage (without native oxide) (a) Low magnification TEM image of silicides formation after annealing 5 secs at 800 °C. Silicide phases formed as small domains contacting each other without clear boundaries or specific sequence. (b-c). Zoom in TEM, high resolution images and corresponding FFT pattern of $\delta\text{-Ni}_2\text{Si}$. (d-e) Zoom in TEM, high resolution images and corresponding FFT pattern of $\theta\text{-Ni}_2\text{Si}$. (h-i) Zoom in TEM, high resolution images and corresponding FFT pattern of NiSi_2 .

(2) The heat of formation of the silicide phases formation are not Si NW size dependant as long as the Ni and Si sources are still abundant. Size dependent phase selection cannot be

explored within the conventional effective heat of formation model, either. We hence suggest effective heat of formation is not the determining factor for phase formation sequence of silicides in 1-D Si NWs.

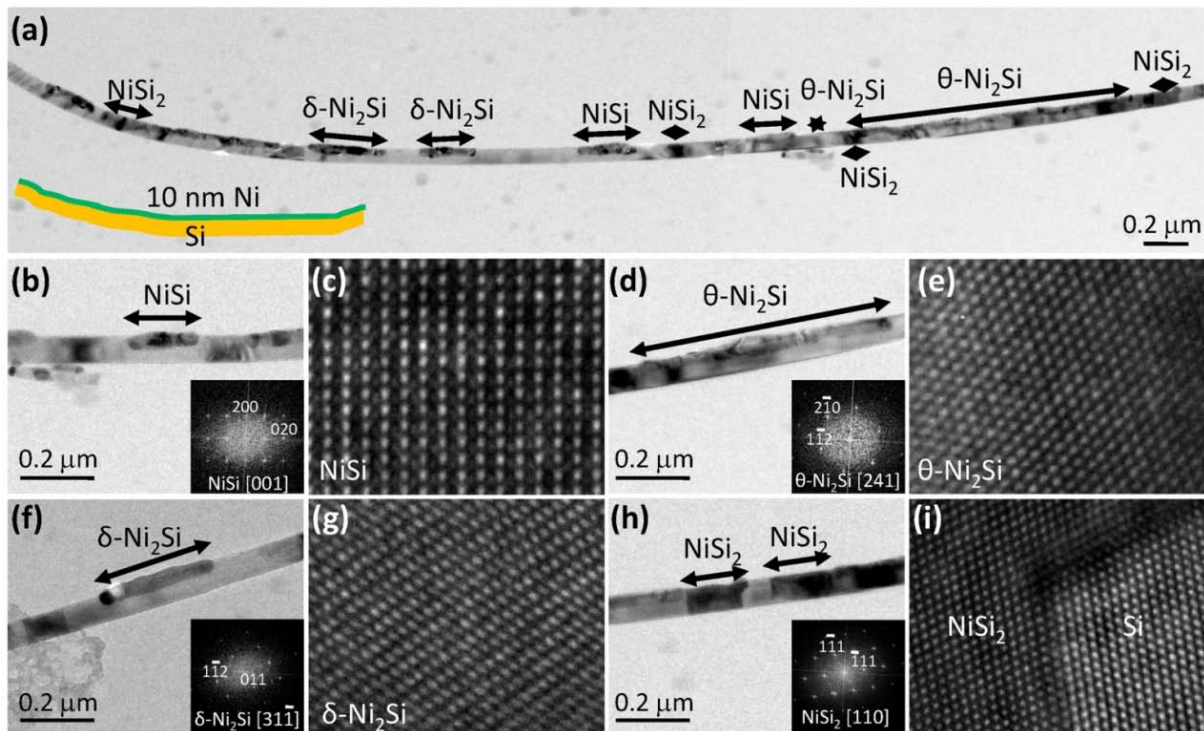


Fig. 8 Coexistence of multiple phases at the initial growth stage (with native oxide between Ni/Si NW). (a) Low magnification TEM image of silicides grown in Si NW template. Si NW is covered by 10 nm Ni at upper side and annealed for 5 secs at 800 °C. (inset) Schematic of 10 nm Ni on Si NW. (b-c) Zoom in TEM, high resolution images and corresponding FFT pattern of NiSi. (d-e) Zoom in TEM, high resolution images and corresponding FFT pattern of θ -Ni₂Si. (f-g) Zoom in TEM, high resolution images and corresponding FFT pattern of δ -Ni₂Si. (h-i) Zoom in TEM, high resolution images and corresponding FFT pattern of NiSi₂.

3.4 Kinetic competition model and multiple phases coexistence in the initial stage

In the kinetic competition model, several phases nucleate at the initial stage and the phase with fastest growth rate wins out and grows as the first phase. However, it is very hard to

directly capture multiple phases coexistence at the initial stage and track individual grain to do kinetic studies in a 2-D structure. Taking the benefits of the 1-D geometry, we can easily operate in-situ TEM and high resolution TEM (HRTEM) without cutting/thinning the NWs to study the initial stage. In order to confirm the existence of multiple phases present at the initial stage of nucleation and growth under Ni pads, and for convenience of observation, we adopt an analogous structure as shown in Fig. 7a. A Si NW is fully covered on one side with 10 nm evaporated Ni and subject to annealing at 800 °C for 5 secs. With limited Ni supply and short annealing time, the formed silicides are captured at the initial stage and the short annealing (5 secs) also prevents the existing silicides from transforming into other phases with remaining Ni or Si sources. HRTEM images of each phase and corresponding FFT patterns are used to identify the observed silicides (Fig. 7 and Fig. 8). As shown in Fig. 7, θ -Ni₂Si, NiSi₂ and δ -Ni₂Si are coexisting as small domains contacting each other without clear boundaries or specific sequence. It indicates that nucleation does not limit the appearance of non-first phase silicides. To further clarify if these phases nucleate independently or are transformed from previous generated silicide with remaining Ni or Si source, a similar structure but with native oxide (<1 nm thick) between Ni and Si NW template (Fig. 8) is examined. In this structure, Ni atoms penetrate through thin shell or local weak points to form separate silicide domains that do not contact with each other. Again, θ -Ni₂Si, NiSi₂, δ -Ni₂Si and NiSi are found coexisting between Ni and Si separately. Diffusion

rate limited phases, θ -Ni₂Si, δ -Ni₂Si and NiSi, form small islands close to the Ni source and interfacial-limited NiSi₂ forms a single crystalline section exhibiting {111} facets and has epitaxial relation of NiSi₂[110]//Si[110], NiSi₂($\bar{1}11$)//Si($\bar{1}11$) with Si. NiSi was only observed in the latter case but did not appear in Fig. 7, where the native oxide is removed and all domains make contact with each other. It might be attributed to the slower growth rate of NiSi which results in its consumption by the faster growing phases in contact. Coexistence of Ni silicide phases in Fig. 7 and Fig. 8a confirms independent nucleation of multiples phases from Ni/Si reaction couple at the initial stage. The observed first phases, NiSi₂ and θ -Ni₂Si, are selected through growth competitions among different phases in 1-D Si NW template.

3.5 Contact area between Ni and Si NW does not limit the Ni supply

Before we study the silicide growth rates, it is very important to analyze the real limiting steps of the silicide growth. NiSi₂ is limited by the interfacial reaction while other phases are limited by the Ni diffusion.²⁵ In our structure, Ni diffusion can be separated into three stages: Ni diffuses from Ni pad to the Ni/Si interface, Ni diffuse through the interface and Ni diffuse in Si or silicide NWs. Firstly, since our annealing time is short and there is always unreacted Ni pads left after the annealing, we can confirm the growth rate and the phase formation are not limited by the amount of Ni atoms in pads. It is also not limited by the Ni diffusion from pad to the metal/NW interface due to the short diffusion distance. Secondly, as Ni diffuses through the interface between Ni and Si NW, contact area might be limiting to the Ni supply

rates. In order to clarify that the formation of NiSi₂ is not the result of limited Ni supply across the interface which is also NW size dependant, we study the phase formation with various ratios of Ni contact/supply area (A) to Si NW volume per unit length (V).

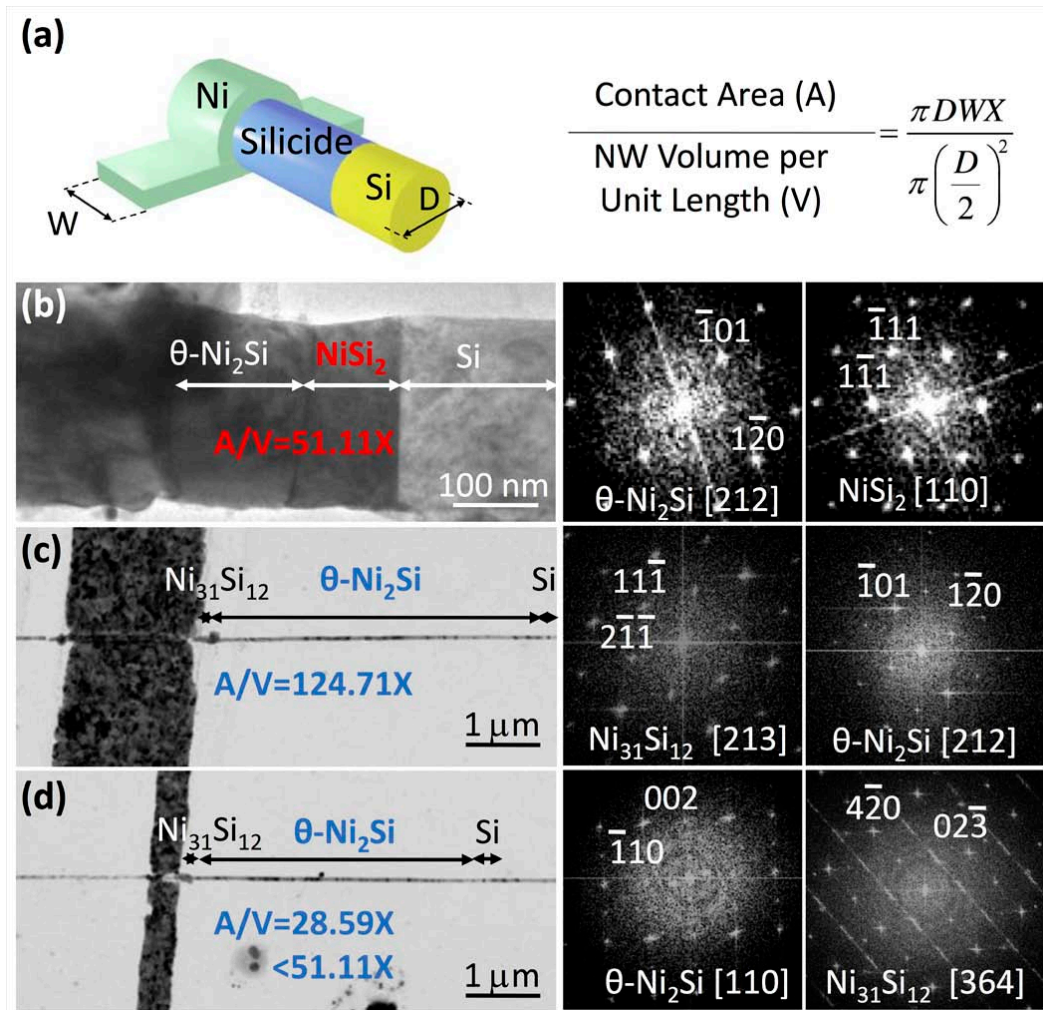


Fig. 9 TEM images and corresponding FFT patterns of silicide formations with different ratios of Ni contact/underneath Si NW volume per unit length (A/V). (a) Schematic and definition of A/V ratio. (b) NiSi₂ forms as the first phase in a 234 nm NW with A/V=51.11X. (c) θ -Ni₂Si forms as the first phase in a 68 nm NW with A/V=124.71X. (d) θ -Ni₂Si still forms as the first phase in a 68 nm NW with A/V=28.59X. It shows the phase formation is independent to the A/V ratios.

Here, we assume the omega-shaped Ni contact covers the same portion (X) of the cross-sectional circumference on all Si NWs (Fig. 9a). Therefore, the A/V ratio is defined as the following:

$$\frac{A}{V} = \frac{\pi DWX}{\pi \left(\frac{D}{2}\right)^2}$$

where D is the diameter of Si NW, W is the width of Ni pad. Through tuning the width of Ni pads, we can match the A/V ratios in NWs with different diameters. As shown in Fig. 9b-c, θ -Ni₂Si forms as the first phase in a small NW with A/V ratio of 124.71X while NiSi₂ forms in a big NW with A/V ratio of 51.11X. This means in a large NW, Ni supply flow across Ni/Si NW interface per unit volume of Si NW underneath the Ni pad in a large NW is smaller than that in a small NW. In order to clarify that the formation of NiSi₂ in a large Si NW is not the result of limited Ni supply source due to volume increase of Si NW, we change the width of the Ni pad to tune the A/V ratio. As shown in Fig. 9d, we found that θ -Ni₂Si still forms as the first phase in a 68 nm Si NW even with an A/V ratio of 28.59X, which is smaller than the large NW (51.11X) in Fig. 9b. This shows the supply of Ni flux per unit Si volume does not limit or significantly contribute to the phase competition here. That clearly indicates the growth rates of diffusion controlled phases are limited by the Ni diffusion through Si NW and silicide NWs.

3.6 Growth rate of Ni silicides and kinetic parameters extracted from in-situ TEM

The predominance of NiSi₂ as the first phase at lower temperatures and the appearance of θ -Ni₂Si and NiSi₂ at higher temperatures can be explained by the kinetic growth competition mechanism in 1-D nanostructures. Comparing to 2-D and 3-D structures, the small size of NWs eliminates the continuous grain boundary in silicides (axial direction) which is a fast path of Ni diffusion.⁴¹ Thus, in 1-D structures, the growth rate of the diffusion-limited phases such as δ -Ni₂Si (conventional first phase in thin film) decreases significantly, which renders the growth of interfacial-limited phase, i.e. NiSi₂, competitive. Among the diffusion-limited phases, θ -Ni₂Si gives the fastest Ni diffusion rate,⁴² which explains the observation that only θ -Ni₂Si phase appears as the competitive phase against NiSi₂ at high temperatures.

In-situ TEM studies are then employed to confirm growth mechanisms and to extract kinetic parameters. Within a single crystal lattice Si NW, in-situ TEM provides high temporal resolution observation of the silicide growth front, from which the accurate kinetic data such as the diffusivity, the reaction rate constant, and the activation barriers of the silicides can be readily extracted to quantitatively explain the observed size-dependent first phase selection at 800 °C. (Fig. 10) In addition, due to single crystal nature of Si NW and the elimination of grain boundaries in this template, the kinetic data will represent the intrinsic lattice properties, which may be compared to the bulk data to differentiate the contributions from various components, e.g. lattice diffusion vs. grain boundary diffusion.

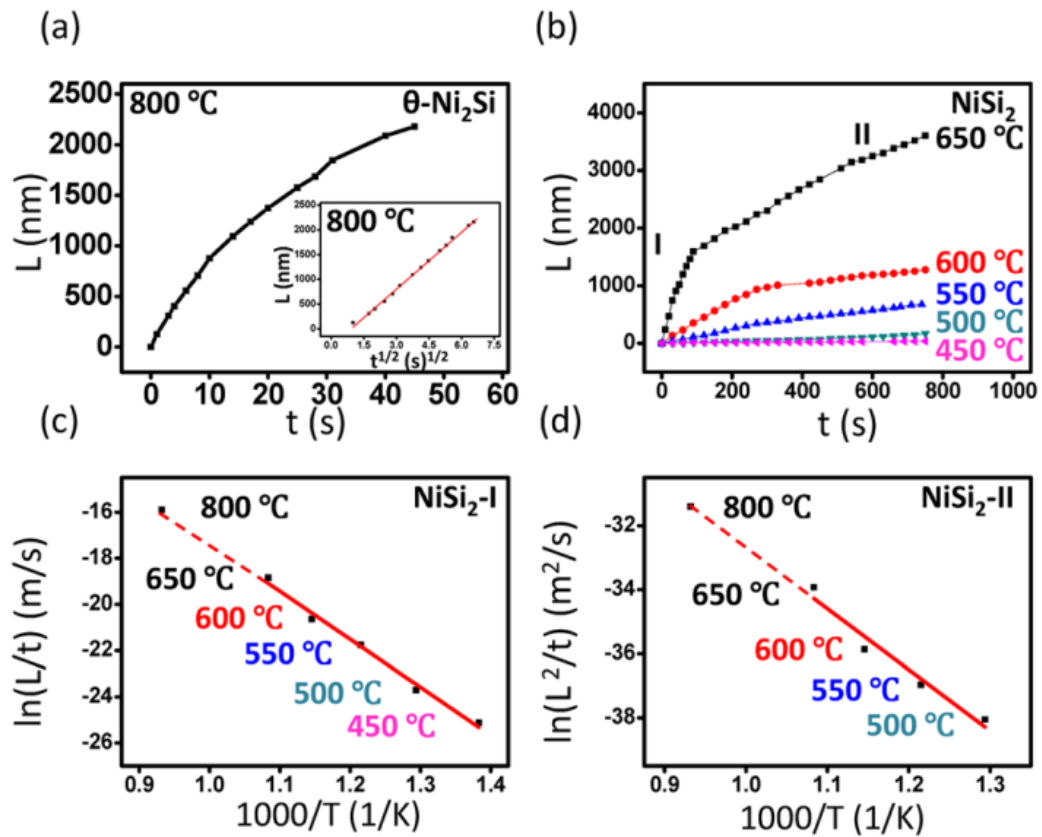


Fig. 10 Growth behaviors of θ -Ni₂Si and NiSi₂ in Si NW templates with diameter of \sim 70 nm from 450 to 800 °C observed with in-situ TEM. (a) Growth length vs. time of θ -Ni₂Si at 800 °C. (inset) Growth length vs. square root of time of θ -Ni₂Si at 800 °C to confirm nature of parabolic growth. (b) Growth length of NiSi₂ vs. time from 450 to 650 °C. Linear to parabolic transitions are observed at 341-1581 nm at 500-650 °C, respectively. (c) Arrhenius' plot of reaction rate of NiSi₂ front with activation barrier of 1.792 ± 0.101 eV/atom from the linear growth region (NiSi₂-I). (d) Arrhenius' plot of Ni diffusion in NiSi₂ with activation barrier of 1.641 ± 0.237 eV/atom, from parabolic region (NiSi₂-II).

We define L as the total length of silicides from Ni source to the silicide/Si interface at time t (Fig. 11) and plot L - t diagram with data captured from in-situ TEM observations. The growth length L of θ -Ni₂Si shows a parabolic relation with growth time t , which indicating that the rate limiting step is Ni diffusion to silicide/Si interface (Fig. 10a). Interestingly, NiSi₂ exhibits clearly two different stages: a linear growth (interfacial-limited) during the first stage

of growth followed by a parabolic growth behavior (diffusion-limited), indicating a linear-parabolic transition (Fig. 10b).⁴³ The in-situ studies show transition lengths of 341 to 1581 nm from 500 to 650 °C. There is no obvious transition at 450 °C due to the short growth length during the observation duration. In our structure, native SiO₂ at the interface of Ni and Si NW is removed by BOE before the deposition of Ni source, hence we do not expect the rate limiting step coming from Ni diffusing through native oxide at Ni/silicide interface. The interfacial-limited behavior therefore is a result of the growth rate limited step at the NiSi₂/Si interface not at Ni/silicide interface.

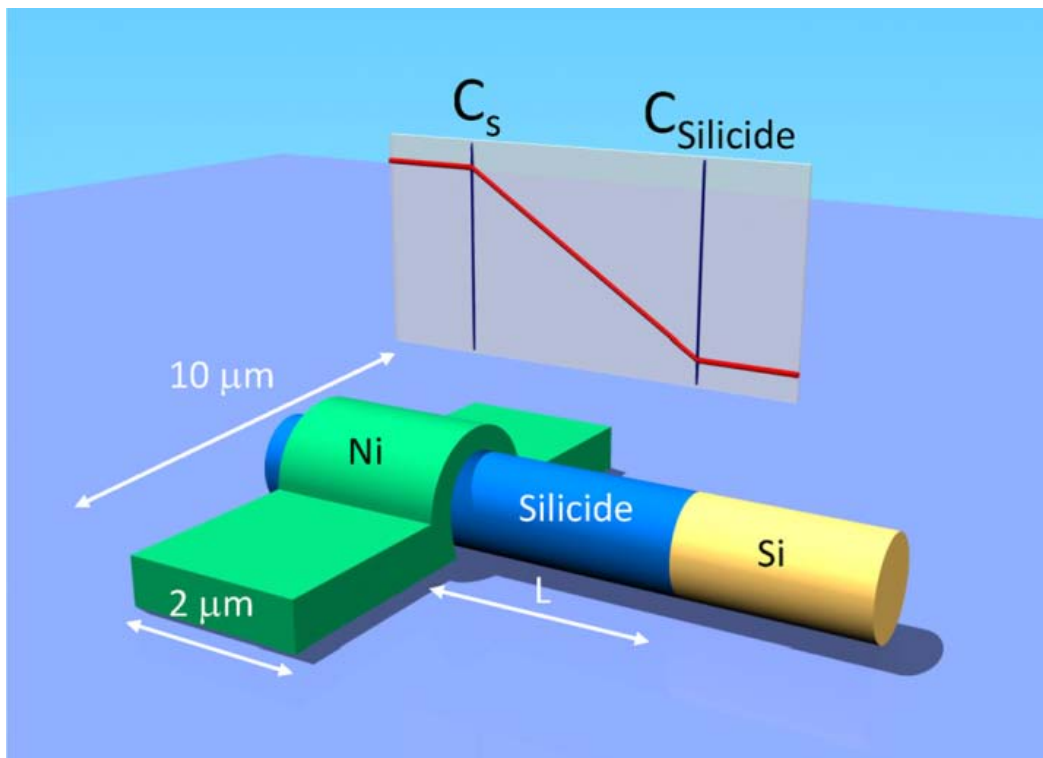


Fig. 11 Schematic of steady state kinetic model. Si NW without native oxide is covered by 2 μm×10μm Ni pad at left side and annealed in vacuum to form silicides.

In the 2-D system, NiSi₂ usually appears at higher temperatures (>750 °C) and as the last

phase following the formation of NiSi. This has hindered the examination of the kinetic behaviors of NiSi₂ formation over a wide range of temperatures and over larger distance, as well as masked the NiSi₂ formation behavior from the intrinsic Ni-Si couple. As a result, to our best knowledge, the kinetic data for NiSi₂ is very limited from bulk studies. The emergence of the NiSi₂ as the first phase in Si NW template, and its persistent existence as the first phase over a wide range of temperatures (~300-800 °C) and over long distance (hundreds of nanometers to micro meters) has allowed us to close interrogate its kinetic behavior for the first time. We clearly captured the two-stage transition of NiSi₂ in single crystal Si lattice, which has allowed the first time derivation of the reaction rate constant K_R of NiSi₂ from regime NiSi₂-I (Fig. 10c), and the diffusivity D during the later parabolic diffusion-limited growth stage, NiSi₂-II (Fig. 10d).

If we simplify the kinetic model by assuming a steady state is reached, i.e. the Ni diffusion flux (J) diffusing toward silicide/Si interface equals to that across silicide/Si interface. Then, the flux can be described as a function of diffusivity (D), concentration gradient or reaction rate constant (K_R).

$$J = D \frac{(C_s - C_{silicide})}{L} = K_R C_{silicide} \quad [1]$$

$$\text{So, } J = \frac{C_s}{\frac{L}{D} + \frac{1}{K_R}} \quad [2]$$

$$\text{from definition of flux } J = NV = \frac{b\rho}{M} \frac{dL}{dt} \quad [3]$$

where N: atoms/unit volume, V: velocity of silicide growth front, b: number of Ni atoms in silicide formula, ρ : density of silicides (NiSi₂: 4.80g/cm³ and θ -Ni₂Si: 6.85g/cm³ measured value; 7.91 g/cm³ theoretical calculated value), M: atomic weight of silicides (NiSi₂: 114.87 g/mol and θ -Ni₂Si: 145.49 g/mol), C_s is the Ni mole concentration per unit volume at the Ni/silicide interface and C_{silicide} is that at silicide/Si interface

$$J = \frac{b\rho}{M} \frac{dL}{dt} = \frac{C_s}{\frac{L}{D} + \frac{1}{K_R}} = \frac{C_s}{K_R L + D} \quad [4]$$

With boundary condition L=L₀ when t=0, we can integrate equation [4] to have:

$$\int_0^t (DK_R MC_s) dt = \int_{L_0}^L b\rho(K_R L + D) dL$$

$$DK_R MC_s t = \frac{K_R b\rho}{2} (L^2 - L_0^2) + Db\rho(L - L_0)$$

$$\frac{L^2 - L_0^2}{2Dt} + \frac{1}{K_R} \frac{L - L_0}{t} - \frac{MC_s}{b\rho} = 0 \quad [5]$$

Solve equation [5], we can obtain the relation of silicide grown length L and time t:

$$L = \frac{A}{2} \left(\sqrt{1 + \frac{(t + \tau)}{A^2 / 4B}} - 1 \right) \quad [6]$$

$$\text{Where } A = \frac{2D}{K_R} \quad [7]$$

$$B = \frac{2DMC_s}{b\rho} \quad [8]$$

$$\tau = \frac{L_0^2 + AL_0}{B} \quad [9]$$

Here, K_R is the reaction rate constant at silicide/Si interface, D is diffusivity of Ni through

silicide, L_0 is the total length of silicide at $t=t_0$ which is zero in our case, b : number of Ni atoms in silicide formula (2 for θ -Ni₂Si and 1 for NiSi₂), M is the atomic weight of silicides, ρ is the density of silicides and C_s is the Ni concentration per unit volume at the Ni/silicide interface.

For a short growth time period, $t \gg A^2/4B$, [6] can be approximated by

$$L = \frac{A}{2} \left(1 + \frac{1}{2} \left(\frac{t}{A^2/4B} \right) - 1 \right) = \frac{Bt}{A} = \frac{MC_s K_R t}{b\rho} \quad [10]$$

For a long growth time period, $t \ll A^2/4B$, [6] can be approximated by

$$L = \frac{A}{2} \sqrt{\frac{t}{A^2/4B}} = \sqrt{Bt} = \sqrt{\frac{2DMC_s t}{b\rho}} \quad [11]$$

Since C_s is the Ni concentration at Ni/silicide interface where Ni is always abundant, we assume C_s equals to the Ni mole concentration per unit volume in Ni source ($C_s=0.1517$ mol/cm³). From equation [10] and [11], we can extract K_R and D values from the L-t relations as shown in Table 1 and the corresponding activation energies. Assuming both the interfacial reaction barrier and the diffusion barrier of Ni in NiSi₂ are the same; then K_R and D values of NiSi₂ at 800 °C (as shown in red number in Table 1) are able to be linear extrapolated from the data of 450-650 °C.

The activation barrier for Ni diffusing through NiSi₂ is 1.641 ± 0.237 eV/atom during the diffusion-limited stage (NiSi₂-II, Fig. 10d), and the activation barrier of NiSi₂ interface reaction is 1.792 ± 0.101 eV/atom at the earlier growth stage (NiSi₂-I, Fig. 10c). There is no

available diffusivity and activation barrier data from thin film studies to describe the Ni diffusion in the NiSi₂, as NiSi₂ usually appears as the last phase in crystalline Si. However, the derived 1.641 ± 0.237 eV/atom activation energy for Ni diffusion in NiSi₂ is very close to the 1.65 ± 0.20 eV/atom barrier height reported in amorphous Si, where diffusion-limited growth of NiSi₂ was observed.⁴⁴ This indicates the grain boundary contribution is not significant in Ni diffusion in NiSi₂, otherwise a much lower diffusivity and higher barrier should be found in single crystal silicide section (in Si NW). Compared the activation energies of NiSi₂ to that of δ -Ni₂Si which is the first formed phase in thin film and bulk system, elimination of continuous grain boundary (axial direction) in 1-D silicide structure raises growth activation barrier of δ -Ni₂Si from 1.30-1.70 eV/atom (grain boundary dominated diffusion) to 2.48 eV/atom (lattice diffusion)⁴¹, which is higher than both the activation barrier of NiSi₂ interface reaction (1.792 ± 0.101 eV/atom) and the activation energy for Ni diffusion in NiSi₂ (1.641 ± 0.237 eV/atom). This data is consistent with our observation that the first phase is flipped from δ -Ni₂Si (in the thin film system) to NiSi₂ (in Si NWs), and confirms the hypothesis that elimination of grain boundaries renders NiSi₂ more competitive in 1-D structure.

With extracted parameters, we are able to compare the transformation rate of NiSi₂ and θ -Ni₂Si and to understand their growth competition in 1-D Si NW template. Here we replace L in [10] and [11] with “d” to represent the diffusion path length at radial direction and

assuming the kinetic parameters are similar in radial and axial directions. According to D and K_R in Table 1, the average transformation rates of θ -Ni₂Si and NiSi₂ (70 nm far from Ni source) are 1.458 $\mu\text{m/s}$ and 0.438 $\mu\text{m/s}$, respectively, at 800 °C. In this region, the average growth rate of θ -Ni₂Si is 3.3 times higher than that of the NiSi₂, consistent with our observation of θ -Ni₂Si appearing as the winning first phase. However, with increasing diffusion path (d), the growth rate of diffusion-limited θ -Ni₂Si will decelerate, while the growth rate of the interfacial-limited NiSi₂ remains constant and will eventually catch up then take over θ -Ni₂Si. By setting $[10]=[11]$ (when both phases grow the same distance at a given time), we arrive at critical values $d_c=234$ nm, beyond which the switch from θ -Ni₂Si to NiSi₂ is possible.

Table 1 Kinetic parameters of Ni silicides extracted from in-situ TEM observations

	Temperature	K (m/s)	D (m ² /s)	D ₀ (m ² /s)
NiSi ₂	450 °C	1.23×10 ⁻¹¹		
	500 °C	5.07×10 ⁻¹¹	2.99×10 ⁻¹⁷	
	550 °C	3.58×10 ⁻¹⁰	8.86×10 ⁻¹⁷	1.20×10 ⁻⁶
	600 °C	1.09×10 ⁻⁹	2.67×10 ⁻¹⁶	
	650 °C	6.57×10 ⁻⁹	1.85×10 ⁻¹⁵	
	800 °C	1.20×10 ⁻⁷	2.33×10 ⁻¹⁴	
θ -Ni ₂ Si	800 °C		3.65×10 ⁻¹⁴	

K is the reaction rate constant at silicide/Si interface

D is the Ni diffusivity in silicides

D₀ is the maximum diffusivity of Ni in silicides

Number in red represents data obtained by linear extrapolation to 800 °C.

In our Si NW system, NiSi₂ was found as first phase in Si NWs with diameter larger than 150 nm, which is reasonably close to the estimated value. The difference may arise from the assumptions of steady state and the simultaneous nucleation of NiSi₂ and θ -Ni₂Si at t_0 . In reality the nucleation of NiSi₂ may initiate earlier than θ -Ni₂Si for the following reasons. NiSi₂ is more stable than θ -Ni₂Si at lower temperatures, which may give NiSi₂ a jump start during the 30 s ramping time in our experiment. Indeed, a control sample annealed at 450 °C for 30 s demonstrates the growth of 210 nm long NiSi₂ from the Ni source (Fig. 5c-d). Thus the inevitable ramping stage gives NiSi₂ the added edge in the competition to win out as the first phase in Si NWs smaller than the predicted critical value.

3.7 Thermal stability of Ni silicides

According to the phase diagram, θ -Ni₂Si is not thermodynamically stable under 816 °C.³⁷ To test the thermal stability of the silicide NWs, a two step annealing is employed. As shown in Fig. 12a-b, sample is annealed at 800 °C for 15 secs, cooled down to room temperature and then annealed at 550 °C for another 15 secs. From the in-situ study, we have learned θ -Ni₂Si is the first phase in a ~60 nm NW at 800 °C. However, after we cool down the sample and reheat it to 550 °C for 15 secs, the first phase is switched to NiSi₂ and followed by δ -Ni₂Si. This is consistent to the thin film study that θ -Ni₂Si is a metastable phase and will transfer to δ -Ni₂Si at low temperature.^{45,46} The first phase NiSi₂ at the interface could be formed during the θ -Ni₂Si to δ -Ni₂Si transition since the Ni concentration in δ -Ni₂Si is higher than that in

θ -Ni₂Si and may take some Ni from surrounding area. It is also possible that the NiSi₂ a product of θ -Ni₂Si or δ -Ni₂Si reacts with unreacted Si.

The thermo stability of NiSi₂ is also tested. NiSi₂ remains as the first phase after a two step annealing at 550 °C for 15 secs, cooled down and then at 800°C for 15 secs (Fig. 12c-d). Even we extend the second annealing at 800°C to 45 secs (Fig. 12e-g), NiSi₂ is still not replaced by the following diffusion controlled phases. This shows the good thermal stability of NiSi₂. After long annealing, the growth rate of diffusion controlled silicides slows down due to the long distance from the interface to the Ni source. The lateral growth competition is similar to thin film structure and can be explained through the kinetic model.¹⁸ From the model, the disappearing phases which are predicted by the equilibrium phase diagram are missing in nano structure due to their kinetic instability. It is believed is the annealing time is long enough and the Ni, Si source are not limited, the phases will all appear in the NW as in a bulk diffusion couple.¹⁸

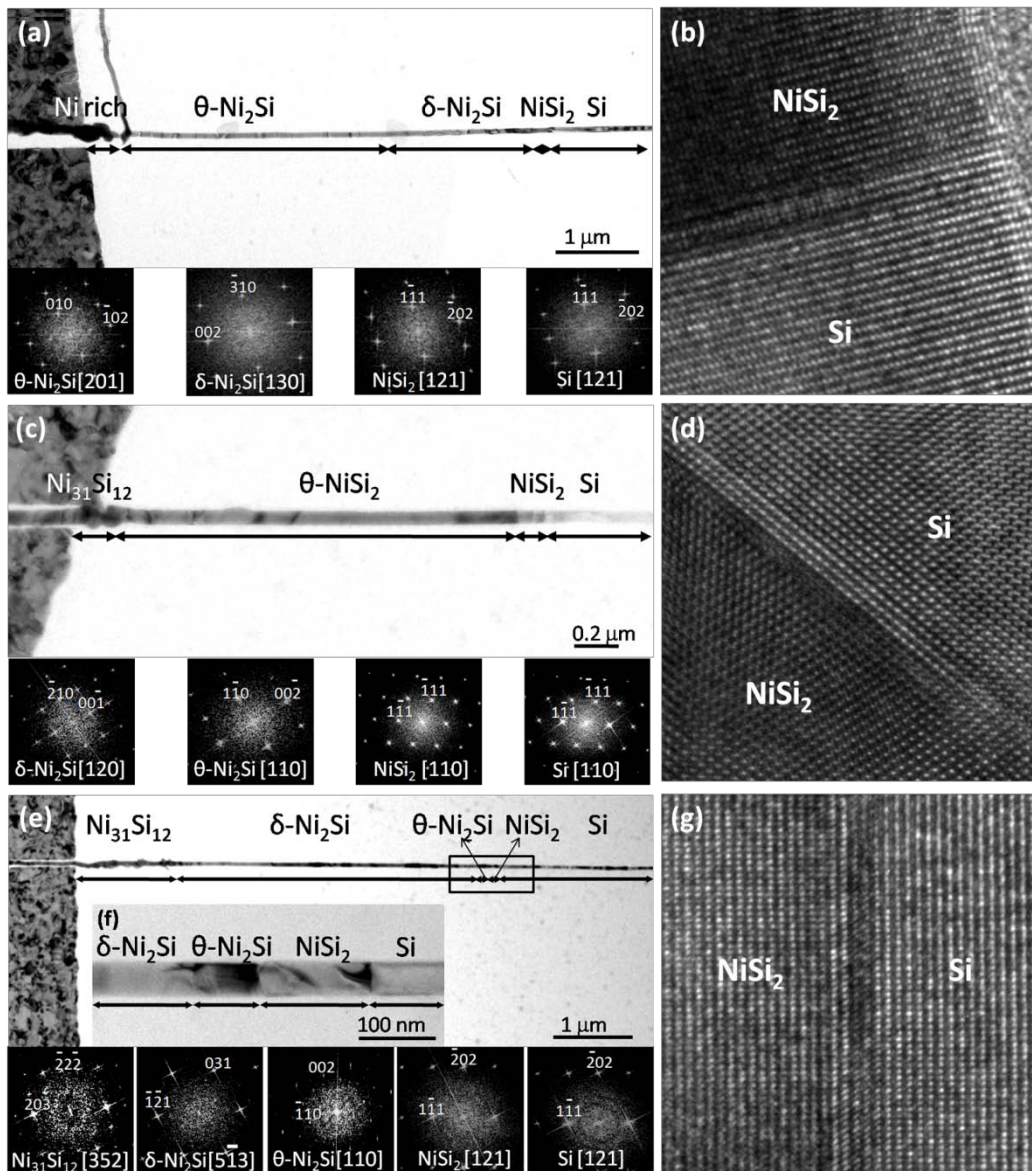


Fig. 12 Ni silicide phase formation after a two step annealing (a-b) Sample is annealed at 800 °C for 15 secs, cooled down to room temperature and then annealed at 550 °C for another 15 secs. (c-d) Sample is annealed at 550 °C for 15 secs, cooled down to room temperature and then annealed at 800 °C for another 15 secs. (e-g) Sample is annealed at 550 °C for 15 secs, cooled down to room temperature and then annealed at 800 °C for another 45 secs. (f) the zoom in image of the interface area in (e) to show the sequence of thin phases. FFT patterns are used for phase identification.

Chapter 4 Phase manipulation through template modulations

4.1 Importance of Ni silicide phase manipulation

Metallic silicides as contacts in Si NW devices have attracted much attention for their ability to achieve superior performances and unique functions in nanoscale electronics and spintronics.^{7,8,47} In order to produce reliable and controllable contacts in small circuits, understanding and manipulating the phase formation of nanoscale silicides are key to their large scale manufacturing. Many known silicides have variable physical properties, including resistivity, maximum current density and work functions that are suitable for various applications.^{9,11} For example, NiSi with lowest resistivity among all silicides is the desired phase for applications such as source, drain and gate contacts in integrated circuits while other Ni silicides with relatively high resistivity are considered as defects (Table 2).⁴⁸⁻⁵⁰ Thus, control towards predictable NiSi formation and extended NiSi manufacturing windows are desirable. However, phase formation in 1-D nanostructure has been reported to be different from that observed in 2-D systems.²²⁻²⁵ Systematic studies and understanding of the material

Table 2 Electrical properties of Ni silicides

	Ni ₃ Si	Ni ₃₁ Si ₁₂	δ-Ni ₂ Si	Ni ₃ Si ₂	NiSi	NiSi ₂
Resistivity (μΩ-cm)	80-90	90-150	24-30	60-70	10.5-18	34-50

Data from Chen, L. J. *Silicide Technology for Integrated Circuits* (The Institute of Electrical Engineers, London, 2004).¹²

behaviors in Si NW templates for reliable phase formation are critical to achieve predictable and reliable high performance contacts at nano scale.^{48,51,52}

Chap. 3 has shown that the emergence of the first phase at the Si/silicide interface in Si NWs is the result of kinetic competition among different silicide phases. In this chapter we show by selectively tuning the growth rates of different phases, one can achieve NiSi₂, θ -Ni₂Si, δ -Ni₂Si, Ni₃₁Si₁₂ and eventually NiSi as the first phase at the Si/silicide interface, respectively. Firstly, structure modifications to the Si NW templates were employed to selectively modulate the growth parameters of different phases, including promoting the growth of diffusion limited phase in porous Si NW structures and hindering the growth of silicides with large unit volume by depositing thick oxide shells around Si NWs. Secondly a Pt interlayer between the Ni source and Si NW template is used to suppress the growth of dominating NiSi₂, which in turn leads to the appearance of otherwise less competitive diffusion limited phases (such as δ -Ni₂Si) as first phase in Si NWs. Finally, with a combination of Pt interlayers to suppress NiSi₂ and thick oxide shells to hinder Ni₃₁Si₁₂, δ -Ni₂Si and θ -Ni₂Si, we can render the slow-growing NiSi as the winning first phase in the growth competitions among silicides in Si NW templates.

4.2 Ni silicides formation in porous Si NWs

It has been demonstrated that in a Si NW template, θ -Ni₂Si is the only competitive diffusion limited phase against the dominating NiSi₂ in wires of smaller diameters (d) and

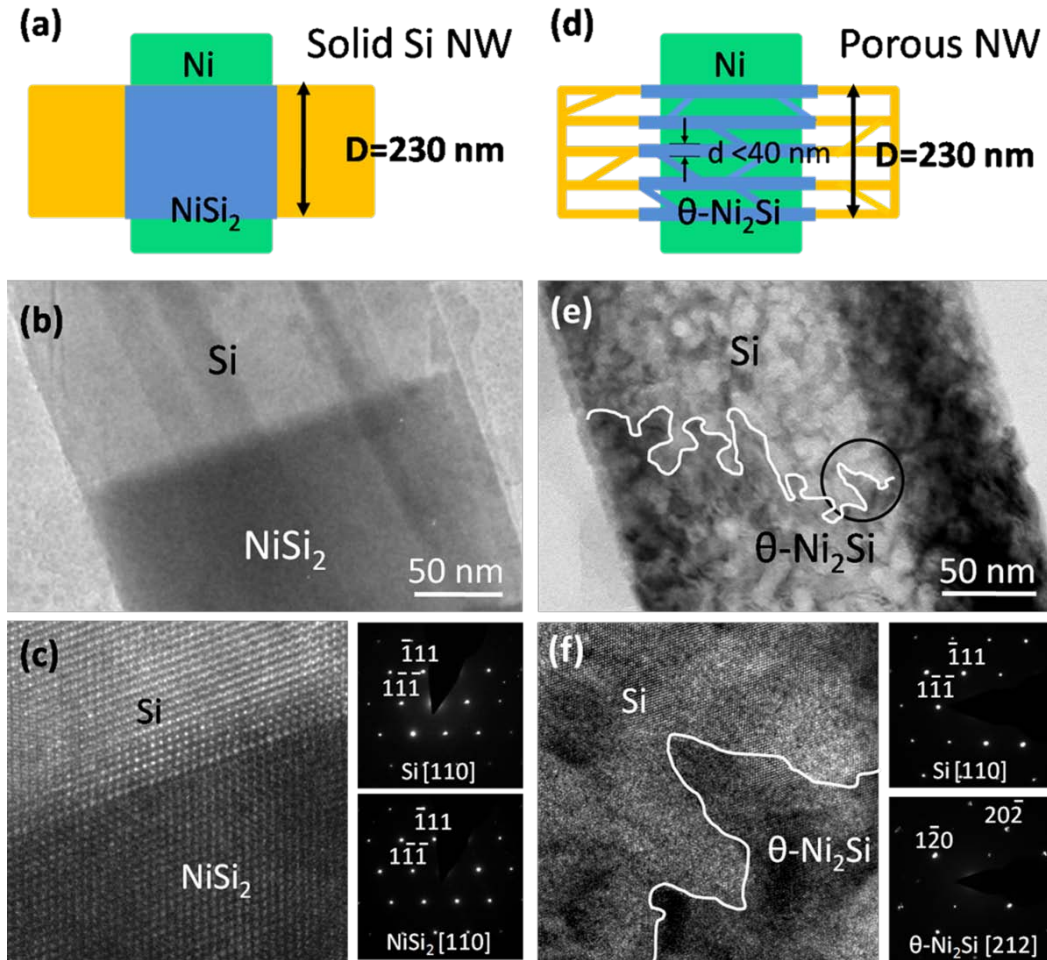


Fig. 13 Enhance growth rate of diffusion limited phase $\theta\text{-Ni}_2\text{Si}$ in 230 nm porous Si NW at 800 °C. (a,d) Schematic of silicide formation in solid and porous Si NWs with the same outer diameters. In porous Si NW, the first phase is switched to diffusion limited phase $\theta\text{-Ni}_2\text{Si}$. (b,c) Low magnification TEM, high resolution TEM images at the silicide/Si interface and corresponding SAED patterns of Si and silicide in 230 nm solid Si NW with NiSi_2 as the first phase. (e,f) Low magnification TEM, high TEM images at the interface and corresponding SAED patterns of Si and silicide in 230 nm porous Si NW with $\theta\text{-Ni}_2\text{Si}$ as the first phase.

only at high temperature (800 °C).²⁵ To this end, a porous NW template with extremely small “d” nanopaths allow the diffusion-limited phase to become competitive in large diameter NWs (Fig. 13) and render another diffusion-limited phase, NiSi , as winning phase at lower temperatures (as $\theta\text{-Ni}_2\text{Si}$ is known as a high temperature phase).³⁷ The porous NW is similar

to a bundle of small Si NWs with each being an individual growth pathway (Fig. 13a,d). As shown in Fig. 14, typical porous NW has outer diameter >200 nm while small interconnected paths with diameter <40 nm (average diameter of 10 nm). The diffraction pattern shows the single crystal nature of porous Si NW (Fig. 14a, inset.) This is also confirmed from high resolution images (Fig. 14c) where no defects such as grain boundaries, twins or dislocations are observed, which are fast diffusion paths and could enhance diffusion locally (not uniformly.) In Fig. 14b, a cross sectional image shows a porous Si NW with an irregular outline without specific dominating facets, and is fully porous without solid core. Thus, the porous Si NW can be considered as a bundle of interconnected single crystal nanopaths with small diameters. From all TEM and HRTEM images, no Ag particles are observed which gets rid of the Ag contribution to the silicide growths and silicide phase selection.

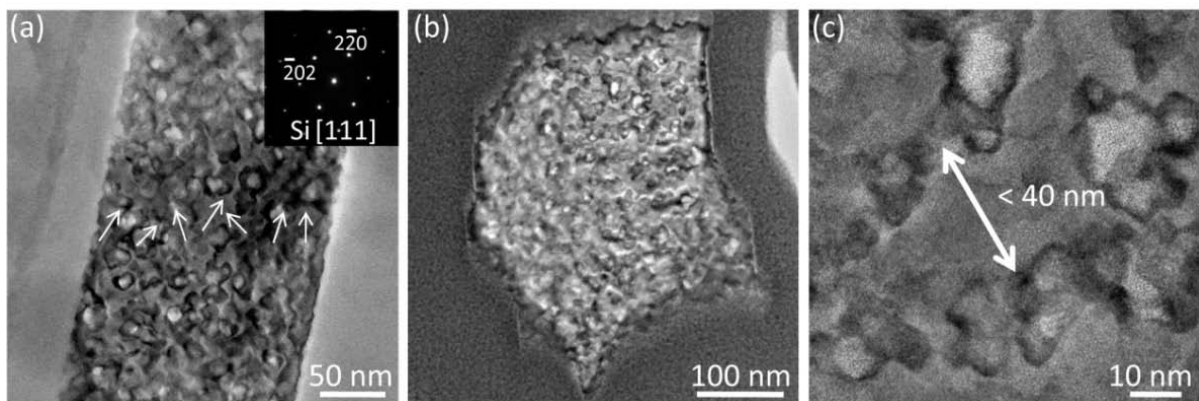


Fig. 14 Characterization of a porous Si NW. (a) TEM image of a typical porous Si NW showing Si nanopaths with average width of 10 nm. Inset in (a) is a SAED pattern of this porous wire. (b) Cross sectional image of porous Si NW without remaining solid core. (c) Zoom in image of (b) showing Si nanopaths with maximum widths smaller than 40 nm.

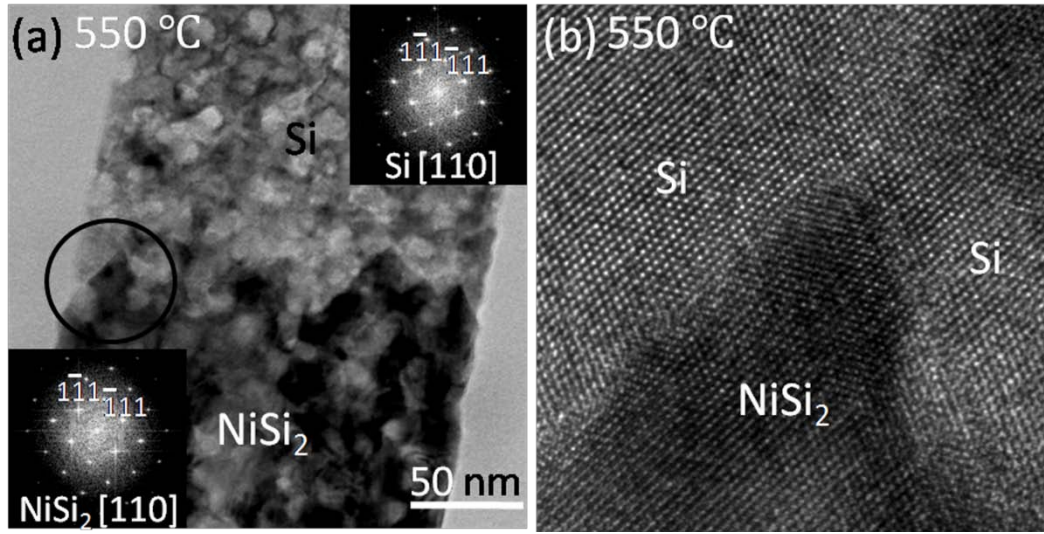


Fig. 15 NiSi₂ is the first phase in a porous NW at 550 °C. (a) Low magnification TEM at interface and corresponding FFT patterns of silicide forms in a porous Si NW with NiSi₂ as the first phase. (b) The high resolution TEM image at the circled area in (a) shows the epitaxial relation between NiSi₂ and Si. The NiSi₂ tends to adopt the shape of Si template. The interface between NiSi₂ and Si is not atomic sharp which may reflect the shape of a nanopath and/or the nature of TEM technique, a projection of a 3-D object into a 2-D image.

Since the nanopaths in porous Si NW are very narrow, as a result, the growth of the diffusion limited phases will be greatly enhanced. This modified kinetics help θ -Ni₂Si become the first phase in a porous 230 nm Si NW at 800 °C (Fig. 13d-f), while NiSi₂ appears as the first phase in a solid 230 nm Si NW (Fig. 13a-c). At lower temperature, NiSi₂ still dominates in both solid NW and porous NW where the θ -Ni₂Si is not as competitive as at 800 °C (Fig. 15). As the Ni diffusivity in NiSi is usually lower than that of other diffusion limited phases,⁴² we need to selectively decrease the growth rates of Ni₃₁Si₁₂, δ -Ni₂Si and θ -Ni₂Si in order to render NiSi the competitive phase.

4.3 Ni silicides formation in solid Si NWs with compressive shells

In order to hinder the growth rate of $\text{Ni}_{31}\text{Si}_{12}$, $\delta\text{-Ni}_2\text{Si}$ and $\theta\text{-Ni}_2\text{Si}$, depositing a thick oxide shell around Si NW by atomic layer deposition (ALD) allows us to selectively decrease the growth rate of silicides with larger unit volume than NiSi, by supplying a compressive stress.^{22,53,54} After patterning the Ni pads by e-beam lithography, a thick (200 cycles of ALD deposition) is deposited on top of the wafer. Since a unit volume expansion usually accompanies the transformation from Si to silicide, the expansion will be suppressed in the confining shells and leads to a compressive stress. The induced stress can significantly hinder Ni diffusion which in turn retards the growth rate of the affected silicides. The diffusivity (D) can be expressed as

$$D = D_0 \exp\left(\frac{-G^*}{k_B T}\right)$$

$$G^* = G_{\text{formation}} + G_{\text{migration}}$$

where D_0 is a material constant and G^* is the diffusion activation energy barrier including formation free energy ($G_{\text{formation}}$) and migration free energy ($G_{\text{migration}}$).²² Under compressive stress, the activation barrier of Ni diffusion ($G_{\text{migration}}$) in the silicide increases and leads to a smaller diffusivity. Therefore, among $\text{Ni}_{31}\text{Si}_{12}$ (39.46 \AA^3), $\delta\text{-Ni}_2\text{Si}$ (32.15 \AA^3), $\theta\text{-Ni}_2\text{Si}$ (30.66 \AA^3), NiSi (24.12 \AA^3) and NiSi_2 (19.75 \AA^3), the $\text{Ni}_{31}\text{Si}_{12}$ will experience the highest suppression and NiSi_2 will face the lowest (Table 3).^{12,55}

Table 3 Volume of Ni Silicides and Si per Si Atom

	Si	Ni ₃₁ Si ₁₂	δ -Ni ₂ Si	θ -Ni ₂ Si	NiSi	NiSi ₂
Volume per Si atom (\AA^3)	20.01	39.46	32.15	30.66	24.12	19.75

Data from:

1. JCPDS Card No. 80-2283⁵⁵
2. Chen, L. J. *Silicide Technology for Integrated Circuits* (The Institute of Electrical Engineers, London, 2004).¹²

θ -Ni₂Si with a larger unit volume than NiSi and NiSi₂ will also face stronger stress in the phase transformation. Interestingly, NiSi₂ is the only phase with a smaller unit volume than Si at room temperature. Therefore NiSi₂ barely experiences compressive stress during nucleation and growth which can keep relatively fast growth rate. Even we take the thermal expansion at 800 °C into account, the volume of Si is 20.21 \AA^3 while NiSi₂ is 20.50 \AA^3 .⁵⁶ The significant volume expansion of θ -Ni₂Si is still about 2.59 times to that of NiSi and 36.03 times to NiSi₂. As a result, when a 22 nm thick Al₂O₃ shell is coated on a 50 nm Si (with native oxide) NW, the first phase at 800 °C switches from θ -Ni₂Si to NiSi₂ suggesting the Al₂O₃ shell has hindered the growth of θ -Ni₂Si (Fig. 16a-d).

Here raises a question: do extra thermal process of ALD Al₂O₃ shell deposition (at 90-250 °C for 100 mins) and the surface condition of Si NW changes have any influence to the phase switch? In order to clarify the shell thickness (and induced compressive stress) is the dominating factor which switches the first phases, we compare the phase formation in four different conditions:

1. Si NW with native oxide coated with thick Al₂O₃ shell (Fig. 16 b-d)
2. Si NW with native oxide coated with thin Al₂O₃ shell (Fig. 16 e-g)
3. Si NW without native oxide coated with thick Al₂O₃ shell (Fig. 17 a-c)
4. Si NW without native oxide coated with thick carbon shell (Fig. 17 d-f)

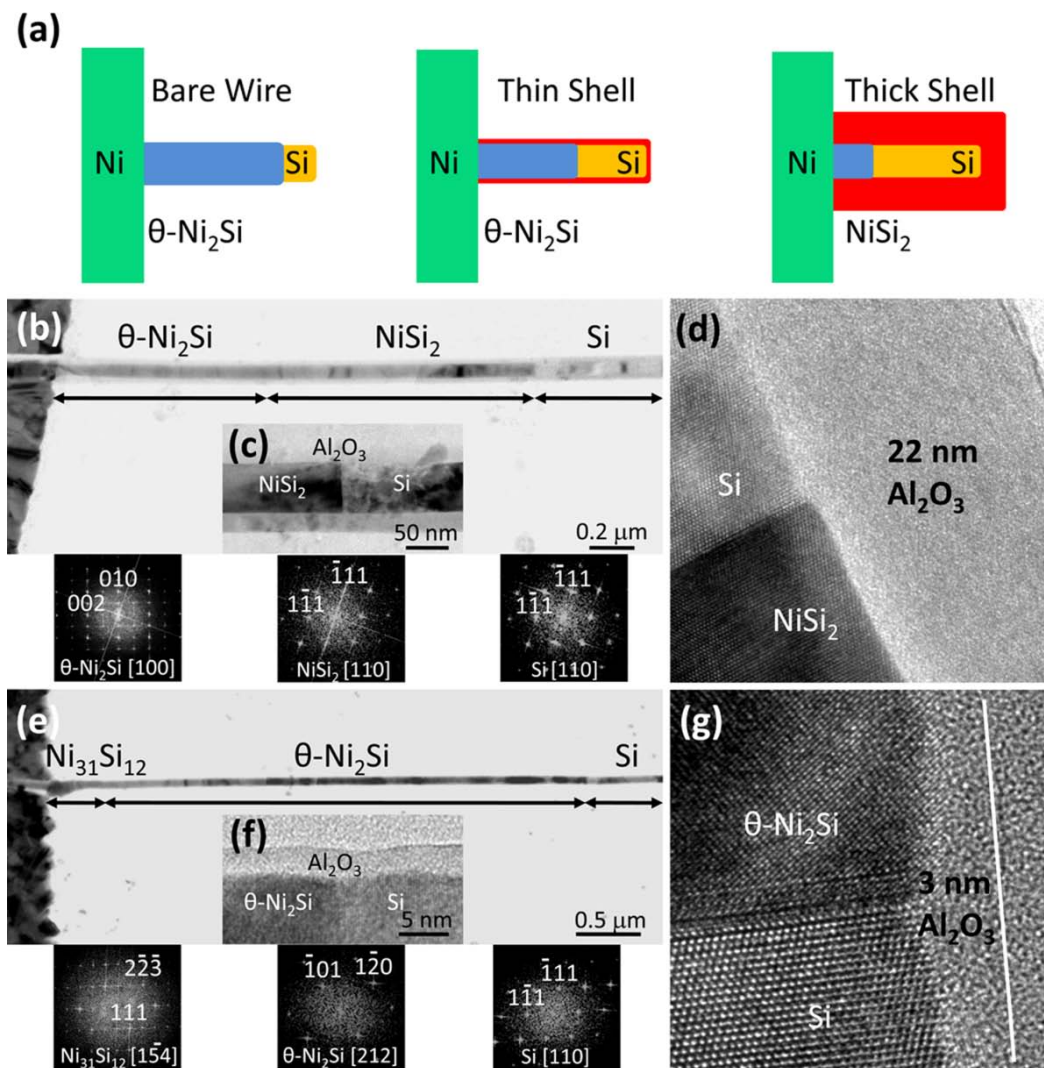


Fig. 16 Suppress growth rate of diffusion limited phase θ -Ni₂Si in 50 nm Si NW with ALD Al₂O₃ shells at 800 °C. (a) Schematic of thin and thick shell influence on suppressing growth rate of diffusion limited phase θ -Ni₂Si. With a thick shell, the first phase is switched to interfacial limited phase NiSi₂. (b-d) TEM images and FFT patterns of silicides and Si in a thick (22 nm) ALD Al₂O₃ shell with NiSi₂ as the first phase. (e-g) TEM images and FFT patterns of silicides and Si in a thin (3 nm) ALD Al₂O₃ shell with θ -Ni₂Si as the first phase.

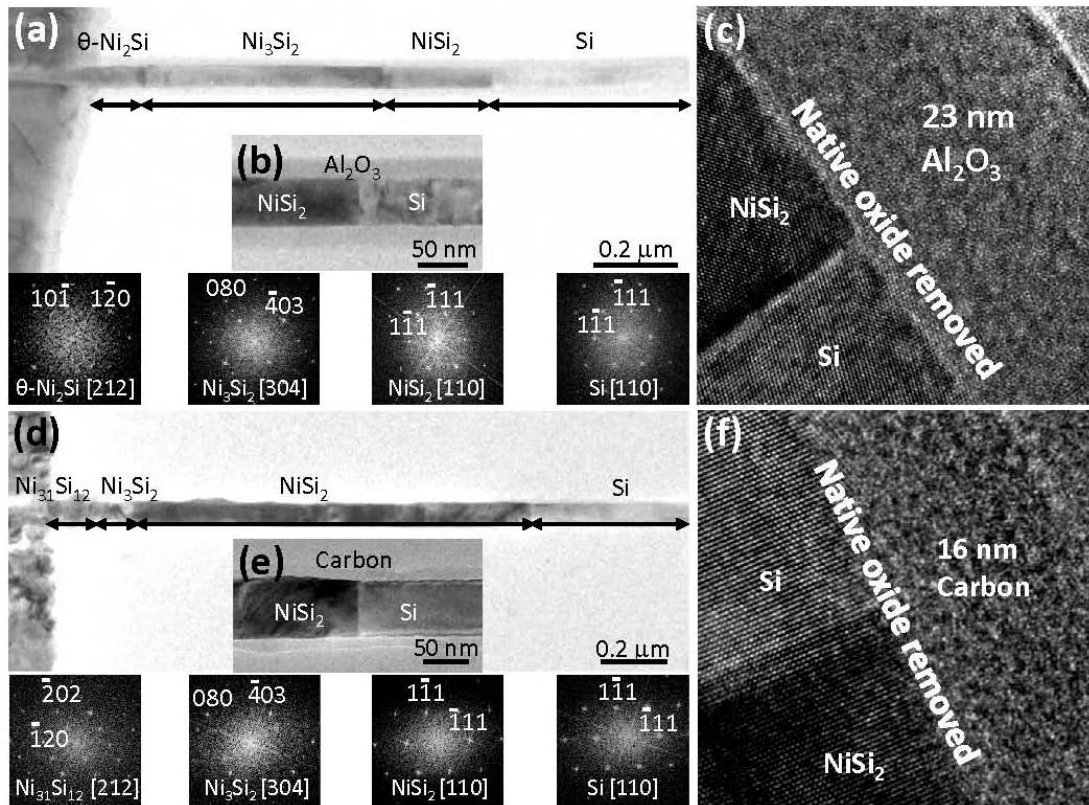


Fig. 17 Image of first phases formed at 800 °C in Al₂O₃ shell and carbon shell without native SiO₂. (a-c) TEM images and FFT patterns of the silicides formed in 23 nm Al₂O₃ shell. NiSi₂ is still found as the first phase. (d-f) TEM image and FFT patterns of the silicides formed in 16 nm carbon shell. NiSi₂ is found as the first phase.

In all cases, once the shell reaches significant thickness (>16 nm), the first phase will be switched to NiSi₂ in a small Si NW template at 800 °C. At the same time, in Si NWs with a 3 nm-thick Al₂O₃ shell, θ -Ni₂Si remains as the first phase (Fig. 16a, e-g). This confirms that compressive stress induced by thick shells is the dominating reason of first phase switching and rules out the noticeable contribution of interfacial energy (e.g. Al₂O₃/Si, SiO₂/Si and C/Si), interfacial diffusion path between the SiO₂/Si or the ALD process thermal treatment. While the compressive stress is effective in limiting the growth of diffusion-limited phases with large volume expansion, this approach is unfortunately not applicable to suppress the

dominant growth of NiSi₂ whose unit volume close to Si.

4.4 Ni silicides formation in solid Si NWs with Pt interlayers

To this end, a Pt interlayer between Si NW and Ni contact is introduced to limit the growth of the dominant phase, NiSi₂. The solubility of Pt in NiSi₂ is much lower than that in NiSi. Since oversaturated Pt must be expelled out of the lattice prior to the formation of NiSi₂, it increases the kinetic barrier of NiSi₂ formation much more than it does to NiSi.^{57,58} As shown in Fig. 18, with a 1-5 nm Pt layer deposited between Ni and Si NW, δ -Ni₂Si overcomes the dominant NiSi₂²⁵ and appears as the first phase after annealing at 550 °C for 30 s. At the same time, the total length of the formed silicide region significantly drops from 1.77 μ m (Fig. 18a, without Pt) to 280 nm (Fig. 18b, with 1 nm Pt) and 195 nm (Fig.18c, with 5 nm Pt), confirming the fastest growing phase NiSi₂ in Si NW is suppressed by the presence of Pt and the slower δ -Ni₂Si wins out in competition instead. The growth rate of δ -Ni₂Si also slows down as the Pt amount increases from 1 nm to 5 nm due to an increased activation barrier which is consistent with that in 2-D structure.⁵⁹ Unfortunately, by simply tuning the thickness of Pt interlayer, we do not obtain the desired NiSi. We have to slow down all other phases at the same time to help NiSi to win in the kinetic competition.

4.5 Ni silicides formation in solid Si NWs with compressive shell and Pt interlayers

To simultaneously suppress Ni₃₁Si₁₂, δ -Ni₂Si, θ -Ni₂Si and NiSi₂, a structure combined with

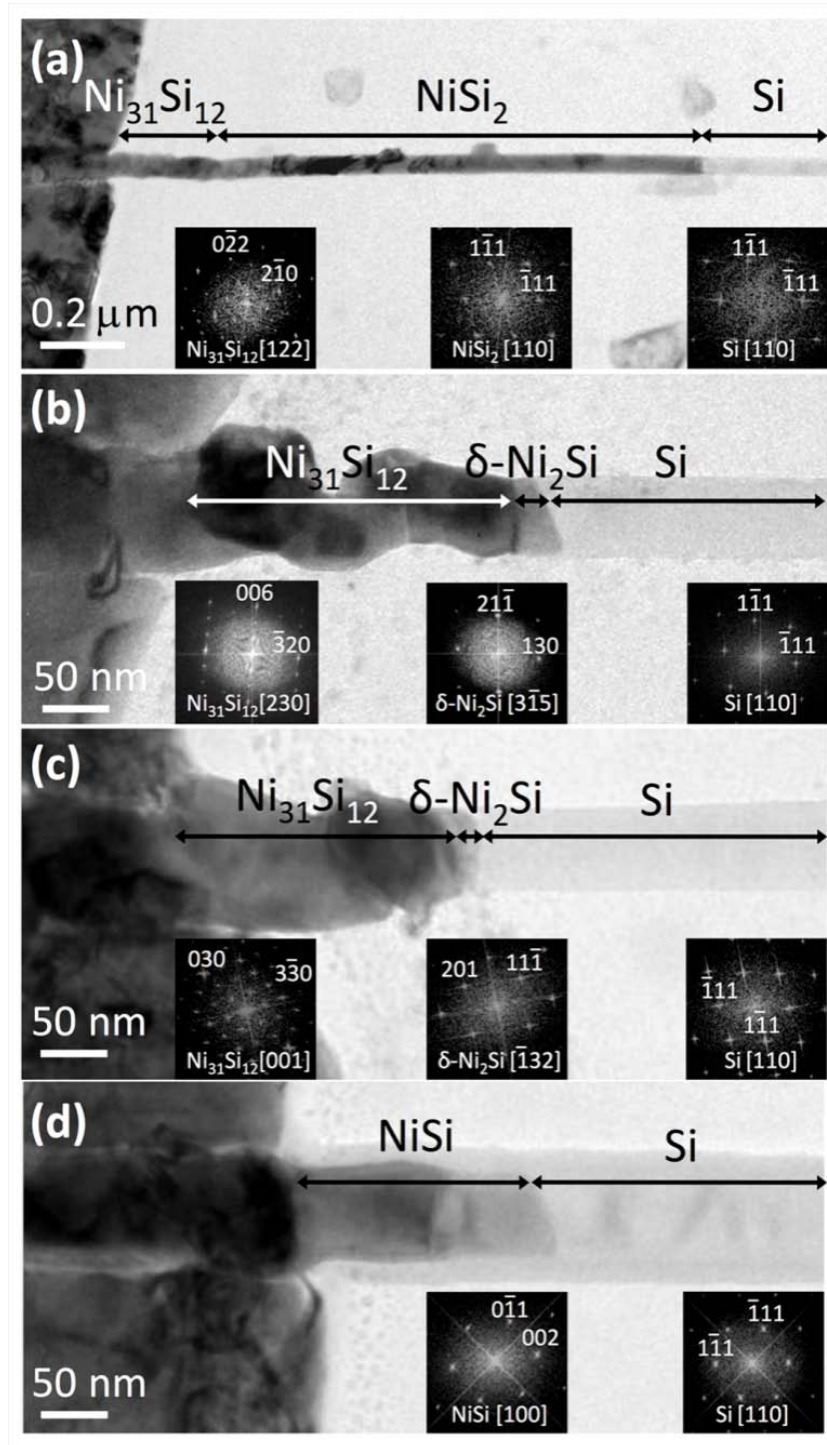


Fig. 18 First phases control in ~70 nm Si NW with 1-5 nm Pt interlayers and ALD Al_2O_3 shells. (a) TEM image and corresponding FFT patterns of silicides and Si in a bare Si NW without Pt interlayer at 550 °C for 30 secs. (b) Silicides formed in a bare Si NW with 1 nm Pt interlayer at 550 °C for 30 secs. (c) Silicides formed in a bare Si NW with 5 nm Pt interlayer at 550 °C for 30 secs. (d) Silicides formed in a Si NW with 5 nm Pt interlayer and 17 nm ALD Al_2O_3 shell at 550 °C for 4 mins.

a Pt interlayer between Ni and Si, and a 17 nm oxide shell around NW is adopted. With the Pt interlayer to suppress NiSi₂ and the thick Al₂O₃ shell to hinder Ni-rich phases, Pt doped NiSi eventually wins out as the first phase (Fig. 18d). Again, the total length of the silicide region decreases to 168 nm (after annealing for 4 minutes). This confirms the slower growth rate of NiSi than NiSi₂, δ -Ni₂Si and θ -Ni₂Si and the slower phase can only appear until the faster growth phases have been slowed down enough. In addition, a Ni richer phase, Ni₃₁Si₁₂ are found in many samples locating next to Ni pads. As Ni atoms keep diffusing into formed silicides region, Ni and these silicides (θ -Ni₂Si, δ -Ni₂Si, NiSi and NiSi₂) will react and transform to Ni₃₁Si₁₂ which is consistent with previous works.^{22,25,60}

4.6 Pt distribution in Ni(Pt)Si crystal structure

TEM and scanning transmission electron microscope (STEM) are used to analyze Pt distribution in NiSi (Fig. 19). The diffraction pattern in Fig. 19a shows the nature of single crystalline structure. Pt concentration is found higher along the core and lower at the edge of the NW corresponding to the thickness profile (Fig. 19b). Along the axial direction, the Pt concentration keeps a significant value and drops sharply at the interface.

These indicate uniform distribution of Pt across entire Ni(Pt)Si portion and occupies Ni site which is consistent with previous reports on thin film studies.^{58,61,62} PtSi and NiSi are known to share the same MnP structure with close lattice constants (NiSi: a=5.233, b=3.258, c=5.659; PtSi: a=5.595, b=3.603, c=5.932) and therefore Pt is more soluble in NiSi than in

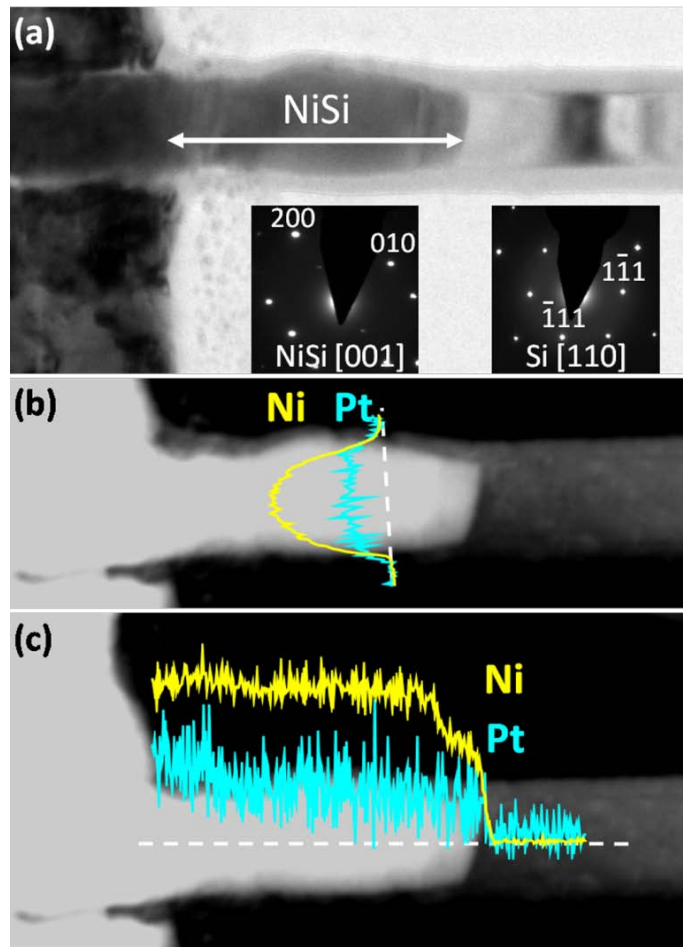


Fig. 19 Pt distribution in Ni(Pt)Si formed in ~ 70 nm Si NW with 5 nm Pt interlayer and thick ALD Al_2O_3 shell at 450°C for 2.5 hr. (a) TEM image and corresponding SAED patterns of NiSi and Si. (b) Line scanning across radial direction. (c) Line scanning across axial direction. Pt intensities in b and c are enhanced by 10 times.

other silicides. The solubility of Pt in NiSi is 2.16-5.50 atom % ($\text{Pt}/(\text{Pt}+\text{Ni})$) and that of the NiSi_2 is 0.30 atom % at 800°C .^{57,58,61-63} If we assume all Pt and Ni atoms react with Si as a homogeneous structure, the amount of Pt atoms (from a 1-5 nm Pt interlayer under an 80 nm Ni film) is 0.88-4.26 atom % of all metal atoms. This concentration range is close to the atomic solubility of Pt in NiSi but much higher than that in NiSi_2 and thus 0.58-3.96 atom % of Pt needs to precipitate before NiSi_2 formation. The repulsion of Pt due to its low solubility

in NiSi₂ greatly increases the growth activation barrier and hinders growth rate of NiSi₂ (Fig. 18a-c). More interestingly, the Ni(Pt)Si/Si epitaxial interface, which in thin film studies is argued to be the main reason for suppressing NiSi₂ formation through lowering the interfacial strain energy and for enhancing Ni(Pt)Si thermostability,^{61,62} is not observed in the NWs. This indicates that the kinetics, rather than interfacial energies, contributes more significantly to the Ni(Pt)Si formation in 1-D system.

To observe the precipitation of Pt during silicides growth, a structure (Fig. 20a,b) with a 10 nm Ni film and a 1 nm Pt interlayer were deposited on the upper side of a Si NW. After annealing at 800 °C for 5 secs, multiple phases are found coexisting, including Ni(Pt)Si and NiSi₂. Short annealing time and thin metal films prevent silicides from contacting and consuming each other. In Fig. 20c-d, a HAADF image and elemental mapping show Ni and Pt atoms distributed across the entire silicide area with bright contrast. Line-scanning shows higher amount of Ni and Pt at the core of Ni(Pt)Si than at the edge, consistent with the thickness profile. On the other hand, the amount of Pt in NiSi₂ is independent of the silicide thickness which indicates Pt precipitation to periphery during silicidation due to low Pt solubility in NiSi₂ (Fig. 20 e-f). A more detailed STEM study shows Pt forms islands on the NiSi₂ surface (Fig. 21). Fig. 21a is a schematic of Pt out-diffuses and forms islands on the surface. A HAADF image in Fig. 21b shows the shape of NiSi₂ grain. In Fig. 21c, Ni peak

intensity is higher at the right side due to thickness difference while Pt intensity is stronger at the left side.

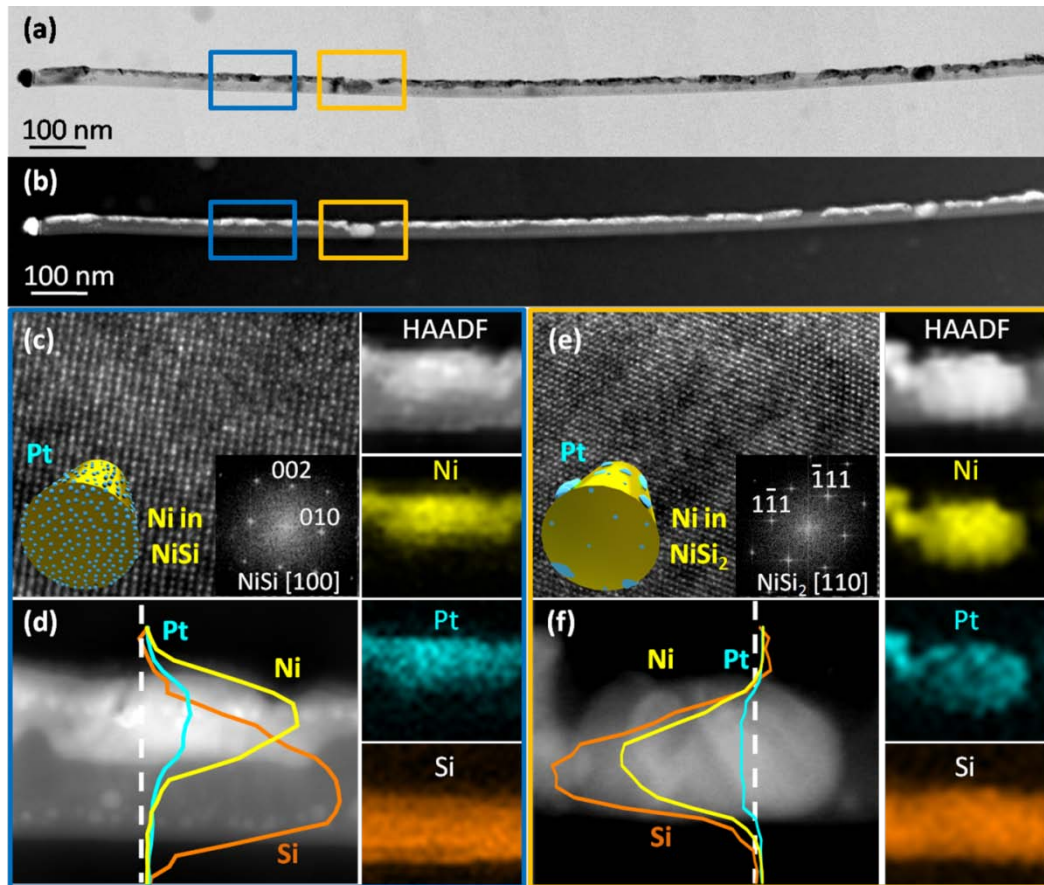


Fig. 20 Pt distribution in Ni(Pt)Si and NiSi₂ and multiple phase coexistence at early growth stage. A 1 nm Pt interlayer is deposited between the 10 nm Ni film and the Si NW and then annealed for 5 secs at 800 °C. (a,b) Bright and dark field TEM images of silicides grown in a Si NW template. Si NW is covered by Pt and Ni films at upper side. (c) High resolution image and corresponding FFT pattern of NiSi. Inset in (c) is the schematic of Pt and Ni distribution in NiSi. (d) Line scanning, element mapping and HAADF image of Pt, Ni and Si atoms distributed across NiSi in NW radial direction. (e) High resolution image and corresponding FFT pattern of NiSi₂. Inset in (e) is the schematic of Pt and Ni distribution in NiSi₂. (f) Line scanning, element mapping and HAADF image of Pt, Ni and Si atoms distributed across NiSi₂ in NW radial direction.

This indicates the Pt intensity comes from Pt islands on the surface and is independent to

the NiSi₂ thickness. In order to show the Pt islands, we tilt the sample a bit more to the right and repeat the mapping (Fig. 21d). Clear Pt islands are observed on the left bottom corner in Pt image. The intensity increase is not shown in Ni image which rules out the thickness contribution at this position. The line scanning also shows two peaks corresponding to locations of Pt islands. This Pt precipitation prior forming NiSi₂ leads to an increased kinetic barrier and suppress NiSi₂ to form with a Pt interlayer presence.

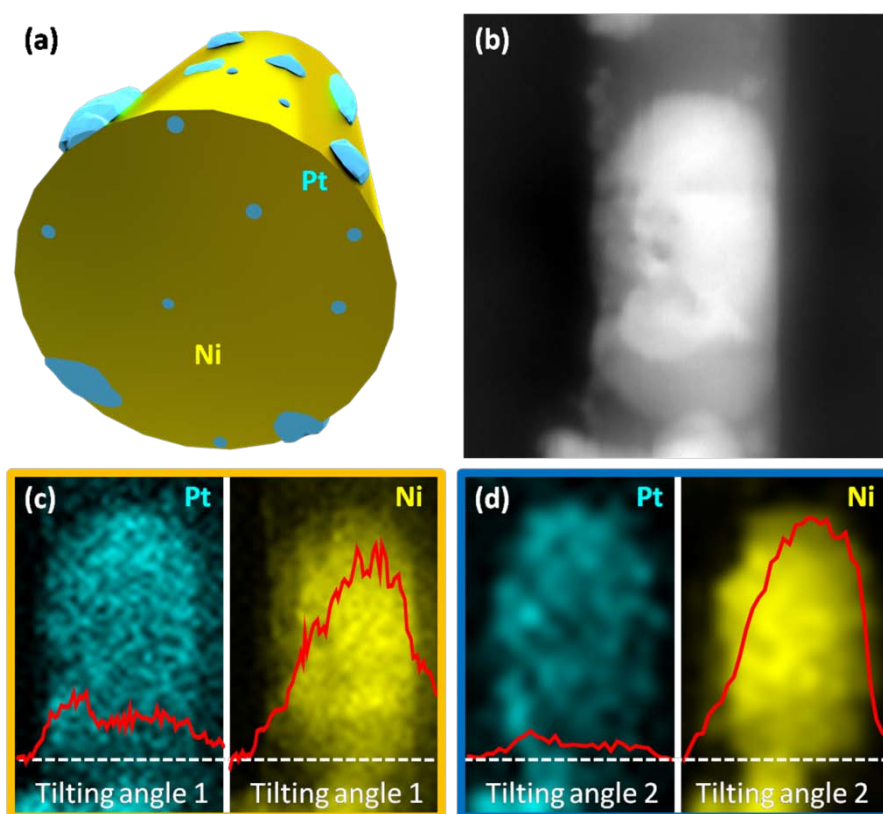


Fig. 21 Detailed STEM characterization of Pt precipitation on NiSi₂ surface. (a) Schematic of Pt precipitates on NiSi₂ surface as islands. (b) HAADF of NiSi₂ (c) Element mapping of Pt and Ni atoms in NiSi₂. Red lines are the counts of Pt and Ni in line scanning across white dash lines. (d) Element mapping of Pt and Ni atoms in NiSi₂ from another tilted angle. Red lines are the counts of Pt and Ni in line scanning across white dash lines at another tilted angle.

4.7 Demonstration of Ni silicides phase control in Si NW templates

Fig. 22 shows the phase formation results under various modulations at 800 °C and confirms the kinetic competition mechanism. In a bare Si NW with diameter of ~70 nm, θ -Ni₂Si the most competitive phase wins as the first phase (Fig. 22a). As we add 1 nm Pt interlayer, θ -Ni₂Si remains as the first phase but the shorter growth length indicates the hindering of θ -Ni₂Si growth (Fig. 22b). To our best knowledge, there is no available data report the solubility of Pt in θ -Ni₂Si. However, considering the Pt solubility in NiSi is way higher than other Ni silicides, we assume that of θ -Ni₂Si is close to that in δ -Ni₂Si (much lower than NiSi)⁶⁴ and thus suggest the hindering of θ -Ni₂Si growth is a result of increasing kinetic barrier with oversaturated Pt presence.

As we increase the Pt thickness to 5 nm, the silicide NW tends to be broken at the interface and the Ni richer phase, Ni₃₁Si₁₂, catches up and consumes previous formed silicides (Fig. 22c). Within a thick oxide shell and 5 nm Pt interlayer, δ -Ni₂Si forms as the first phase with confining shell to suppress large unit volume Ni₃₁Si₁₂ (Fig. 22d). Compared to a similar case without Pt interlayer where NiSi₂ forms as the first phase, oversaturated Pt suppresses the NiSi₂ growth. The possible reason of forming δ -Ni₂Si instead of Ni(Pt)Si (as at 550 °C) is the higher Pt solubility in δ -Ni₂Si at 800 °C than at 550 °C. The higher Pt solubility in silicides will cause less suppression on δ -Ni₂Si growth.

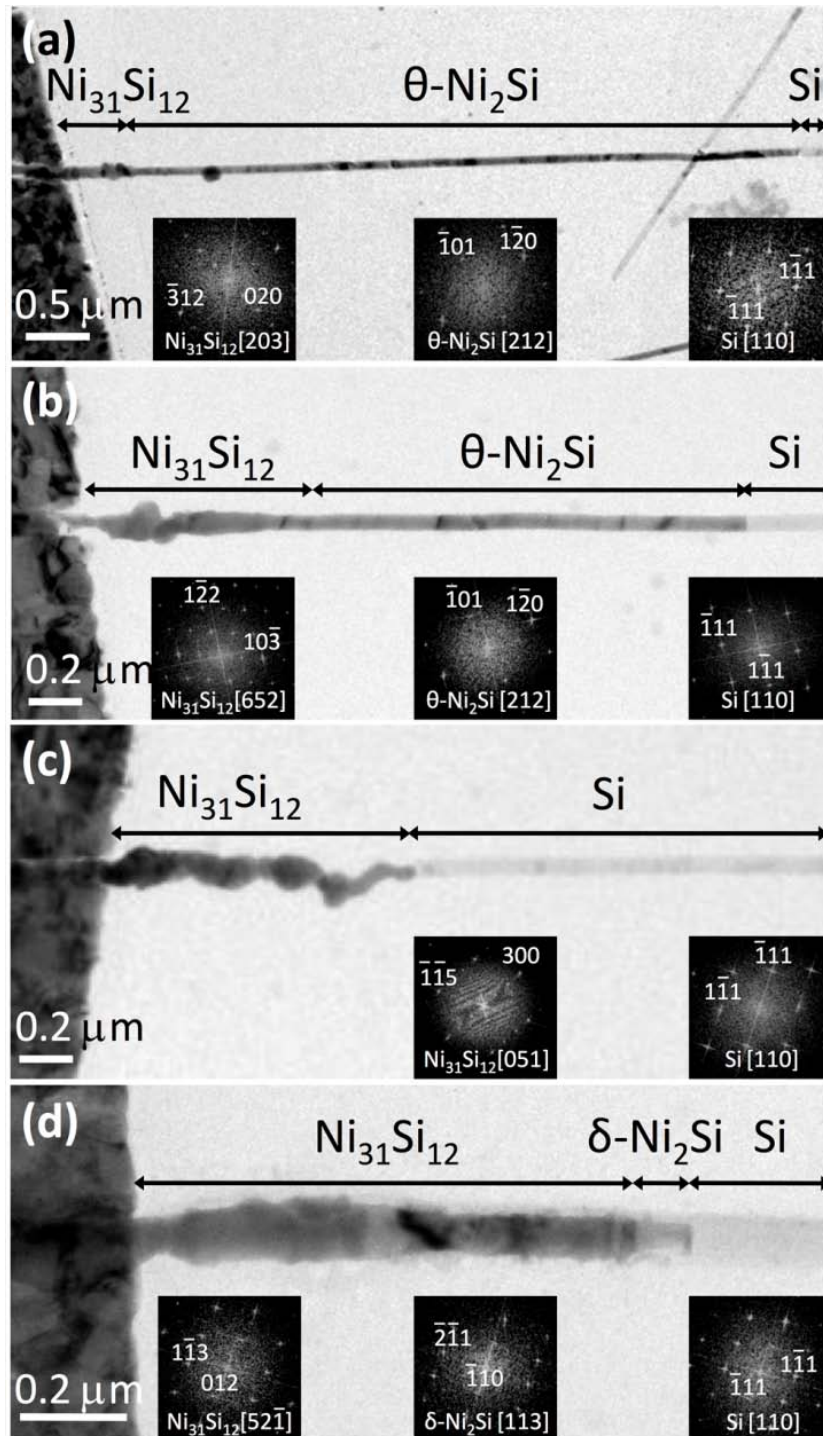


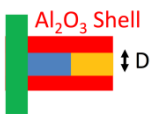

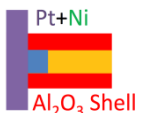


Fig. 22 First phases control in ~70 nm Si NW with Pt interlayer and ALD Al_2O_3 shells at 800 °C. (a) TEM image and corresponding FFT patterns of silicides formed in bare Si NW without Pt interlayer at 800 °C. (b) TEM image and corresponding FFT patterns of silicides formed in bare Si NW with 1 nm Pt interlayer at 800 °C. (c) TEM image and corresponding FFT patterns of silicides formed in bare Si NW with 5 nm Pt interlayer at 800 °C. (d) TEM image and corresponding FFT patterns of silicides formed in Si NW with 5 nm Pt interlayer and 17 nm ALD Al_2O_3 shell at 800 °C.

Table 4 Results of first phase formation in modified Si NW templates with different growth conditions.

Structure modification	First phase at 550 °C	First phase at 800 °C	Notes
Small bare NW 	NiSi ₂	θ-Ni ₂ Si	D<70nm
Large bare NW 	NiSi ₂	NiSi ₂	D>150nm
Al ₂ O ₃ shell 	NiSi ₂	NiSi ₂	D<70nm t>16 nm
Pt interlayer 	δ-Ni ₂ Si	θ-Ni ₂ Si Ni ₃₁ Si ₁₂	D<70nm Pt: 1-5nm
Pt interlayer and Al ₂ O ₃ shell 	Ni(Pt)Si	δ-Ni ₂ Si	D<70 nm t>16 nm Pt: 1-5nm

D: outer diameter of NWs

t: thickness of the Al₂O₃ shell

Pt: thickness of Pt interlayer

Since the 5 nm Pt amount is already close to Pt solubility in NiSi, this suppression relief at high temperature will be more significant to δ-Ni₂Si than NiSi and thus render δ-Ni₂Si as the first phase. Further studies will be needed to discover the Pt solubility difference in all

silicides for quantitative discussion. Together with results in Fig. 18 and Fig. 22, we have demonstrated how to manipulate $\text{Ni}_{31}\text{Si}_{12}$, $\delta\text{-Ni}_2\text{Si}$, $\theta\text{-Ni}_2\text{Si}$, Ni(Pt)Si and NiSi_2 to form as the first phase under different template structure and growth conditions. By selectively controlling the growth rate of Ni silicides and tuning the first phase, we confirm the kinetic competition mechanism determines the phase formation in 1-D structures. The conditions to form these silicides are summarized in Table 4.

Chapter 5 Influence of the additional Pt atoms on NiSi formation and its electrical properties

5.1 Electrical properties of Ni(Pt)Si NWs from two terminal measurements

The electrical properties of Ni(Pt)Si NW are tested as a benchmark of NW's quality. Two Ni pads with a narrow gap (~250 nm) in between are patterned by e-beam lithography to make the Si NW in gap fully silicided. As shown in Fig. 23, the resistivity and the maximum current density of Ni(Pt)Si are found to be $20.02 \mu\Omega\text{-cm}$ and $1.31 \times 10^8 \text{ A cm}^{-2}$ from the two terminal measurement, which are close to the reported values of NiSi.⁶⁵ According to other studies, Ni(Pt)Si has a shorter mean free path, lower junction leakage and higher thermal stability than pure NiSi.^{65,66} Therefore, Ni(Pt)Si NW is a promising candidate for nano-interconnects, nanocontacts and is more flexible for post-silicidation annealing.

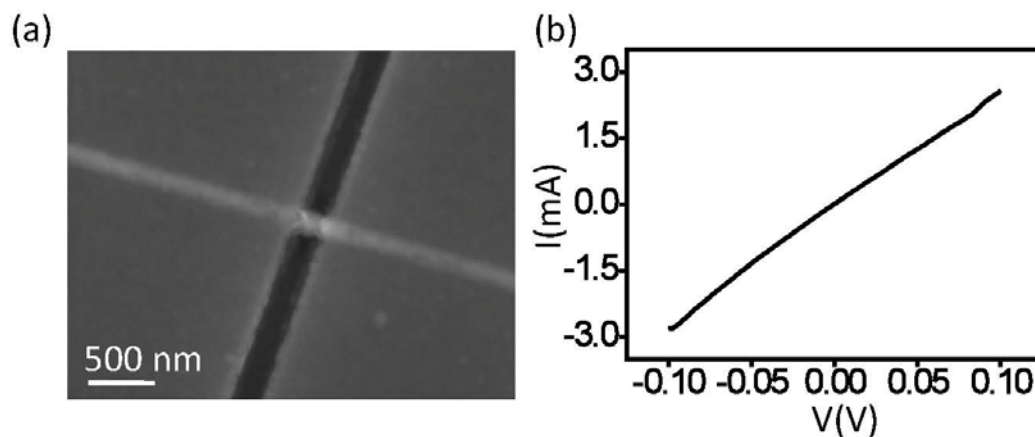


Fig. 23 Two terminal measurement of Ni(Pt)Si resistivity. (a) SEM image of two terminal measurement for Ni(Pt)Si form in Si NW with a 5 nm pt interlayer and a 22 nm Al_2O_3 shell. (b) I_d - V_d curve with two terminal measurements.

5.2 Fabrication of long Ni(Pt)Si NWs

To measure the real resistivity of Ni(Pt)Si without contact resistance between Ni pad and silicides, longer Ni(Pt)Si NWs is required. However, from the lateral structure in Fig. 23, it is hard to have long, pure Ni(Pt)Si NW without forming Ni richer phases after a long annealing time. Therefore, a new metal/Si NW diffusion structure is adopted as shown in Fig. 24.

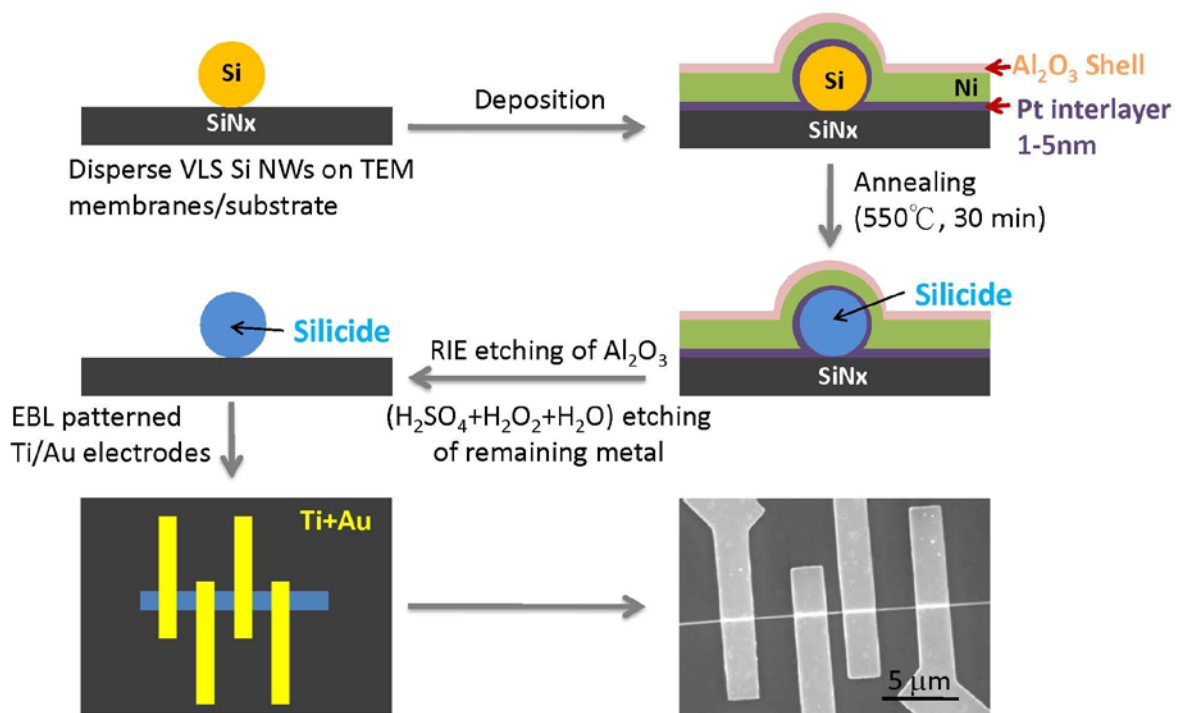


Fig. 24 Process flow to fabricate long Ni(Pt)Si NWs.

Si NWs are first dispersed on TEM membranes or Si nitride substrates. Native oxide on the Si NW is removed by BOE and 1-5 nm Pt interlayer and 6-15 nm Ni films are deposited to cover the whole NW in an e-beam evaporator. A 20-30 nm thick ALD Al₂O₃ film is deposited on top of the metal films to serve as a protecting layer. Samples are then heated at 550 °C for 30 mins to form Ni(Pt)Si. After reaction, Al₂O₃ film is etched by RIE and excess metal films

are then etched in a $\text{H}_2\text{SO}_4:\text{H}_2\text{O}_2:\text{H}_2\text{O}=1:1:4$ solution for 5 mins. Ti and Au pads are patterned through e-beam lithography to serve as contacts in the four terminal measurements. Four terminal measurements are operated in Lakeshore TTP4 probe station from 300-360 K.

5.3 Electrical properties of Ni(Pt)Si NWs from four terminal measurements

With the structure described in section 5.2, we are able to perform the four terminal measurements on a long NiSi NW to get rid of the contact resistance. The resistivity of 44.2 to 90 nm Ni(Pt)Si NWs are summarized in Table 5. As the diameter of the Ni(Pt)Si NW scales down to 44.2 nm, the resistivity does not increase but is somehow scattered. This is a result the over estimation of the NW diameter from top down SEM images with limited resolution and side effect. Therefore, we pick two NWs with close diameters to prepare cross sectional TEM samples by FIB.

Table 5 Resistivity of Ni(Pt)Si NW as a function of diameter

Diameter (nm)	44.2	53.0	55.5*	60.0*	60.4	70.0	73.0	90.0
Resistivity ($\mu\Omega\text{-cm}$)	30.43	20.00	15.35 (5.48)	9.13 (4.95)	29.84	27.80	23.92	17.92
Current density ($\times 10^7 \text{A/cm}^2$)	4.02	2.41	3.79 (7.23)	4.34 (10.18)	4.63	4.38	4.21	2.12

Diameters of Ni(Pt)Si NW are estimated from top down SEM images

*Phase confirmed as Ni(Pt)Si and diameter recalculated by FIB prepared cross sectional TEM sample. Numbers in parenthesis are recalculated by TEM

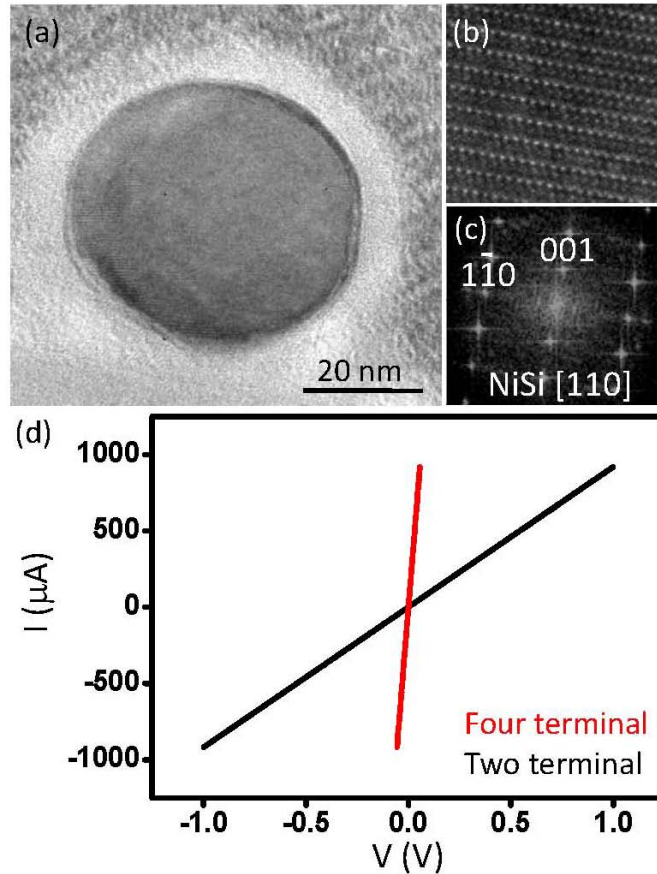


Fig. 25 (a) Cross sectional TEM image of a Ni(Pt)Si NW in Table 5. (b-c) High resolution image and FFT pattern of the NW. (d) Two and four terminal IV curve of the NW.

As shown in Fig. 25, the measured diameter of the Ni(Pt)Si NW from a TEM image is much smaller than that from a SEM image. The 55.5 nm NW (estimated from SEM, 15.35 $\mu\Omega\text{-cm}$) is actually 31.5 nm with a resistivity of 5.48 $\mu\Omega\text{-cm}$. The other 60 nm NW (from SEM) is also overestimated and its real resistivity is 4.95 $\mu\Omega\text{-cm}$. This indicates the scattered resistivity in Table 5 is a result of diameter and cross sectional area overestimation. From TEM characterizations, we confirm the phases of the two FIB cut NWs are indeed Ni(Pt)Si. Interestingly, the recalculated resistivity (close to 5 $\mu\Omega\text{-cm}$) are lower than the reported data

in thin film which is $19\text{-}24\ \mu\Omega\text{-cm}$ with $5\text{-}10\%$ Pt.⁶⁵ The lower resistivity might be attributed to the nature of single crystal Ni(Pt)Si NW without grain boundary scattering. A similar effect has also been reported in a single crystal NiSi NW with resistivity of $9.8\ \mu\Omega\text{-cm}$ (without a precise diameter estimation from FIB and TEM) while its thin film resistivity is $15\ \mu\Omega\text{-cm}$.^{6,65} From the TEM images and FFT pattern in Fig. 25a-c, we also rule out the possibility of excess metals (Ni or Pt) as parallel conducting paths. The clear surface shows the excess metals after silicidation are totally etched away.

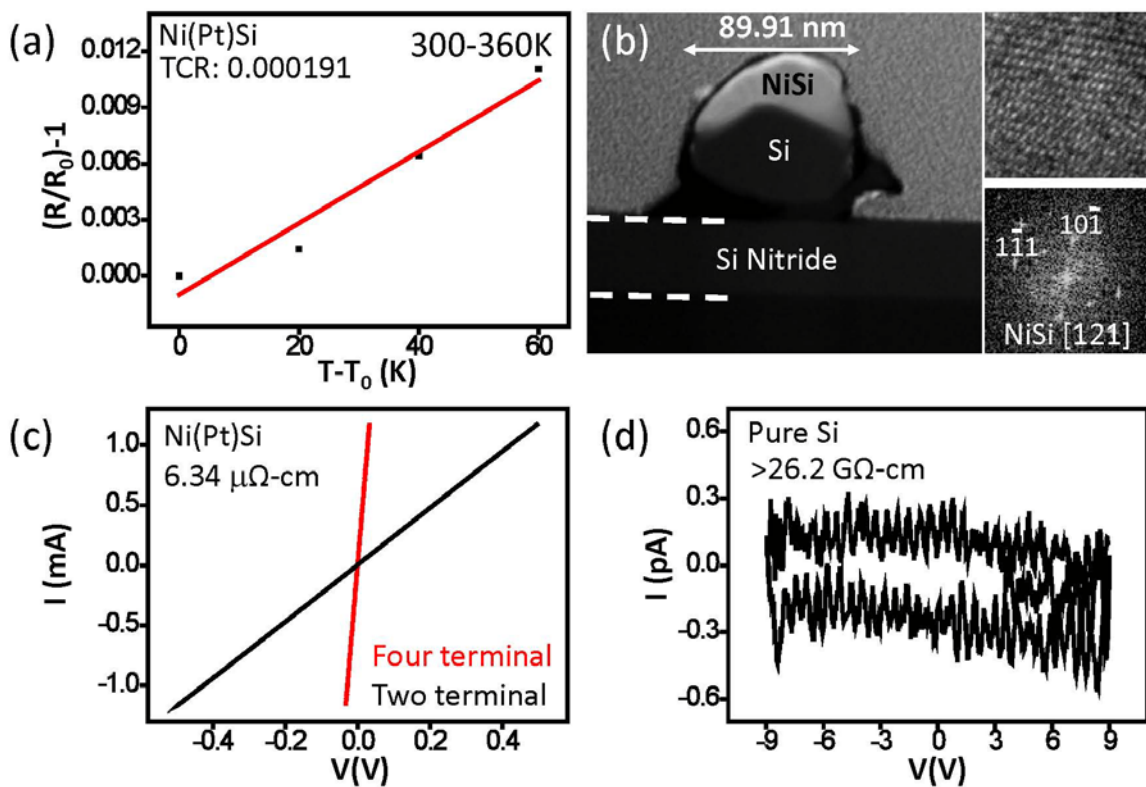


Fig. 26 (a) TCR value of the Ni(Pt)Si NW. (b) Cross sectional TEM image of the Ni(Pt)Si NW. The phase is identified from high resolution image and FFT pattern. (c) Two and four terminal measurement of the Ni(Pt)Si NW. (d) Resistivity of a pure Si NW.

We also measure the resistance of Ni(Pt)Si NW from 300-360K and to extract the temperature coefficient of resistance (TCR) value. The resistivity of a Ni(Pt)Si NW with diameter of 89.91 nm has been measured (Fig. 26). Since the NW is half reacted, we use Image J to estimate the cross sectional area of silicide part and use this number to calculate the resistivity (Fig. 26b). The resistivity of pure Si NW (without silicidation) is >26.2 GΩ-cm which makes its contribution to the conducting negligible (Fig. 26d). The phase is identified from high resolution image and FFT pattern.

The definition of TCR is as follow:

$$\frac{R}{R_{RT}} = \alpha(T - T_{RT}) + 1$$

where the R is the resistance at temperature T, R_{RT} is the resistance at room temperature, T_{RT} is 300 K and α is the TCR. As shown in Fig. 26a, the TCR value of the NW is 0.000191. This number is one order lower than the reported number of NiSi NW (TCR=0.0022).⁶⁷ In some of the metal solid solutions, the TCR are found lower as the concentration of solute increases.⁶⁸ More electrical properties measurements should be studies to understand the Pt effect to the resistivity and TCR lowering.

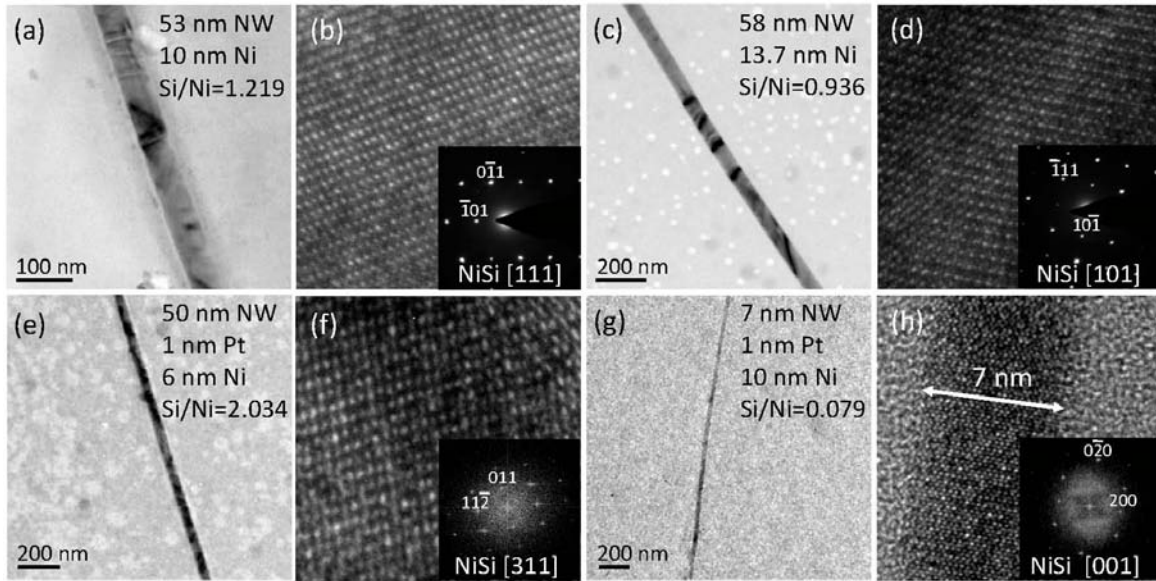


Fig. 27 Process window to form NiSi in samples with and without Pt interlayer. (a-d) Samples with an atomic ratios of Si/Ni=0.936-1.219 form NiSi without Pt interlayer. (e-h) Samples with an atomic ratio of Si/Ni=0.079-2.034 form NiSi with 1 nm Pt interlayer.

5.4 Wider processing windows of Ni(Pt)Si than pure NiSi

As mentioned in Chap. 4, Pt has higher solubility in NiSi than that in NiSi₂ and δ -Ni₂Si which suppresses the growth of those low resistivity phases. Indeed, as we optimize the thickness of Ni film and the diameter of the NWs to obtain NiSi and Ni(Pt)Si NWs, samples with Pt interlayer has a much wider processing window. As shown in Fig. 27a-d, the atomic ratio of as prepared Si NW with a Ni film on top to form NiSi is 0.936-1.219 without Pt interlayer. Here we assume only the top half surfaces of the NWs are contacted with metal films. Under the same annealing condition, the ratio to form NiSi with a 1 nm Pt interlayer has been made wider to 0.079-2.034 (Fig. 27e-h). In fact, 6-15 nm Ni films with 1 nm Pt can transfer Si NWs to 7-93 nm Ni(Pt)Si which gives more tolerance to the size of Si NW and uniformity of Ni film thickness in the lithography, etching and deposition prior the

silicidation for a large scale manufacturing. This can significantly increase the yield to form Ni(Pt)Si contacts and interconnection in integrated circuit and save money.

Chapter 6 Phase formation in other silicide systems

6.1 Phase formation of Co silicide

In Chap. 3 and 4, the kinetic growth competition is used to explain the first phase selection and to manipulate the phase formation through template modulation. In order to confirm this model can also be applied to other silicide systems, we show the phase formation results of Co and Pd silicide systems in this chapter.

Co-Si system is chosen for its well studied kinetic behaviors in 2-D system and similarities of crystal structure and phase formation sequence to Ni silicides. Cubic CoSi_2 (space group 225, $Fm\bar{3}m$, $a=5.365 \text{ \AA}$) shares the same atomic structure with NiSi_2 (space group 225, $Fm\bar{3}m$, $a=5.416 \text{ \AA}$) with close lattice constants while orthogonal Co_2Si (space group 62, $Pnma$, $a=4.918 \text{ \AA}$, $b=3.738 \text{ \AA}$ and $c=7.109 \text{ \AA}$) can be paired up with $\delta\text{-Ni}_2\text{Si}$ (space group 62, $Pnma$, $a=4.990 \text{ \AA}$, $b=3.720 \text{ \AA}$ and $c=7.030 \text{ \AA}$).^{40,69-71} Among Co silicides, Co_2Si forms as the first phase in 2-D structure due to its fastest growth rate which is also similar to $\delta\text{-Ni}_2\text{Si}$.⁷² In addition, Co silicide is also known for its phase formation sequence: diffusion controlled Co_2Si first forms at a low temperature and transfers into another diffusion controlled phase, CoSi at 450-500 °C. After a annealing at 750-900 °C, CoSi will react with Si and transfer into a nucleation controlled phase CoSi_2 .^{12,73} All these similarities valuable kinetic data make Co-Si system a good candidate to double check the kinetic competition model.

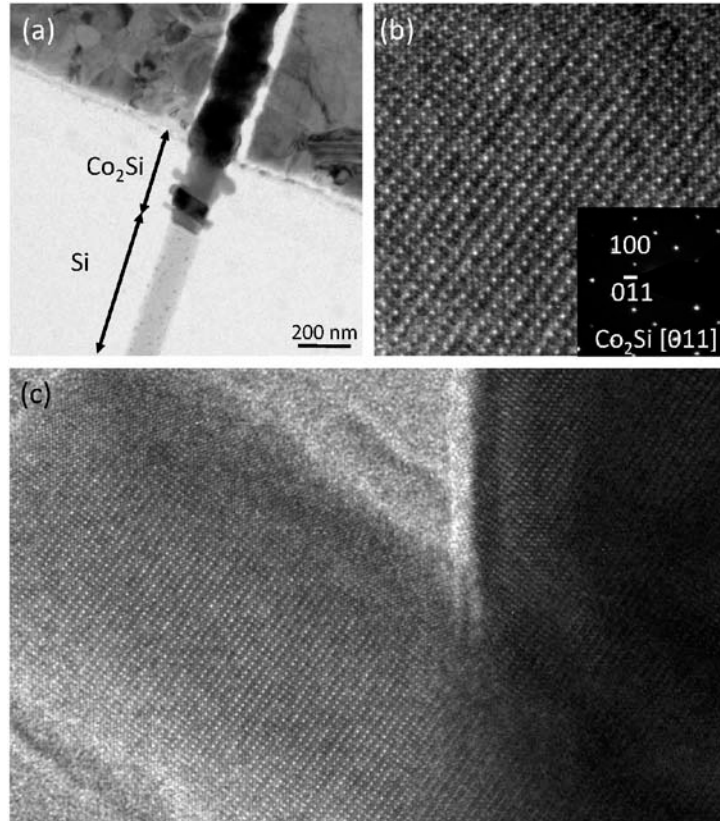


Fig. 28 Co silicide formation after annealed at 800 °C for 3 mins. (a) TEM image of the NW which breaks at the interface. (b) High resolution image and SAED pattern of Co_2Si . (c) High resolution image shows the extrusion of Co silicides with a continuous lattice structure from the stem.

As shown in Fig. 28, after annealed at 800 °C for 3 mins, Co_2Si form as the first phase in a 140 nm Si NW. In the growth, some extrusions from the stem with continuous lattices are observed on the surface of the NW (Fig. 28c). This is very different from the results in Ni-Si system where the NiSi_2 dominates as the first phase due to the elimination of grain boundary along axial direction in 1-D structures.

To discuss the growth rate of the Co silicides, we have to determine the diffusive species in all these phases. Unlike Ni and Pd silicides, where metals are always much more diffusive

than Si, the moving species in Co-Si system switches between Co and Si.⁷⁴⁻⁷⁶ In Co_2Si , Co diffusion is 10 times faster than Si, while in CoSi , Si is the dominant moving species. On the other hand, in CoSi_2 , the Co and Si diffusion are close and both contribute to the growth rate of CoSi_2 . Therefore to discuss the growth rates of Co silicides, we have to use the concept of integrated diffusivity \tilde{D}_{int} to consider the interdiffusion of Co and Si.

The definition of integrated diffusivity is

$$\tilde{D}_{\text{int}} = \int \tilde{D} dX$$

Where \tilde{D} is the interdiffusion coefficient

$$\tilde{D} = X_{\text{Co}} D_{\text{Co}} + X_{\text{Si}} D_{\text{Si}}$$

X_{Co} and X_{Si} are the molar fractions of Co and Si, D_{Co} and D_{Si} are diffusion coefficients of Co and Si. Since interdiffusion coefficients are not always a constant, we need to integrate \tilde{D} at various molar fraction regions.

To fairly compare the integrated diffusivities of Co silicides, we can only use data from one single group since the measurements from different research groups might contain systematic errors. In van Dal's study, the integrated diffusion coefficient of Co_2Si at 1100 °C is $2.13 \times 10^{-14} \text{ m}^2/\text{s}$ which is much larger than that of CoSi ($4.36 \times 10^{-15} \text{ m}^2/\text{s}$) and CoSi_2 ($7.80 \times 10^{-16} \text{ m}^2/\text{s}$).⁷⁶ Consider the activation barrier of Co_2Si (2.03-2.26 eV/atom) is lower than that of CoSi (2.17-2.61 eV/atom) and CoSi_2 (2.77-3.25 eV/atom),⁴¹ the integrated diffusion coefficient of Co_2Si at lower temperature (800 °C) will be much larger than that of CoSi and

CoSi₂ which makes Co₂Si more competitive and to form as the first phase in polycrystal structures.

In our case, the geometry of NW eliminates the continuous grain boundary of silicides along axial direction and thus the Co/Si diffusion in single crystal silicides should also be considered. In Co₂Si, the majority of Co diffuses through Co₂Si lattice with a vacancy mediated mechanism which makes its diffusivity and activation barrier in a single crystal structure remain similar values as in a polycrystal structure since the grain boundary contribution is not significant.⁷⁶ However, in CoSi₂, the activation barrier of Co and Si raises from 2.5 eV/atom (Co through grain boundary diffusion) and 2.7 eV/atom (Si through grain boundary diffusion) to 2.8 eV/atom (Co through lattice diffusion) and 3.2 eV/atom (Si through lattice diffusion), respectively. The increased activation barrier makes the Co as the only diffusive species in a single crystal CoSi₂ and slows down growth rate of CoSi₂ significantly. In CoSi, since the Si diffusion is much faster than Co, Si atoms in the nanowire will diffuse into the Co pad to form CoSi in the reaction. Therefore, CoSi can never grow out from the pad area into the Si NW and to compete with other phases. This is similar to Ti-Si system, where the Si diffusivity is two orders higher than Ti, Ti silicides do not grow out from the Ti pad even after a long annealing (Fig. 29).^{77,78}

The modified kinetics in 1-D structure makes Co₂Si even more competitive than in 2-D structure. This explains why the Co₂Si forms as the first phase in 1-D structure while δ -Ni₂Si

is replaced by NiSi₂. The kinetic competition model is again confirmed by the Co-Si system.

Unfortunately, the Co₂Si NW easily breaks at the silicide/Si interface and stops growing after a short annealing time which makes it hard to further study under in-situ TEM and extract the kinetic parameters as we did in Ni-Si system.

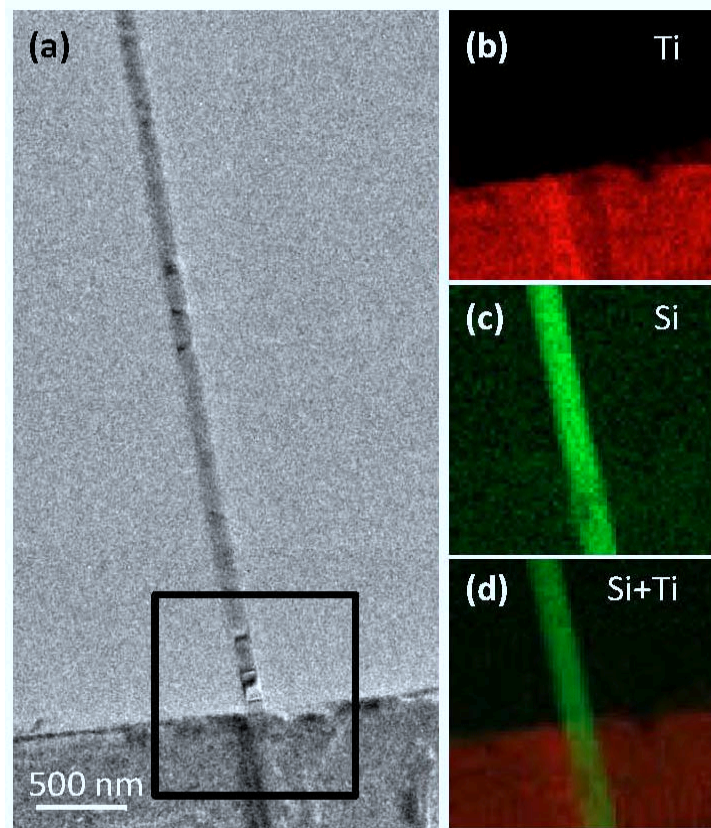


Fig. 29 No Ti silicide grows out from the Ti pad after annealing at 800 °C. (a) Bright field image of the nanowire and Ti pad. (b-d) Elemental mapping of the NW and Ti pad at the squared area in (a).

6.2 Phase formation of Pd silicide

Pd silicide has also been systematically studied in thin film structure due to its importance on the diffusion mechanism and Schottky barrier height engineering.⁷⁹⁻⁸¹ Pd₂Si, the first and

only formed phase in 2-D structure, is very competitive in growth and thermally stable (up to 800 °C) which simplifies the kinetic studies as a single phase system and offers a wide temperature range to study.^{81,82} Therefore, Pd silicide is an important lesson to understand the dynamic interdiffusion between metal and Si.

Very interestingly, the dominant diffusion species in the growth of Pd₂Si can be switched between Pd and Si from the reported data with inert markers and radioactive markers.^{75,82,83} In the formation of polycrystalline Pd₂Si, Si is the dominant diffusive specie with an kinetic barrier of 1.5-1.7 eV/atom through grain boundary of Pd₂Si. Meanwhile, in a single crystal Pd₂Si, the kinetic barrier of Si will be raised to 2.1 eV/atom and make the Pd becoming the dominant diffusion species. It is worth to mention that Pd₂Si forms as the first phase in both 2-D single crystal and polycrystal structures which indicates it is very competitive to other Pd silicides.

In our case, Pd₂Si forms at 550 °C in a Si NW template as shown in Fig. 30a-b. Again, the geometry of NW eliminates the possibility of grain boundary along axial direction in the wire and makes the interdiffusion similar to that in a single crystalline 2-D structure where Pd is the dominant diffusive species. The contrast switching between two Pd₂Si grains in Fig. 30a-b is due to different tilting angle of the sample in TEM. As the grain zone axis is aligned with the electron beam, more electrons will be scattered and not able to penetrate the sample which shows darker contrast in the images. Meanwhile, the Pd₂Si formed in the NW

underneath and in the Pd pads is similar to a polycrystalline thin film since and the grain boundary in the radial direction also contributes as a fast path for Si to diffuse into Pd. Therefore, Si is more diffusive than Pd underneath and in the Pd pad. As a result, Pd diffusion might be limited and slows down the growth of Pd₂Si due to the formation of Kirkendall voids in the supply channel underneath the Pd pad.

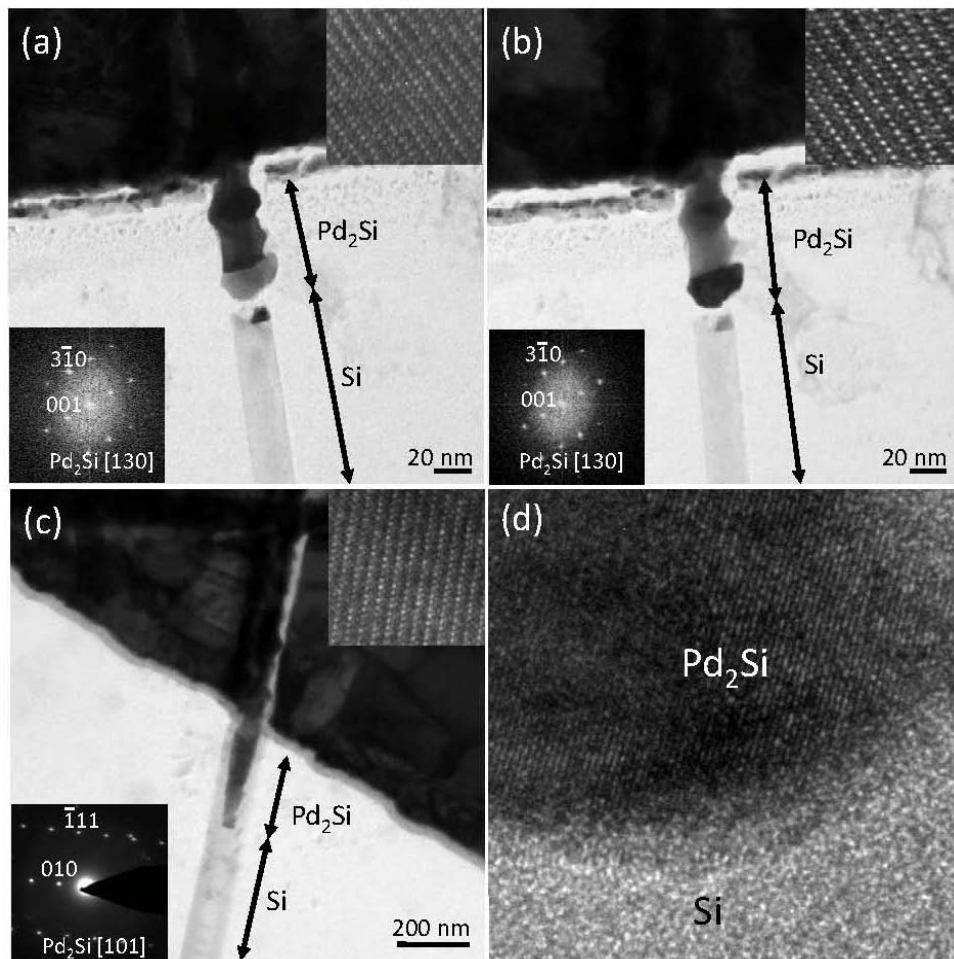


Fig. 30 Phase formation of Pd silicide after annealed at 550 °C. (a) and (b) are the same wire at different tilting angles. Pd₂Si form in a Si NW template and the NW is broken at the silicide/Si interface. (c) Pd₂Si forms in a Si NW with thick ALD Al₂O₃ shell without breaking the NW. (d) High resolution image at the Pd₂Si/Si interface in (c). No epitaxial relation is found. The phases are identified from FFT/SAED patterns and high resolution images in insets.

It is interesting that the NW in Fig. 30a-b is broken at the interface. From the in-situ TEM, we saw the wire is broken during the annealing which rules out the contribution of thermal stress to break the NW when it cools down. According to the Poisson's effect, when the NW expands in the radial direction during the phase transformation, it will simultaneously tend to shrink in the axial direction. This shrinking of the silicide region may pull at the interface and eventually break the NW since Si part is attached to the substrate due to the capillary force.

To confirm the capillary force is strong enough to hold the Si NW, we dispersed the Si NW on the substrate as stand process in Chap. 2 then poked it with an omni probe in FIB. The Si NW is found strongly attached to the substrate and do not move when the probe touches it. As we push harder and harder, the Si NW beaks instead of bends which shows the strong connection between the NW and the substrate.

To suppress this breaking formation, a thick ALD Al_2O_3 is deposited to cover the NW before annealing. Again, as the silicide grows into NW, the volume expansion is suppressed and the growth rate is slowed down as shown in Ni silicide system. The less expansion of Pd_2Si in the thick shell decrease the pulling force to the interface and helps the Pd_2Si to grow without breaking (Fig. 30c-d). No epitaxial interface form between Pd_2Si and Si (Fig. 30d). More kinetic studies especially with in-situ TEM are needed to understand the complicated interdiffusion with the switching dominant diffusive species.

Chapter 7 Summary

We have demonstrated that the size-dependent phase formation in Si NW templates can be understood with a kinetic competition mechanism. Coexistence of multiple phases at initial stage confirms nucleation does not limit the appearance of non-first phases. Our studies suggest diffusion-limited δ -Ni₂Si (conventional first phase in thin film) is suppressed in the Si NW due to the elimination of grain boundary diffusion, instead, interfacial-limited NiSi₂ appears as the dominant first phase in Si NWs. In the 1-D nanotemplate, linear-parabolic transition was observed for NiSi₂ in crystalline Si lattice, which enables the first time extraction of the activation energies for Ni diffusion in NiSi₂ lattice and for interface reaction at Si/NiSi₂. In specific, similar value of activation barrier and diffusivity of Ni diffusion in single crystal NiSi₂ (in Si NW) and in polycrystalline NiSi₂ suggests grain boundary diffusion is not a significant contribution. The studies also demonstrate that the activation barriers of NiSi₂ are lower than that of δ -Ni₂Si for lattice diffusion, but higher than the diffusion barrier of δ -Ni₂Si through grain boundaries, confirming that the elimination of grain boundaries renders NiSi₂ more competitive, leading to its replacement of δ -Ni₂Si as the first phase in Si NW. The extracted parameters are then used to explain the kinetic competition which leads to the size dependant first phase selection observed at 800 °C.

In addition, the manipulation of Ni₃₁Si₁₂, δ -Ni₂Si, θ -Ni₂Si, NiSi₂ and finally NiSi as the first phase by tuning the growth rates of targeted silicides has been demonstrated. Firstly, the

growth rate of silicides can be selectively tuned through template structure modifications. In a porous template, the growth rate of the diffusion limited phase is more enhanced as opposed to the interface limited phase due to shorter diffusion length. With thick shells, the growth rate of silicides will be selectively decreased depending on volume expansion during silicidation. Secondly, a Pt interlayer can suppress the formations of low Pt solubility silicides, especially dominating NiSi₂. Finally, with a combination of Pt interlayer and oxide shells, we can open a processing window for desired NiSi by suppressing NiSi₂ with a Pt interlayer and hindered Ni₃₁Si₁₂, δ -Ni₂Si and θ -Ni₂Si with thick shells. Element mapping and line scanning confirm the Pt distribution difference in NiSi and NiSi₂. Pt uniformly exists in NiSi while the majority of Pt precipitates to the surface of NiSi₂ causing a higher kinetic barrier and suppression of the NiSi₂ formation. Interestingly, epitaxial interface between NiSi (with Pt substitution) and Si, which is arguably the determining factor of enhanced NiSi growth in thin film, is not observed in NWs which further indicates herein kinetic modulation rather than interfacial energies determines the formation of NiSi over NiSi₂ with Pt present. Resistivity of single crystal Ni(Pt)Si NW from two and four terminal measurements are compatible to pure NiSi. With shorter mean free path, Ni(Pt)Si has a lower resistivity than NiSi in small scale which makes it a perfect material for being nano contacts.

Phase formations of Co silicide and Pd silicide have also been studied. Conventional first phase in Co-Si 2-D structure, Co₂Si, is still the primary phase in 1-D system. This is because

the majority of Co diffuses through lattice and thus the elimination of grain boundary along the axial direction does not impede the growth of dominating Co_2Si as it does to $\delta\text{-Ni}_2\text{Si}$. In Pd-Si system, Pd_2Si , dominates in 1-D structure with a huge volume expansion and leads to a broken interface. An Al_2O_3 thick shell is found effective to suppress the formation of the breaking interface by applying a compressive stress to the NW. This study demonstrated the potential for reliable and predictable phase formation for high performance nanodevices through fundamental understanding of the kinetics of material behaviours at nanoscale. With the understanding of silicide competition growth mechanism, we can kinetically manipulate desired phase, such as Ni(Pt)Si , to form in 1-D structures.

References

- (1) McFadden, S. X.; Mishra, R. S.; Valiev, R. Z.; Zhilyaev, A. P.; Mukherjee, A. K. Low-Temperature Superplasticity in Nanostructured Nickel and Metal Alloys. *Nature* **1999**, *398*, 684–686.
- (2) Boukai, A. I.; Bunimovich, Y.; Tahir-Kheli, J.; Yu, J.-K.; Goddard, W. A.; Heath, J. R. Silicon Nanowires as Efficient Thermoelectric Materials. *Nature* **2008**, *451*, 168–171.
- (3) Wang, Z. L. ZnO Nanowire and Nanobelt Platform for Nanotechnology. *Mater. Sci. Eng., R* **2009**, *64*, 33–71.
- (4) Léonard, F.; Talin, A. A. Size-Dependent Effects on Electrical Contacts to Nanotubes and Nanowires. *Phys. Rev. Lett.* **2006**, *97*, 026804.
- (5) Norris, D. J.; Bawendi, M. G. Measurement and Assignment of the Size-Dependent Optical Spectrum in CdSe Quantum Dots. *Phys. Rev. B* **1996**, *53*, 16338–16346.
- (6) Wu, Y.; Xiang, J.; Yang, C.; Lu, W.; Lieber, C. M. Single-Crystal Metallic Nanowires and Metal/semiconductor Nanowire Heterostructures. *Nature* **2004**, *430*, 61–65.
- (7) Lin, Y.-C.; Lu, K.-C.; Wu, W.-W.; Bai, J.; Chen, L. J.; Tu, K. N.; Huang, Y. Single Crystalline PtSi Nanowires, PtSi/Si/PtSi Nanowire Heterostructures, and Nanodevices. *Nano lett.* **2008**, *8*, 913–918.
- (8) Lin, Y.-C.; Chen, Y.; Shailos, A.; Huang, Y. Detection of Spin Polarized Carrier in Silicon Nanowire with Single Crystal MnSi as Magnetic Contacts. *Nano Lett.* **2010**, *10*, 2281–2287.
- (9) Chen, L. J. Metal Silicides : An Integral Part of Microelectronics. *JOM* **2005**, *57*, 24–30.
- (10) Chen, L. J. Solid State Amorphization in metal/Si Systems. *Mater. Sci. Eng., R* **2000**, *29*, 115–152.
- (11) Murarka, S. P. Silicide Thin Films and Their Applications in Microelectronics. *Intermetallics* **1995**, *3*, 173–186.
- (12) Lavoie, C.; Detavernier, C.; Besser, P. *Silicide Technology for Integrated Circuits*; Chen, L. J., Ed.; The Institute of Electrical Engineers: London, 2004; pp. 95–151.

- (13) Walser, R. M.; Bené, R. W. First Phase Nucleation in Silicon–transition-Metal Planar Interfaces. *Appl. Phys. Lett.* **1976**, *28*, 624.
- (14) Pretorius, R. Phase Sequence of Silicide Formation at Metal-Silicon Interfaces. *Vacuum* **1990**, *41*, 1038–1042.
- (15) Pretorius, R.; Marais, T. K.; Theron, C. C. Thin Film Compound Phase Formation Sequence: An Effective Heat of Formation Model. *Mater. Sci. Eng., R* **1993**, *10*, 1–83.
- (16) Pretorius, R. Prediction of Silicide Formation and Stability Using Heats of Formation. *Thin Solid Films* **1996**, *290-291*, 477–484.
- (17) Pretorius, R.; Theron, C. C.; Vantomme, A.; Mayer, J. W. Compound Phase Formation in Thin Film Structures. *Crit. Rev. Solid State Mater. Sci.* **1999**, *24*, 1–62.
- (18) Gosele, U.; Tu, K. N. Growth Kinetics of Planar Binary Diffusion Couples: “Thin-Film Case” versus “Bulk Cases.” *J. Appl. Phys.* **1982**, *53*, 3252–3260.
- (19) d’Heurle, F. M.; Gas, P. Kinetics of Formation of Silicides: A Review. *J. Mater. Res.* **1986**, *1*, 205–221.
- (20) Tu, K. N.; Ottaviani, G.; Gosele, S. U.; Folic, H. Intermetallic Compound Formation in Thin-Film and in Bulk Samples of the Ni-Si Binary System. *J. Appl. Phys.* **1983**, *54*, 758–763.
- (21) Tinani, M.; Mueller, A.; Gao, Y.; Irene, E. a.; Hu, Y. Z.; Tay, S. P. In Situ Real-Time Studies of Nickel Silicide Phase Formation. *J. Vac. Sci. Technol. B* **2001**, *19*, 376.
- (22) Lin, Y.-C.; Chen, Y.; Xu, D.; Huang, Y. Growth of Nickel Silicides in Si and Si/SiO_x Core/shell Nanowires. *Nano Lett.* **2010**, *10*, 4721–4726.
- (23) Weber, W. M.; Geelhaar, L.; Unger, E.; Chèze, C.; Kreupl, F.; Riechert, H.; Lugli, P. Silicon to Nickel-Silicide Axial Nanowire Heterostructures for High Performance Electronics. *Phys. Status Solidi B* **2007**, *244*, 4170–4175.
- (24) Chou, Y. C.; Wu, W.-W.; Lee, C.-Y.; Liu, C.-Y.; Chen, L.-J.; Tu, K.-N. Heterogeneous and Homogeneous Nucleation of Epitaxial NiSi₂ in [110] Si Nanowires. *J. Phys. Chem. C* **2011**, *115*, 397–401.

- (25) Chen, Y.; Lin, Y.-C.; Huang, C.-W.; Wang, C.-W.; Chen, L.-J.; Wu, W.-W.; Huang, Y. Kinetic Competition Model and Size-Dependent Phase Selection in 1-D Nanostructures. *Nano Lett.* **2012**, *12*, 3115–3120.
- (26) Lu, K.-C.; Wu, W.-W.; Wu, H.-W.; Tanner, C. M.; Chang, J. P.; Chen, L. J.; Tu, K. N. In Situ Control of Atomic-Scale Si Layer with Huge Strain in the Nanoheterostructure NiSi/Si/NiSi through Point Contact Reaction. *Nano Lett.* **2007**, *7*, 2389–2394.
- (27) Dellas, N. S.; Liu, B. Z.; Eichfeld, S. M.; Eichfeld, C. M.; Mayer, T. S.; Mohny, S. E. Orientation Dependence of Nickel Silicide Formation in Contacts to Silicon Nanowires. *J. Appl. Phys.* **2009**, *105*, 094309.
- (28) Chou, Y.; Wu, W.; Chen, L.; Tu, K. Homogeneous Nucleation of Epitaxial CoSi₂ and NiSi in Si Nanowires. *Nano Lett.* **2009**, *9*, 2337–2342.
- (29) Holmberg, V. C.; Panthani, M. G.; Korgel, B. A. Phase Transitions, Melting Dynamics, and Solid-State Diffusion in a Nano Test Tube. *Science* **2009**, *326*, 405–407.
- (30) Chen, Y.; Lin, Y.-C.; Zhong, X.; Cheng, H.-C.; Duan, X.; Huang, Y. Kinetic Manipulation of Silicide Phase Formation in Si Nanowire Templates. *Nano Lett.* **2013**, *13*, 1–6.
- (31) Duan, X.; Niu, C.; Sahi, V.; Chen, J.; Parce, J. W.; Empedocles, S.; Goldman, J. L. High-Performance Thin-Film Transistors Using Semiconductor Nanowires and Nanoribbons. *Nature* **2003**, *425*, 274–278.
- (32) Zhong, X.; Qu, Y.; Lin, Y.-C.; Liao, L.; Duan, X. Unveiling the Formation Pathway of Single Crystalline Porous Silicon Nanowires. *Acs Appl. Mater. Interfaces* **2011**, *3*, 261–270.
- (33) Morkved, T. L.; Lopes, W. A.; Hahm, J.; Sibener, S. J.; Jaeger, H. M. Silicon Nitride Membrane Substrates for the Investigation of Local Structure in Polymer Thin Films. *Polymer (Guildf)*. **1998**, *39*, 3871–3875.
- (34) Lee, C.; Lu, M.; Liao, K.; Lee, W.; Huang, C.; Chen, S.; Chen, L. Free-Standing Single-Crystal NiSi₂ Nanowires with Excellent Electrical Transport and Field Emission Properties. *J. Phys. Chem. C* **2009**, *113*, 2286–2289.
- (35) Song, Y.; Schmitt, A. L.; Jin, S. Ultralong Single-Crystal Metallic Ni₂Si Nanowires with Low Resistivity. *Nano Lett.* **2007**, *7*, 965–969.

- (36) Lee, C.-Y.; Lu, M.-P.; Liao, K.-F.; Wu, W.-W.; Chen, L.-J. Vertically Well-Aligned Epitaxial Ni₃₁Si₁₂ Nanowire Arrays with Excellent Field Emission Properties. *Appl. Phys. Lett.* **2008**, *93*, 113109.
- (37) Miettinen, J. Thermodynamic Description of the Cu–Ni–Si System in the Copper-Rich Corner above 700 °C. *Calphad* **2005**, *29*, 212–221.
- (38) Tsubouchi, N.; Horino, Y. Ni Silicide Layer Formation Using Low-Energy Ion Beams. *Nucl. Instr. Meth. Phys. Res. B* **2005**, *232*, 338–342.
- (39) JCPDS Card No. 75-0589.
- (40) JCPDS Card No. 43-0989.
- (41) Colgan, E. G.; Heurle, F. M. Kinetics of Silicide Formation Measured by in Situ Ramped Resistance Measurements. *J. Appl. Phys.* **1996**, *79*, 4087–4095.
- (42) Gulpen, J. H.; Kodentsov, A. A.; Loo, F. J. van. Growth of Silicides in Ni-Si and Ni-SiC Bulk Diffusion Couples. *Z. Met.* **1995**, *86*, 530–539.
- (43) Gas, P.; d’Heurle, F. M. Formation of Silicide Thin Films by Solid State Reaction. *Appl. Surf. Sci.* **1993**, *73*, 153–161.
- (44) Lien, C.-D.; Nicolet, M. A.; Lau, S. S. Low Temperature Formation of NiSi₂ from Evaporated Silicon. *Phys. stat. sol.* **1984**, *81*, 123–128.
- (45) Putero, M.; Mangelinck, D. Effect of Pd on the Ni₂Si Stress Relaxation during the Ni-Silicide Formation at Low Temperature. *Appl. Phys. Lett.* **2012**, *101*, 111910.
- (46) De Keyser, K.; Van Bockstael, C.; Detavernier, C.; Van Meirhaeghe, R. L.; Jordan-Sweet, J.; Lavoie, C. Epitaxial Formation of a Metastable Hexagonal Nickel-Silicide. *Electrochem. Solid-State Lett.* **2008**, *11*, H266.
- (47) Dasgupta, N. P.; Xu, S.; Jung, H. J.; Iancu, A.; Fasching, R.; Sinclair, R.; Prinz, F. B. Nickel Silicide Nanowire Arrays for Anti-Reflective Electrodes in Photovoltaics. *Adv. Funct. Mater.* **2012**, *22*, 3650–3657.
- (48) Lin, Y.-C.; Chen, Y.; Huang, Y. The Growth and Applications of Silicides for Nanoscale Devices. *Nanoscale* **2012**, *4*, 1412–1421.

- (49) Hensel, J. C.; Tung, R. T.; Poate, J. M.; Unterwald, F. C. Electrical Transport Properties of CoSi_2 and NiSi_2 Thin Films. *Appl. Phys. Lett.* **1984**, *44*, 913–915.
- (50) Lavoie, C.; d’Heurle, F. M.; Detavernier, C.; Jr, C. C. Towards Implementation of a Nickel Silicide Process for CMOS Technologies. *Microelectron. Eng.* **2003**, *70*, 144–157.
- (51) Léonard, F.; Talin, a A. Electrical Contacts to One- and Two-Dimensional Nanomaterials. *Nat. Nanotech.* **2011**, *6*, 773–783.
- (52) Schmitt, A. L.; Higgins, J. M.; Szczech, J. R.; Jin, S. Synthesis and Applications of Metal Silicide Nanowires. *J. Mater. Chem.* **2010**, *20*, 223–235.
- (53) Lin, Y.-C.; Chen, Y.; Chen, R.; Ghosh, K.; Xiong, Q.; Huang, Y. Crystallinity Control of Ferromagnetic Contacts in Stressed Nanowire Templates and the Magnetic Domain Anisotropy. *Nano Lett.* **2012**, *12*, 4341–4348.
- (54) Tang, J.; Wang, C.-Y.; Xiu, F.; Lang, M.; Chu, L.-W.; Tsai, C.-J.; Chueh, Y.; Chen, L.-J.; Wang, K. L. Oxide-Confined Formation of Germanium Nanowire Heterostructures for. *ACS Nano* **2011**, *5*, 6008–6015.
- (55) JCPDS Card No. 80-2283.
- (56) Smeets, D.; Vanhoyland, G.; D’Haen, J.; Vantomme, A. On the Thermal Expansion Coefficient of CoSi_2 and NiSi_2 . *J. Phys. D Appl. Phys.* **2009**, *42*, 235402.
- (57) Loomans, M. E.; Chi, D. Z.; Chua, S. J. Monosilicide-Disilicide-Silicon Phase Equilibria in the Nickel- Platinum-Silicon and Nickel-Palladium-Silicon Systems. *Met. Mater. Trans. A* **2004**, *35A*, 3053–3061.
- (58) Mangelinck, D.; Gas, P.; Gay, J. M.; Pichaud, B.; Thomas, O. Effect of Co, Pt, and Au Additions on the Stability and Epitaxy of NiSi_2 Films on (111)Si. *J. Appl. Phys.* **1998**, *84*, 2583–2590.
- (59) Demeulemeester, J.; Smeets, D.; Comrie, C. M.; Barradas, N. P.; Vieira, a.; Van Bockstael, C.; Detavernier, C.; Temst, K.; Vantomme, a. On the Growth Kinetics of Ni(Pt) Silicide Thin Films. *J. Appl. Phys.* **2013**, *113*, 163504.
- (60) Tang, W.; Dayeh, S. A.; Picraux, S. T.; Huang, J. Y.; Tu, K.-N. Ultrashort Channel Silicon Nanowire Transistors with Nickel Silicide Source/drain Contacts. *Nano lett.* **2012**, *12*, 3979–3985.

- (61) Mangelinck, D.; Dai, J. Y.; Pan, J. S.; Lahiri, S. K. Enhancement of Thermal Stability of NiSi Films on (100)Si and (111)Si by Pt Addition. *Appl. Phys. Lett.* **1999**, *75*, 1736–1738.
- (62) Liu, J. F.; Chen, H. B.; Feng, J. Y.; Zhu, J. Improvement of the Thermal Stability of NiSi Films by Using a Thin Pt Interlayer. *Appl. Phys. Lett.* **2000**, *77*, 2177.
- (63) Wang, R. N.; Feng, J. Y. Comparison of the Thermal Stabilities of NiSi Films in Ni/Si, Ni/Pd/Si and Ni/Pt/Si Systems. *J. Phys. Condens. Matter* **2003**, *15*, 1935–1942.
- (64) Demeulemeester, J.; Smeets, D.; Van Bockstael, C.; Detavernier, C.; Comrie, C. M.; Barradas, N. P.; Vieira, a.; Vantomme, a. Pt Redistribution during Ni(Pt) Silicide Formation. *Appl. Phys. Lett.* **2008**, *93*, 261912.
- (65) Zhang, Z.; Zhang, S.-L.; Yang, B.; Zhu, Y.; Rosnagel, S. M.; Gaudet, S.; Kellock, A. J.; Jordan-Sweet, J.; Lavoie, C. Morphological Stability and Specific Resistivity of Sub-10 Nm Silicide Films of Ni_{1-x}Pt_x on Si Substrate. *Appl. Phys. Lett.* **2010**, *96*, 071915.
- (66) Lee, P. S.; Pey, K. L.; Mangelinck, D.; Ding, J.; Chi, D. Z.; Chan, L. New Salicidation Technology with Ni(Pt) Alloy for MOSFETs. *IEEE Electron Device Lett.* **2001**, *22*, 568–570.
- (67) Zhang, Z.; Hellström P.-E.; Ostling M.; Zhang, S.-L.; Lu, J. Electrically Robust Ultralong Nanowires of NiSi, Ni₂Si, and Ni₃₁Si₁₂. *Appl. Phys. Lett.* **2006**, *88*, 043104.
- (68) *Springer Handbook of Condensed Matter and Materials Data*; Martienssen, W.; Warlimont, H., Eds.; Springer, 2005.
- (69) JCPDS Card No. 74-1371.
- (70) JCPDS Card No. 89-4181.
- (71) JCPDS Card No. 73-2092.
- (72) Tu, K. N.; Ottaviani, G.; Thompson, R. D.; Mayer, W.; Introduction, I. Thermal Stability and Growth Kinetics of Co₂Si and CoSi in Thin-Film Reactions. *J. Appl. Phys.* **1982**, *53*, 4406–4410.

- (73) Kikkawa, T.; Inoue, K.; Imai, K. *Silicide Technology for Integrated Circuits*; Chen, L. J., Ed.; The Institute of Electrical Engineers: London, 2004; pp. 77–94.
- (74) Baglin, J. E. E.; Twater, H. A. A.; Gupta, D.; d’Heurle, F. M. Radioactive Ni* Tracer Study of the Nickel Silicide Growth Mechanism. *Thin Solid Films* **1982**, *93*, 255–264.
- (75) Zingu, E. C.; Mayer, J. W.; Comrie, C.; Pretorius, R. Mobility of Pd and Si in Pd₂Si. *Phys. Rev. B* **1984**, *30*, 5916–5922.
- (76) Van Dal, M. J. .; Huibers, D. G. G. .; Kodentsov, A. .; van Loo, F. J. . Formation of Co-Si Intermetallics in Bulk Diffusion Couples. Part I. Growth Kinetics and Mobilities of Species in the Silicide Phases. *Intermetallics* **2001**, *9*, 409–421.
- (77) Yu, J.; Wang, Y.; Lu, J.-Q.; Gutmann, R. J. Low-Temperature Silicon Wafer Bonding Based on Ti/Si Solid-State Amorphization. *Appl. Phys. Lett.* **2006**, *89*, 092104.
- (78) Chu, W. K.; Krautle, H.; J. W. Mayer; Muller, H.; Nicolet, M. A.; Tu, K. N. Identification of the Dominant Diffusing Species in Silicide Formation. *Appl. Phys. Lett.* **1974**, *25*, 454.
- (79) Chand, S.; Kumar, J. Current-Voltage Characteristics and Barrier Parameters of Pd₂Si/p-Si(111) Schottky Diodes in a Wide Temperature Range. *Semicond. Sci. Technol.* **1995**, *10*, 1680–1688.
- (80) Belyaev, A. E.; Boltovets, N. S.; Konakova, R. V.; Kudryk, Y. Y.; Sachenko, A. V.; Sheremet, V. N. Temperature Dependence of Contact Resistance of Au-Ti-Pd₂Si-n⁺-Si Ohmic Contacts. *PACS* **2010**, *13*, 436–438.
- (81) Ho, P. S.; Rubloff, G. W.; Lewis, J. E.; Moruzzi, V. L.; Williams, A. R. Chemical Bonding and Electronic Structure of Pd₂Si. *Phys. Rev. B* **1980**, *22*, 4784–4790.
- (82) Wittmer, M.; Tu, N. Growth Kinetics and Diffusion Mechanism in Pd₂Si. *Phys. Rev. B* **1983**, *27*, 1173–1179.
- (83) Comrie, C. M.; Egan, J. M. Diffusion of Silicon in Pd₂Si during Silicide Formation. *J. Appl. Phys.* **1988**, *64*, 1173.